FIELD, PETROGRAPHIC AND $^{40}Ar/^{39}Ar$ CONSTRAINTS ON THE TECTONIC HISTORY OF THE CENTRAL MANZANO MOUNTAINS, CENTRAL NEW MEXICO

Joseph Robert Marcoline

Department of Earth and Environmental Science
New Mexico Institute of Mining and Technology
Socorro, New Mexico

Submitted in partial fulfillment of the requirements for the degree of
Master of Science in Geology

December 1996

ABSTRACT

The Proterozoic rocks in the Capilla Peak area of the Manzano Mountains of central New Mexico preserve evidence, on all scales, for multiple deformation events. The dominant NNE trending foliation (S_2) overprints an older, nearly perpendicular foliation (S_1). In schists and metarhyolites S_2 is a crenulation cleavage, while in quartz mylonites and amphibolites, S_2 is a mylonitic fabric. Within the amphibolites S_1 is preserved as a relict foliation subparallel to S_1 in the schist and metarhyolites.

Petrographic, microprobe and $^{40}Ar/^{39}Ar$ studies have been performed on rocks and mineral separates from the Capilla Peak area to help constrain the timing, and characterize, the deformational and metamorphic history in the Manzano Mountains. Quartz microstructures and crystallographic preferred orientations indicate that D_2 was accommodated at upper greenschist to lower amphibolite facies conditions, in a non-coaxial, general shear zone. This estimate of metamorphic grade is refined on the basis of petrographic studies and microprobe data from amphibolites. These data indicate that two distinct periods of amphibole growth occurred, resulting in an older (D_1) actinolite and a younger (D_2) hornblende. The hornblende indicates that (D_2) took place under lower amphibolite facies conditions. The younger hornblendes and biotites yield $^{40}Ar/^{39}Ar$ cooling ages of 1.4 Ga indicating that the area cooled through the hornblende and biotite closure temperatures by 1.4 Ga. Muscovites yield $^{40}Ar/^{39}Ar$ ages between 1320 and

1400 Ma indicating that the crust cooled relatively rapidly to 250-300°C by 1.35 Ga.

Data presented support a model of deformation during upper greenschist to lower amphibolite facies conditions ca. 1.45-1.4 Ga.

ACKNOWLEDGMENTS

I sincerely thank the members of my committee Kent Condie, Laurel Goodwin, Matt Heizler and Steve Ralser, all of whom made significant contributions to this manuscript and more importantly, helped me become a better scientist.

I benefited from insightful discussions with, and critical reviews from John Abbott, Paul Bauer, John Hall, Mic Heynekamp and Kurt Vollbrecht, their help is greatly appreciated.

Special thanks goes to Dr. Barbara Tewksbury whose teachings and guidance drew me into geology and inspired me to pursue a masters degree and a career in geology.

This research was funded by NSF grant EAR-9316474 and generous support from the New Mexico Bureau of Mines and Mineral Resources Geochronology Research Laboratory.

TABLE OF CONTENTS

LIST OF FIGURES

Part I: FIELD AND MICROSTRUCTURAL OBSERVATIONS FROM THE CAPILLA PEAK AREA IN THE MANZANO MOUNTAINS, CENTRAL NEW MEXICO

Part II: STRUCTURAL AND 40Ar/39Ar CONSTRAINTS ON MIDDLE PROTEROZOIC DEFORMATION AND METAMORPHISM IN THE MANZANO MOUNTAINS, CENTRAL NEW MEXICO

LIST OF TABLES

Part II: STRUCTURAL AND 40Ar/39Ar CONSTRAINTS ON MIDDLE PROTEROZOIC DEFORMATION AND METAMORPHISM IN THE MANZANO MOUNTAINS, CENTRAL NEW MEXICO

LIST OF APPENDICES

Part II: STRUCTURAL AND 40Ar/39Ar CONSTRAINTS ON MIDDLE PROTEROZOIC DEFORMATION AND METAMORPHISM IN THE MANZANO MOUNTAINS, CENTRAL NEW MEXICO

INTRODUCTION

In the last decade, work in the Proterozoic of the southwestern United States has focused on understanding the extent, the character, and the driving force behind 1.4 Ga tectonism (Bowring and Karlstrom, 1990; Karlstrom and Bowring, 1991; Bowring, 1991; Shastri and Bowring, 1992; Bauer and Williams, 1993). Many of the studies have concentrated on the numerous 1.4 Ga plutons and their metamorphic aureoles, while few have tried to understand the 1.4 Ga tectonism outside the aureoles. The central Manzano Mountains is an optimal location to study the effects of 1.4 Ga tectonism because of the excellent exposure and varying lithologies, including 1.4 Ga intrusives. The study area was chosen greater than 10 km from the margins of the Priest and Ojita granodiorites in order to characterize and date the metamorphism and deformation from an area which has not experienced the thermal and deformational effects of 1.4 Ga plutonism.

Due to ongoing research and abundant unanswered questions related to 1.4 Ga tectonism, this thesis is presented in the form of two separate papers which will be published in order to make the data available for others studying or interested in the Proterozoic of New Mexico.

Part I is a description of the structural relationships observed in the Capilla Peak area of the Manzano Mountains. The emphasis is on understanding the character of the latest deformational event through detailed analysis of microstructures and the microfabrics preserved in the rocks.

Part II is a presentation of new structural, microprobe and $^{40}Ar/^{39}Ar$ data supporting a model for deformation and metamorphism at 1.4 Ga in the Manzano Mountains. This model is somewhat controversial, but is becoming more widely accepted as the idea of "anorogenic" plutonism at 1.4 Ga is being questioned.

This thesis is a contribution to the ongoing studies of Proterozoic crustal evolution. Additional information, even within the Capilla Peak area of the Manzano Mountains, is needed in order to fully understand the middle to late Proterozoic in the southwestern United States.

Part I

FIELD AND MICROSTRUCTURAL OBSERVATIONS FROM THE CAPILLA PEAK AREA IN THE MANZANO MOUNTAINS, CENTRAL NEW MEXICO.

ABSTRACT

Proterozoic rocks in the Capilla Peak area of the Manzano Mountains preserve evidence for two distinct phases of deformation including folding of a pre-existing foliation and two phases of mineral growth. Little information about the character of the first deformation remains due to extensive overprinting. However, microstructural and crystallographic preferred orientations provide valuable information about the deformational history of the second event and place constraints on the metamorphic grade and character of this deformation. Microstructures and fabrics are typical of those forming during an upper greenschist to lower amphibolite grade metamorphic event. Quartz c-axis preferred orientations display both slightly asymmetric and symmetric patterns with respect to foliation and lineation, which is interpreted to suggest that deformation occurred under a combination of coaxial and non-coaxial strain. Asymmetric quartz c-axis distributions and microscopic and outcrop-scale kinematic indicators from quartz mylonites, metarhyolites, amphibolites and schists are interpreted to suggest a dominant east-side-up sense of shear. Metamorphic conditions inferred from crystallographic and microstructural fabrics are interpreted to be upper greenschist to lower amphibolite during deformation in the area of Capilla Peak, which is consistent with amphibole composition (Part II). The rocks in the Capilla Peak area are proposed to have accumulated high strain (inferred from microstructures and c-axis patterns) in a zone of general ductile shear.

INTRODUCTION

The Manzano Mountains are an eastward-tilted fault block composed primarily of Proterozoic metasedimentary, metavolcanic, and plutonic rocks. The mountain range is approximately 70 km long and 15 km wide and defines the eastern margin of the Rio Grande Rift between the Manzanita Mountains and Abo Pass(Fig. 1-1). The study area is in the central Manzano Mountains, located between Capilla Peak and Trigo Canyon (Fig. 1-1). The Capilla Peak area of the Manzano Mountains consists of a structurally complex sequence of multiply deformed Proterozoic quartzites, pelitic schists, metarhyolites, and amphibolites (Fig. 1-2). The Sevilleta metarhyolite is believed to be the oldest rock in the sequence; five Rb-Sr results define an isochron and yield an age of 1700 ±58 Ma (Bolton, 1976) and a U-Pb zircon age of 1680 Ma is also reported (Bowring et al., 1983).

The Monte Largo shear zone (MLSZ) has been mapped in the Manzano Mountains (Bauer, 1988; Thompson et al., 1991), and was first recognized in Monte Largo Canyon by Bauer (1988) as a 2m wide ductile fault. Structural mapping at 1:12,000 and petrologic investigations from Trigo Canyon north to Capilla Peak have shown that the MLSZ, as observed in Monte Largo Canyon, is not one discrete shear zone; rather, is just one localized high strain zone

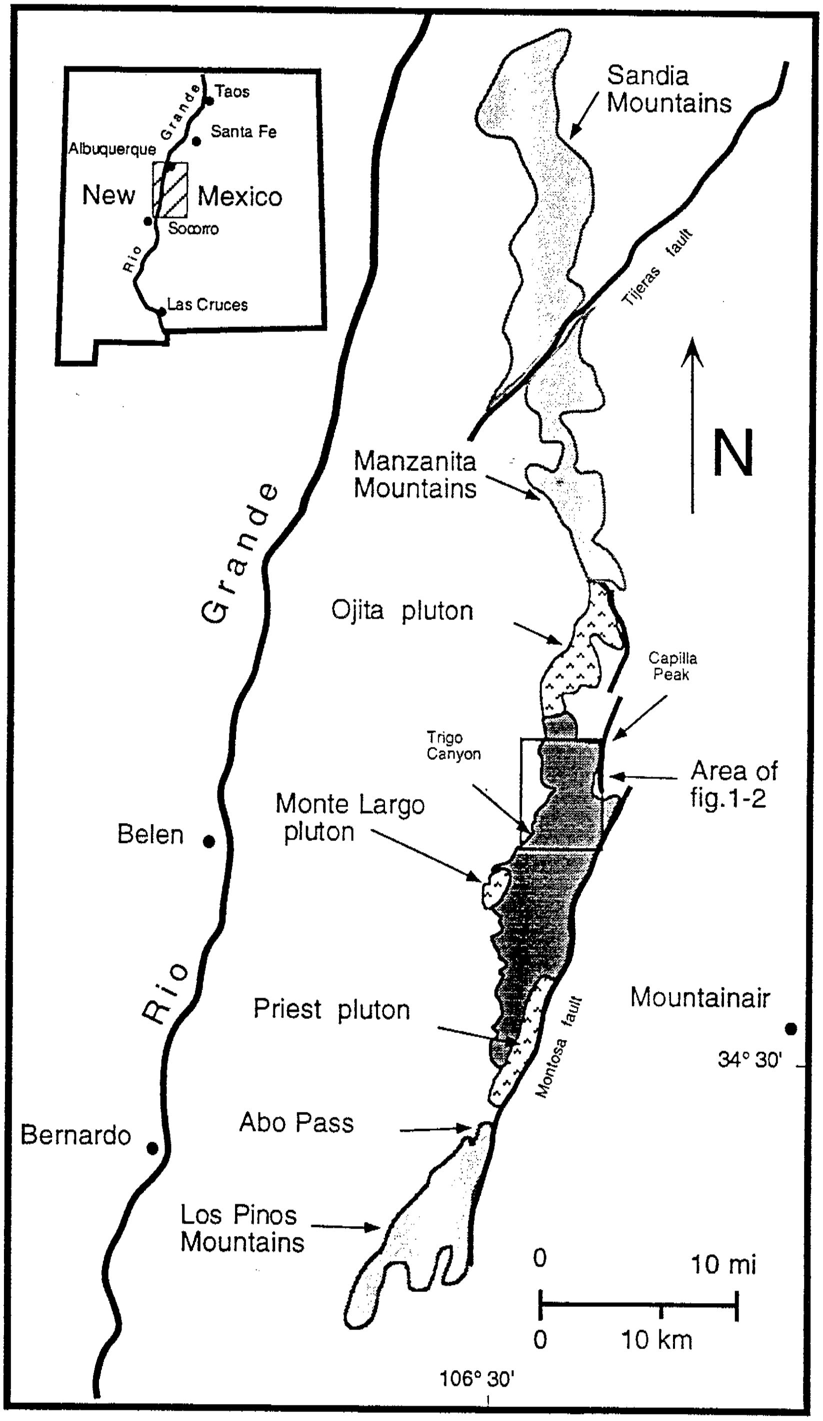

Figure 1-1. Geologic map of Proterozoic outcrops in central New Mexico showing the location of the study area.

within a larger deformation zone. Discontinuous zones of high strain appear to be lithologically controlled and have been mapped from Trigo canyon on the western edge of the range to Capilla Peak where they are overlain unconformably by Pennsylvanian limestones. The high-strain zones trend parallel, and adjacent to, the contact between the Blue Springs schist and structurally overlying Sevilleta metarhyolite (Fig 1-2). It is proposed in this paper that the Proterozoic rocks currently exposed in the Manzano Mountains were all part of a large ductile shear zone. The timing of this deformation is postulated to have occurred at 1.4 Ga based on $^{40}Ar/^{39}Ar$ geochronology of amphibole, muscovite and biotite from the Capilla Peak area (Part II).

The purpose of this paper is to describe the structural relationships and the deformational conditions of the 1.4 Ga event, in the Capilla Peak area of the Manzano Mountains. Our goal is to document these relationships and make interpretations in order to better understand the character and significance of the 1.4 Ga deformation event in New Mexico.

PREVIOUS WORK

The geology and structure of the Manzanita Mountains and the northern Manzano Mountains was first studied by Reiche (1949). In the Southern Manzano Mountains, Stark (1956) made correlations with observations of

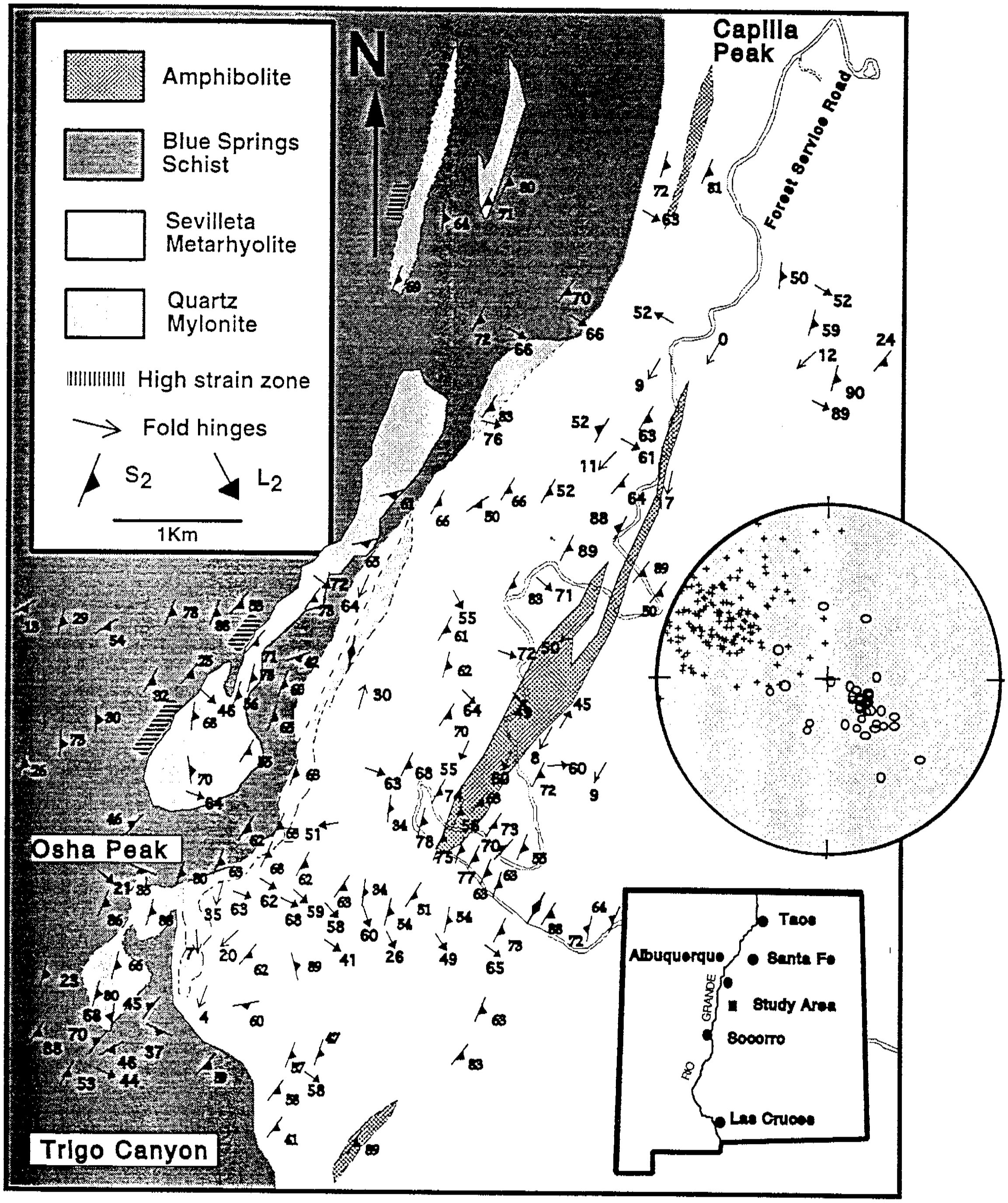

Figure 1-2. Geologic map of the study outlined in figure 1-1, showing the distribution of geologic units, fold hinges, the main foliation S_2 and the lineation L_2. Poles to foliation (+) and mineral lineations (O) are plotted on a lower hemisphere equal area net.

Reiche's; and made a correlation between parts of the stratigraphic section in the Los Piños Mountains (Stark and Dapples, 1946) with that in the Southern Manzano Mountains. Stark (1956) suggested that the Precambrian rocks in the Manzano Mountains were only moderately metamorphosed and therefore assumed an upright stratigraphic sequence. Within this sequence, Stark (1956) interpreted the quartz layers within the Blue Springs schist as vein quartz. After 1956 little work was performed in the Manzano Mountains until Grambling (1982) produced a map of Precambrian structures in Trigo Canon. Grambling documented evidence for three phases of folding, disproving the idea that the original stratigraphic sequence was preserved. Bauer (1982) produced a detailed geologic map and structural interpretation of the southern Manzano Mountains. Like Grambling (1982), Bauer (1982) recognized three phases of folding in the Manzano Mountains: early isoclinal folding, a strong crenulation cleavage and third, open folds in quartz-rich rocks and small crenulations in shistose rocks. Bauer (1982) also observed crossbedding in the quartz layers within the Blue Springs schist disproving Stark's (1956) conclusion that the layers were veins. In Monte Largo Canyon, Bauer (1982) mapped the MLSZ as a probable fault, and Thompson et al. (1991) recognized this structure as a shear zone separating two different terranes based on contrasting metamorphic grade. She proposed that the MLSZ juxtaposed the greenschist grade Blue Springs schist from the overriding amphibolite grade Sevilleta metarhyolite. Northrup (1991) studied the geochemical fluid-rock interaction within the MLSZ in Monte Largo Canyon and conclude that several episodes of hydrothermal veining had occurred.

The rocks present in the Capilla Peak area are similar to those described in the Los Pinos and southern Manzano Mountains by Stark and Dapples (1946) and Bauer (1982) and are summarized below.

Blue Springs schist

The Blue Springs schist of Stark and Dapples (1946) is intruded in the south by the 1656±10 Ma (Bauer et al., 1992) Monte Largo pluton and trends NNE for approximately 17 km, where it is overlain by Pennsylvanian limestones. The schist exposure is approximately 4 km wide, covered on the west by overlying pediment gravels and bound on the east by the White Ridge quartzite. Three dominant rock types exist within the Blue Springs schist: metasiltstones, phyllites, and muscovite-chlorite schists (Stark 1956; Bauer 1982).

The metasiltstones are typically folded, fine-grained pink, gray and green, finely-laminated rocks. S_1 is parallel to compositional laminae. Folds in S_1 are tight to isoclinal and slightly disharmonic. The phyllites are composed dominantly of quartz and muscovite and preserve a strong foliation S_2. The muscovite-chlorite schists range from gray-green to reddish brown in color, and are found throughout the Blue Springs schist. Folds in S_1 in the schists include 0.5-4 cm crenulations and 1-3 cm chevron folds. Between 30 and 40% of the muscovite-chlorite schists consist of folded and boudined quartz layers aligned parallel to the crenulated and chevron folded foliation S_1 in the schist.

Quartz mylonites

The quartz mylonites within the Manzano Mountains have previously been subdivided into the Sais and the White Ridge quartzites within the Blue Springs schist by Stark and Dapples (1946), Reiche (1949), Stark (1956) and Bauer (1982). The Sais quartzite does not outcrop in the study area. The quartz mylonites outcrop in discontinuous layers parallel to the foliation trend within the Blue Springs schist, whereas the White Ridge quartzite outcrops between the Blue Springs schist and the Sevilleta metarhyolite (Fig 1-2). Due to regional folding, compositional variations and the possibility of original cyclic deposition, it is unclear whether the quartz mylonites should be subdivided into separate formations. The White Ridge quartzite and quartz "reefs" in the field area are macroscopically and microscopically similar and will be grouped together as quartz mylonites for discussion in this paper. Quartz mylonite layers range from less than one meter to more than a kilometer in width. Compositions of the mylonites range from 90 to 99% quartz and 1-10% muscovite, with minor magnetite, biotite and epidote. Locally color ranges from pure white to purplish-gray depending on biotite and magnetite percentages. Outcrops range in character from massive to schistose.

Sevilleta metarhyolite

The Sevilleta metarhyolite of Stark and Dapples (1946), outcrops predominately on the east side of the range in the Capilla Peak area. It is a pink to brown, well foliated and lineated, metamorphosed rhyolite. In lower strain areas, the metarhyolite contains 1-2 mm equidimensional quartz and feldspar porphyroclasts. In the higher strain zones, porphyroclasts are elongate parallel to the foliation and lineation. The matrix is predominantly fine-grained quartz, feldspar and biotite with minor opaques.

Amphibolites

Amphibolite layers occur only within the Sevilleta Metarhyolite and are interpreted to be early mafic dikes (Stark and Dapples, 1946). The amphibolite layers are one to twenty meters wide and up to 400 meters long. The outcrop character ranges from highly schistose to massive. The amphibolites are petrologically complex and contain two amphibole phases, a hornblende and an actinolite, plagioclase, biotite, quartz, epidote and minor amounts of magnetite and pyrite (see Part II).

STRUCTURE

Macrostructural relationships

The dominant structure in the central Manzano Mountains is a pervasive NE-striking steeply SE dipping foliation (Fig. 1-2). The NE-striking foliation in the schistose units is a crenulation cleavage, cutting a well defined earlier foliation (S_1). In the non-schistose units, the main foliation (S_2) is defined by aligned minerals. S_2 is locally absent to well developed and is subparallel to lithologic contacts with the exception of areas of disharmonic folding where S_2 is variable. Where S_2 is absent to poorly developed, S_1 is the dominant foliation; this relationship is observed in several locations within the Blue Springs schist and in a few locations within the metarhyolites. The character of the macroscopic folding is integrally related to the degree of S_2 development and the rock type. Where S_2 is well developed, S_1 and S_0 are typically not observed.

The main foliation (S_2) in the Blue Springs schist exhibits the highest degree of variation, both in character and in orientation. S_2 in the Blue Springs schist is parallel to the regional foliation trend and in most places is a crenulation cleavage (Fig. 1-3). S_2 in the phyllites and the quartz-rich zones of the muscovite-chlorite schists is a well developed planar foliation, striking approximately 030° and dipping 60-80° SE. However, S_2 in the majority of the muscovite-chlorite schist is non-planar. S_2 anastamoses between the numerous folded quartz layers with

orientations ranging from 0-050°, 60-90° SE. A few areas within the schists exhibit an asymmetrical chevron fold crenulation with the limbs 1 to 3 cm in length (Fig. 1-3), and S_2 axial planar to the folds. The two limbs have the same strike and are oriented approximately 030°, dipping 85° SE and 55° NW with the main foliation subparallel to the SE dipping limbs. The metasiltstones are

Figure 1-3. Asymmetric chevron folding within the Blue Springs schist. S_2 is nearly vertical and is a crenulation cleavage. The limbs of the crenulations are 1-3 cm in length. Long dimension of photograph is approximately 30 cm.

characterized by small disharmonic folding of the compositional layering. The main foliation in the metasiltstones is poorly developed and highly irregular in orientation. The foliation is axial planar to the disharmonic folding which may explain the large variation in orientation of S_2.

A distinctive, narrow zone of highly deformed Blue Springs schist is seen in three locations. The most continuous outcrop is located on the west side of the contact between the ridge-forming quartz mylonite layer and the Blue Springs schist (Fig. 1-2). Two other highly deformed zones are located along strike within the schist, adjacent to one of the smaller quartz mylonite layers. The contact between the highly deformed zone and the schist is gradational. The character of the Blue Springs schist changes with increasing proximity to the zones; from containing abundant quartz-rich layers, to discontinuous and boudinaged quartz layers in the contact zone, to no quartz layers in the highly deformed zone. The highly deformed zones are less than a meter wide and defined by a well developed, highly planar foliation.

The Sevilleta metarhyolites have a moderate to well-developed NNE-striking foliation (S_2) and a locally well-developed down dip lineation. The foliation is defined by aligned biotite and lens-shaped quartz and feldspar porphyroclasts. A older foliation (S_1) is observed in a few locations where S_2 is poorly developed. No evidence is preserved for original compositional layering.

Folds in S_1 within the metarhyolite include both small 0.5-1 m isoclinal folds and 3-5 m open folds in foliation. These folds plunge 0-50° to the SW and are seen with a strong down dip lineation. Where crenulations are observed, S_2 is a crenulation cleavage. S_2 is axial planar to the outcrop scale folds, but is typically not observed in folded areas.

S_2 in the amphibolite layers is poorly to well-developed and is usually parallel to the foliation in the surrounding metarhyolite. One amphibolite layer contains distinctive 1-10 cm less deformed `pods' (Fig. 1-4). A well developed foliation wraps around these pods. The pods have length to width ratios ranging from 1:1 - 2:1 and are characterized by 1-3 mm, unaligned, green to black amphibole crystals surrounded by strongly foliated fine-grained amphibolite. The pods are sigmoidal in shape and asymmetric with respect to the main foliation, showing a consistent east-side-up sense of shear. Several 0.5-1 m scale asymmetric sigmoidally shaped structures within the amphiboite layers are also observed. These structures are similar to the 1-10 cm pods but contain an internal foliation parallel to, but weaker, than the surrounding foliation.

The quartz mylonites have a strong mylonitic foliation (S_2) oriented approximately 025°, dipping 60-80° SE (Fig. 1-5). In areas with a higher percentage of muscovite, the foliation is better developed.

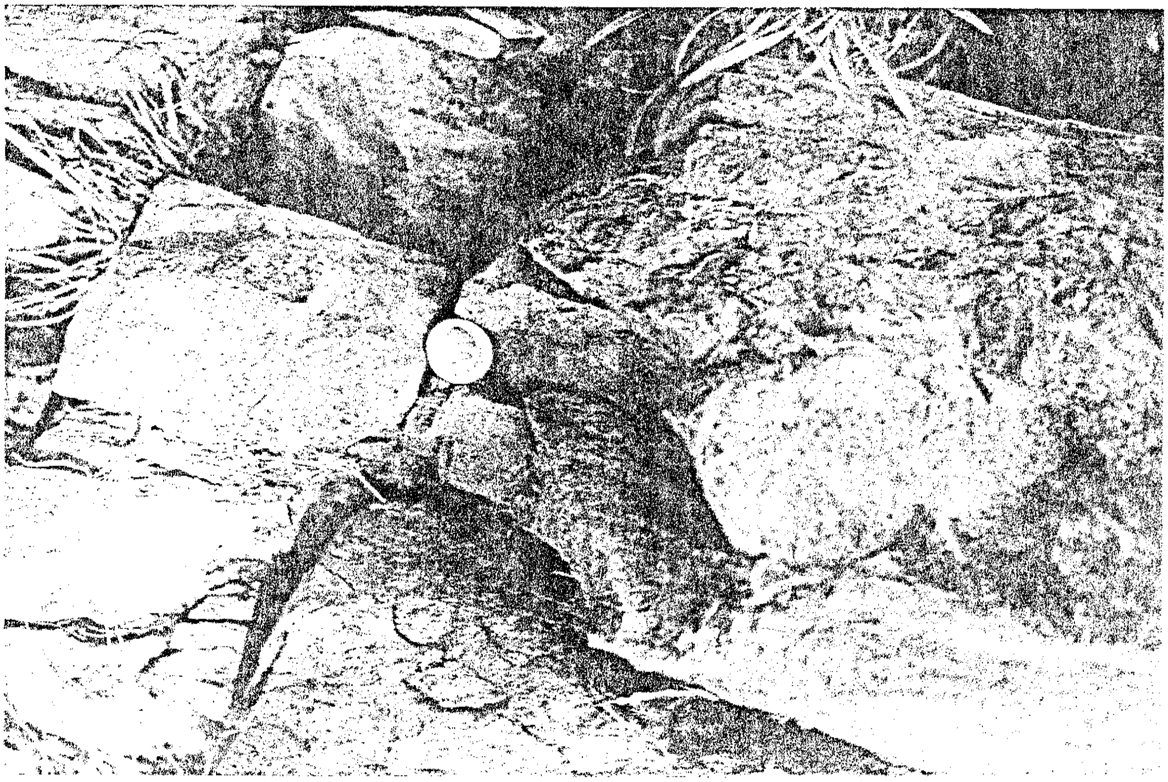

Figure 1-4. Photograph of asymmetric sigmoidal structure developed around the pods within the amphibolite layers. The pods are zones of relatively undeformed amphibolite within a strongly deformed amphibolite layer. Long dimension of photo is approximately 50 cm.

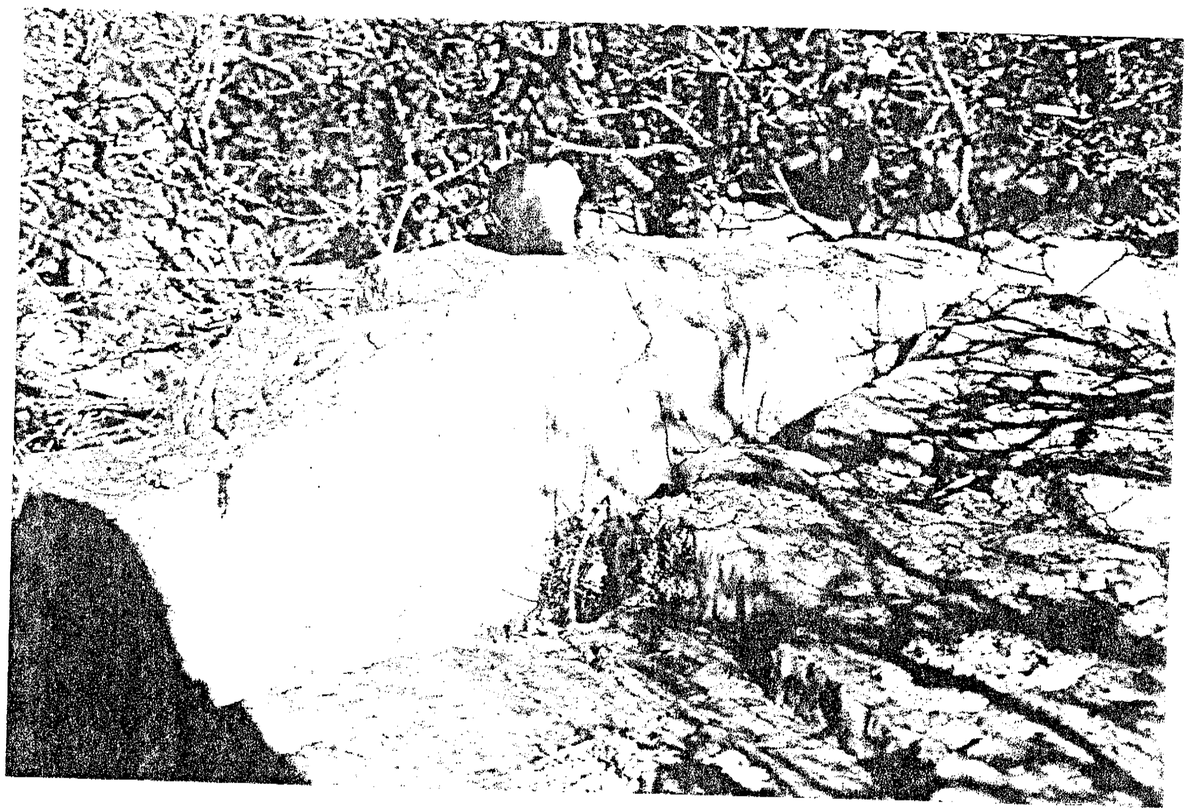

Figure 1-5. Field photograph of highly foliated quartz mylonite. The dominant foliation, S_2, is nearly vertical.

Open to isoclinal folds in S_1 are common in the quartz mylonites, and locally the axial planar foliation S_2 is observed. Folds in the quartz mylonites appear to be preserved in the lower strain zones. The discontinuous quartz mylonite layers within the Blue Springs schist may be repeated by large-scale folding, however, no direct evidence for this has been observed in the Capilla Peak area.

Microstructural relationships

In the following section, the microstructural relationships related to the youngest deformation event are described.

Blue Springs schist microstructures

In thin section, the character of the Blue Springs schist is as variable as it is at the outcrop scale (Fig. 1-6). In general the S_2 crenulation cleavage is best developed adjacent to the quartz mylonites. With greater S_2 development the cleavage plane spacing is decreased. In zones with a higher amount of quartz, recrystallized grains preserve a grain shape preferred orientation at a 45° angle to S_2.

Sevilleta metarhyolite microstructures

The metarhyolites are characterized by 1 to 2 mm quartz and feldspar porphyroclasts in a fine-grained (0.1-0.25 mm) quartz and feldspar matrix. The majority of the feldspar porphyroclasts are symmetric with respect to the

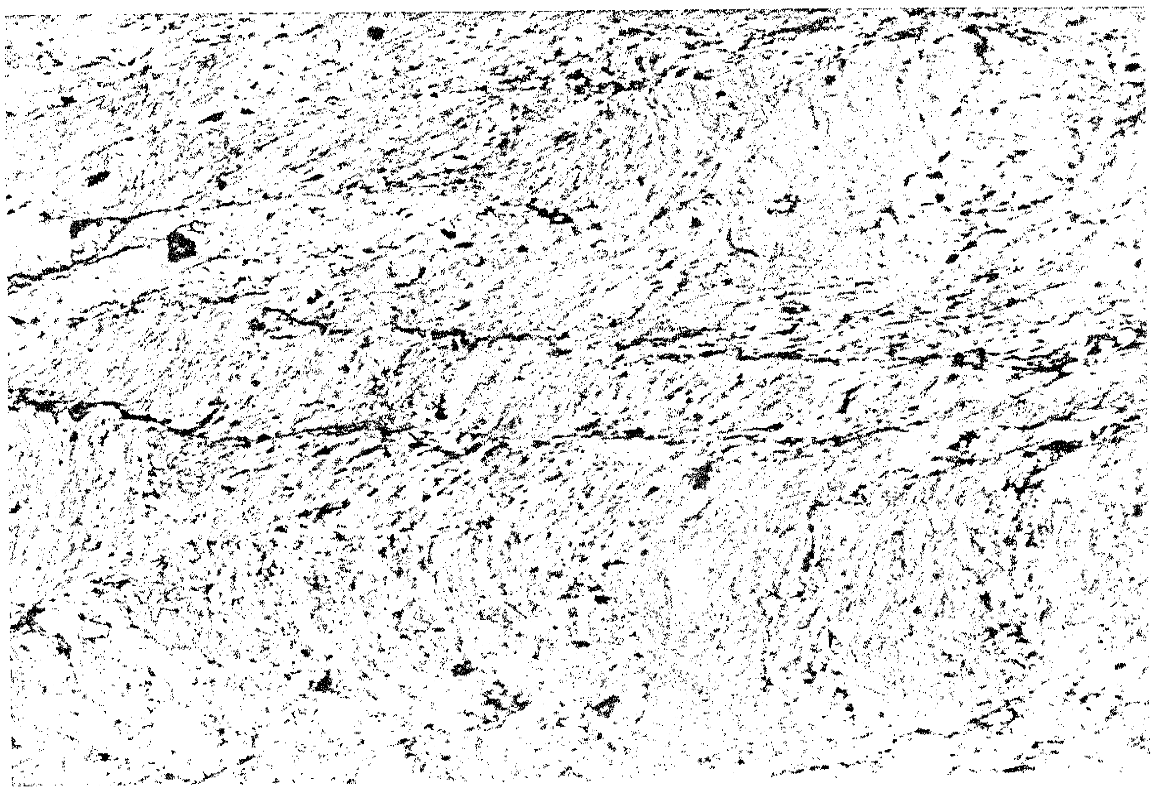

Figure 1-6. Photomicrograph from the Blue Springs. Long dimension of photo is parallel to S_2 and approximately 2mm.

foliation, however asymmetric delta-shaped porphyroclasts are present (Fig. 1-7). Asymmetries are also preserved by quartz grain-shape-preferred orientations within the matrix and porphyroclast tails, but are often ambiguous.

Amphibolite microstructures

The amphibolites exhibit the most complex microstructures in the study area and are dealt with in more detail in Part II. The amphibolites contain two chemically and structurally distinct amphibole phases, an older actinolite and a younger hornblende, plagioclase, biotite, quartz and epidote. The older anhedral actinolite is cross-cut and overgrown by the foliation-forming euhedral hornblendes (Fig 1-8). The actinolites contain inclusion trails that mark an older foliation parallel to cleavage plane traces within the actinolites and nearly perpendicular to the well defined hornblende foliation. The amphibole phases are chemically distinct (Table 2-1 Part II) and it is proposed in Part II that the younger hornblende crystals grew at lower amphibolite facies conditions, probably around 500°C.

Quartz mylonite microstructures

Quartz mylonites from the central Manzano Mountains exhibit a variety of microstructures which can be divided into three groups. Samples ML 11-3, ML 7-15 and ML 6-2 are characterized by 0.1 to 0.25 mm recrystallized quartz grains (Fig. 1-9). Quartz grains typically have a strong to moderate grain-shape preferred orientation (GSPO) which defines a foliation at an angle between 45°

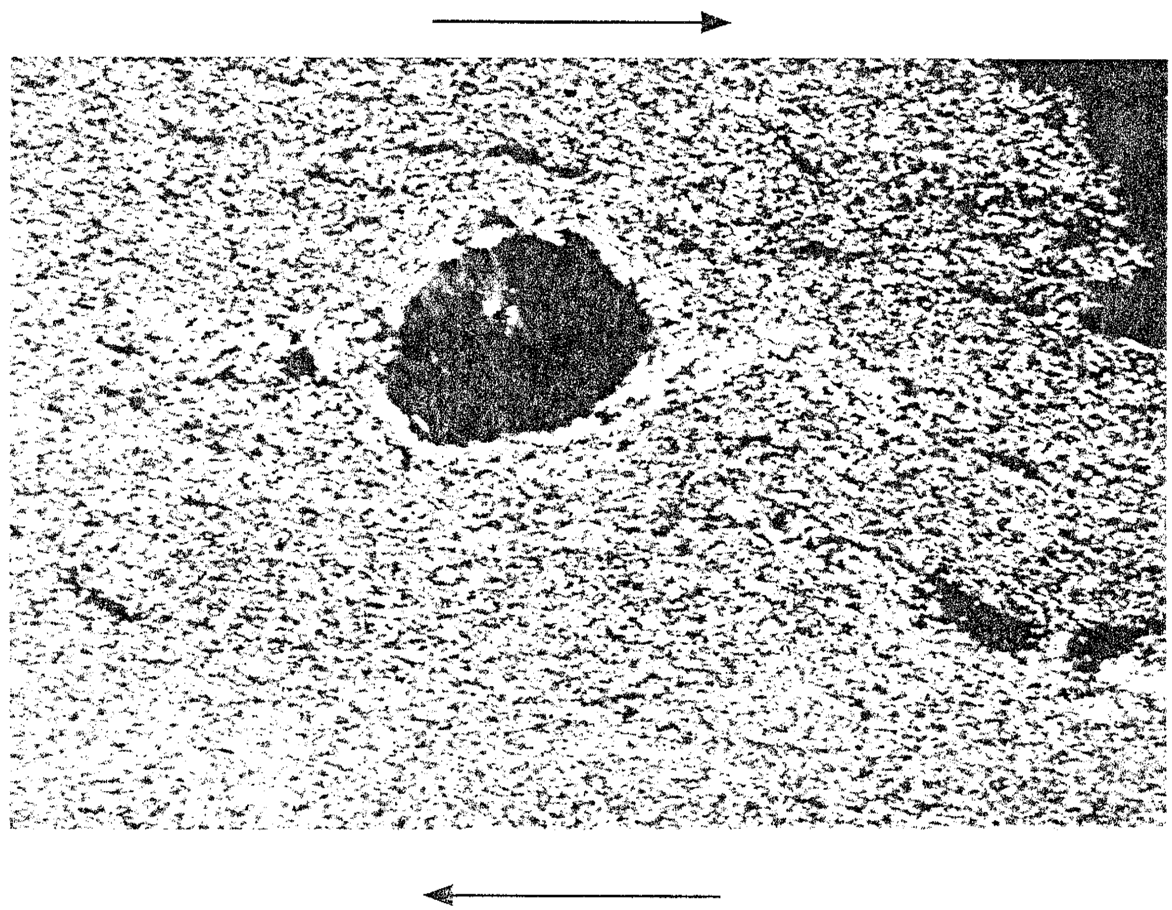

Figure 1-7. Photomicrograph from the Sevilleta Metarhyolite. Note the delta-type porphyroclasts asymmetry indicating an east-side-up sense of shear. Photomicrograph view is to the south, parallel to L_2. Long dimension of photo is approximately 6mm.

Figure 1-8. Photomicrograph from amphibolite layer showing two amphibole phases. Note the anhedral tan actinolite (A) has mineral inclusions nearly perpendicular to the main foliation defined by the green euhedral hornblendes (B). Long dimension of photo is approximately 6mm.

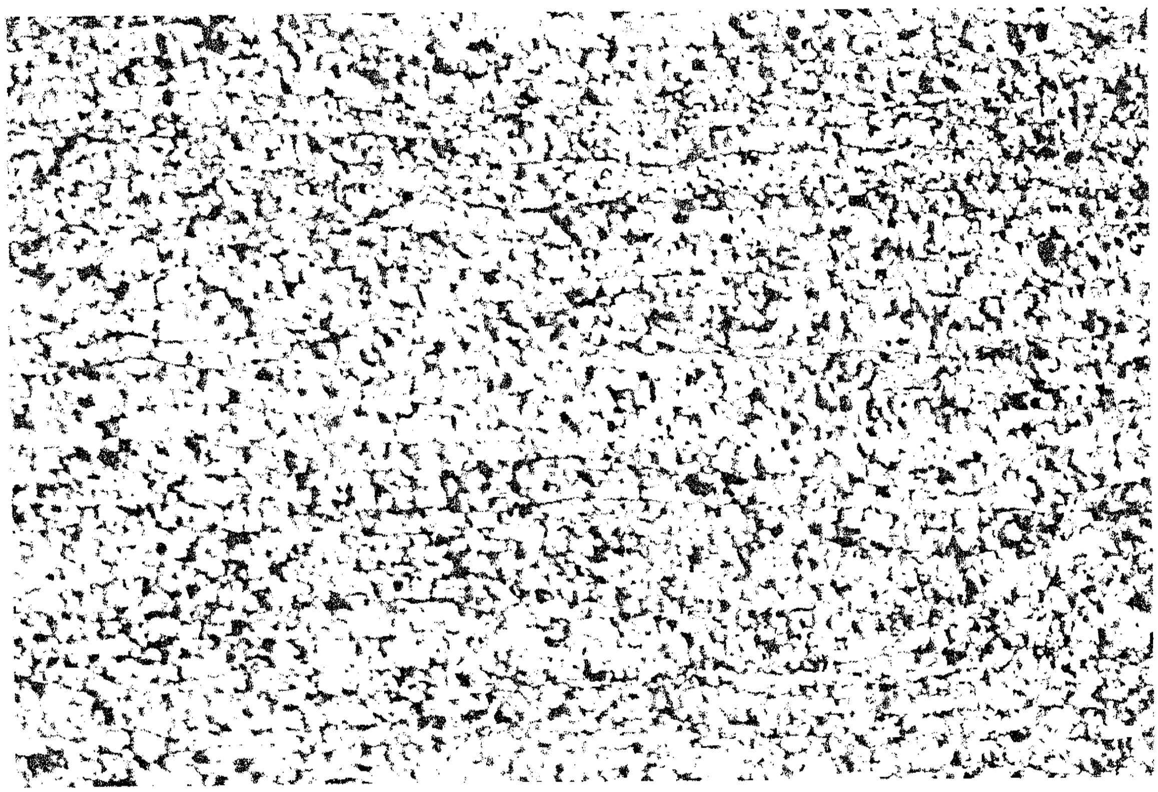

Figure 1-9. The first group of quartz microstructures is characterized by a fine-grained fabric with 0.1 to 0.25 mm equigranular quartz crystals. Note the foliation ~50° from S_2. View is perpendicular to S_2 and L_2. The long dimension of the photo is approximately 6mm.

and 60° from S_2. The second group of quartz mylonites (ML 7-1 and ML 7-3) are characterized by fine-grained 0.1 to 0.25 mm recrystallized quartz grains with relict monocrystalline quartz ribbons (Fig. 1-10). Relict ribbons are 1 to 3 mm long, with a 4:1 length to width ratio. The third group (ML 1-2, Ml 5-10) is characterized by 3 to 20+ mm long monocrystalline quartz ribbons (Fig. 1-11). Ribbons exhibit undulose extinction with minor subgrain formation and the rocks locally exhibit S-C fabrics. In all mylonite samples, micas are included within the recrystallized quartz grains as well as between grains indicating a high degree of grain boundary mobility; this suggests either deformation at high temperature or low strain rate (Lister and Dornseipen, 1982).

c-axis crystallographic preferred orientations

In combination with the quartz microstructures, c-axis crystallographic preferred orientations can be a helpful tool for determining both the sense of shear in the mylonite and the conditions of deformation (cf. Hobbs, 1972). As with microstructural studies, several factors need to be taken into account when interpreting the observed c-axis crystallographic preferred orientations.

Temperature, strain rate, trace impurity content, type of strain (coaxial or non-coaxial) and OH content are factors which determine how quartz deforms therefore influencing the development of the crystallographic preferred orientation (e.g. Lister and Dornsiepen, 1982; Schmid and Casey, 1986). Kronenberg (1981) has proposed

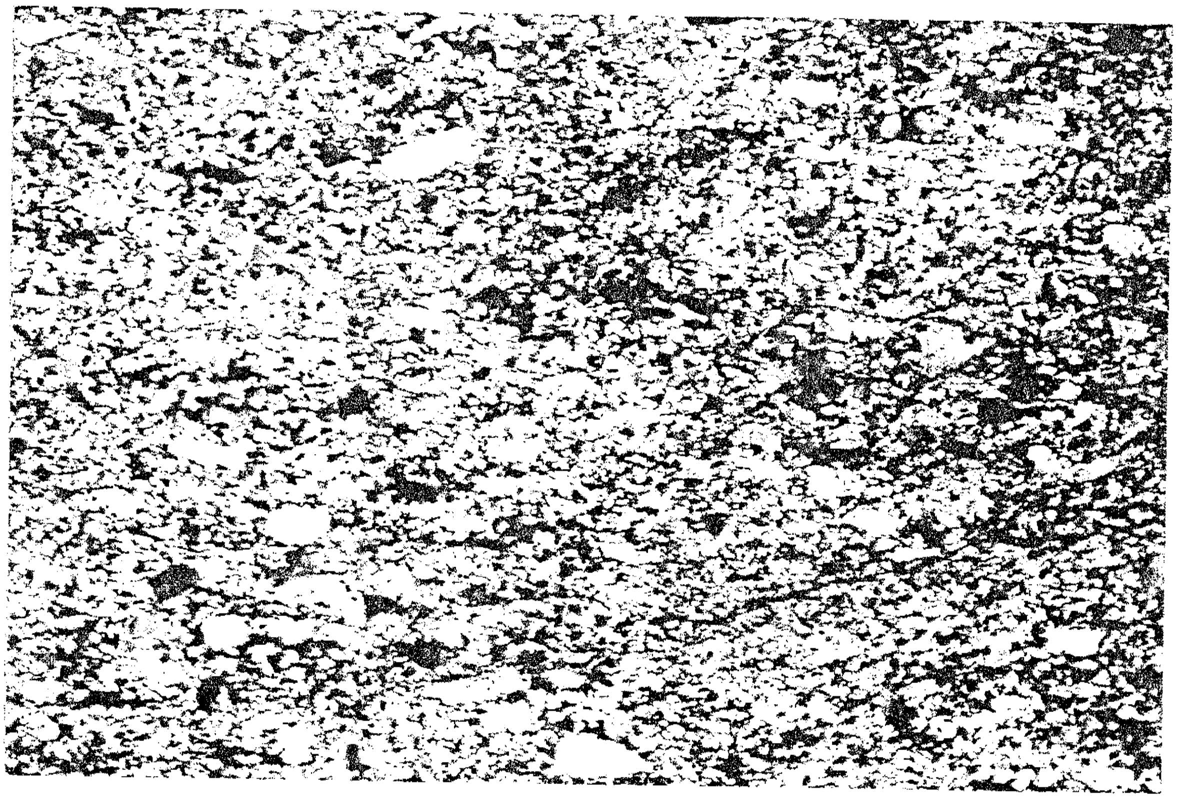

Figure 1-10. The second microstructural group is characterized by a bi-modal grain size distribution. The larger grains have sutured grain boundaries and are elongate parallel to the main foliation. The recrystallized grains are 0.1 to 0.25 mm in width. The fabric is relatively symmetric with respect to S_2 and L_2. View is perpendicular to S_2 and L_2. The long dimension of the photo is approximately 6mm.

Figure 1-11. The third microstructural group is characterized by 1-10 mm slightly undulose monocrystalline quartz ribbons and <5% white mica. Ribbon boundaries are sutured and exhibit significant subgrain formation. These fabrics are typically asymmetric and exhibit S-C relationships. View is perpendicular to S_2 and L_2. Long dimension of photo is approximately 6mm.

that the development of c-axis preferred orientation patterns in quartz is also strongly effected by the presence of phyllosilicates. In this situation slip may be preferentially accommodated by the phyllosilicates with optimal orientations. It has also been proposed by Lister et al. (1982) that increasing OH has the same effect on the fabric as does decreasing the temperature. It is very difficult to isolate the influence of each of the factors since all influence deformation (Schmid and Casey, 1986). However, the influence of temperature and strain rate on fabrics is better constrained. Experimental studies show that an increase in temperature or a decrease in strain rate corresponds to an increase in girdle angle (on the c-axis plot) and a difference in location of c-axis maxima (Tullis et al., 1973). The type of strain also has an effect on the fabric, for example small circle girdles are indicative of flattening, while cross girdles are often indicative of plane strain and similarly, single girdles indicate constrictional strain (Schmid and Casey, 1986). The above factors affecting c-axis patterns complicate identification of the active slip systems. This identification of active slip systems is necessary in order to interpret the deformation conditions. In general, TEM analysis of structures associated with slip is necessary to determine the active slip systems in naturally deformed rocks (e.g. Law, 1990; Ralser, 1990); however, similarities between experimentally and naturally deformed quartzites (Tullis et al., 1973) make it possible to use c-axis crystallographic preferred orientations to infer the relative activity of different slip systems. If the dominant slip systems can be identified, it may be possible to work backwards and estimate temperature or strain rate during deformation (Lister et al., 1978). From c-axis fabrics it has been shown (Lister and Hobbs, 1977) that an asymmetry of the c-axis pole figures with respect to the foliation and lineation reflects the sense of shear that the sample has experienced. This asymmetry also indicates non-coaxial deformation. Caution must be used when interpreting sense of shear from asymmetric c-axis patterns in multiply deformed terranes. In such a situation, it may be difficult to distinguish whether the asymmetry results from non-coaxial deformation or from a pre-existing asymmetry (Ralser, 1990).

Description of Crystallographic Preferred Orientations

Two hundred c-axis orientations from each of the representative quartz mylonite samples were measured from thin sections cut perpendicular to the lineation and foliation (Fig. 1-12). Data were then plotted on equal area, lower hemisphere projections and rotated so that the trace of the foliation is horizontal and the lineation is horizontal and plunging to the right.

Three different patterns are observed in the quartz mylonite samples. Incomplete small circle girdles about the pole normal to the foliation are developed in three samples (ML 11-3, ML 7-3 and ML 7-15; Fig. 1-12). In each girdle, two maxima are symmetrically distributed on either side of the pole to the foliation; however, the size of the maxima on either side of pole to the foliation vary.

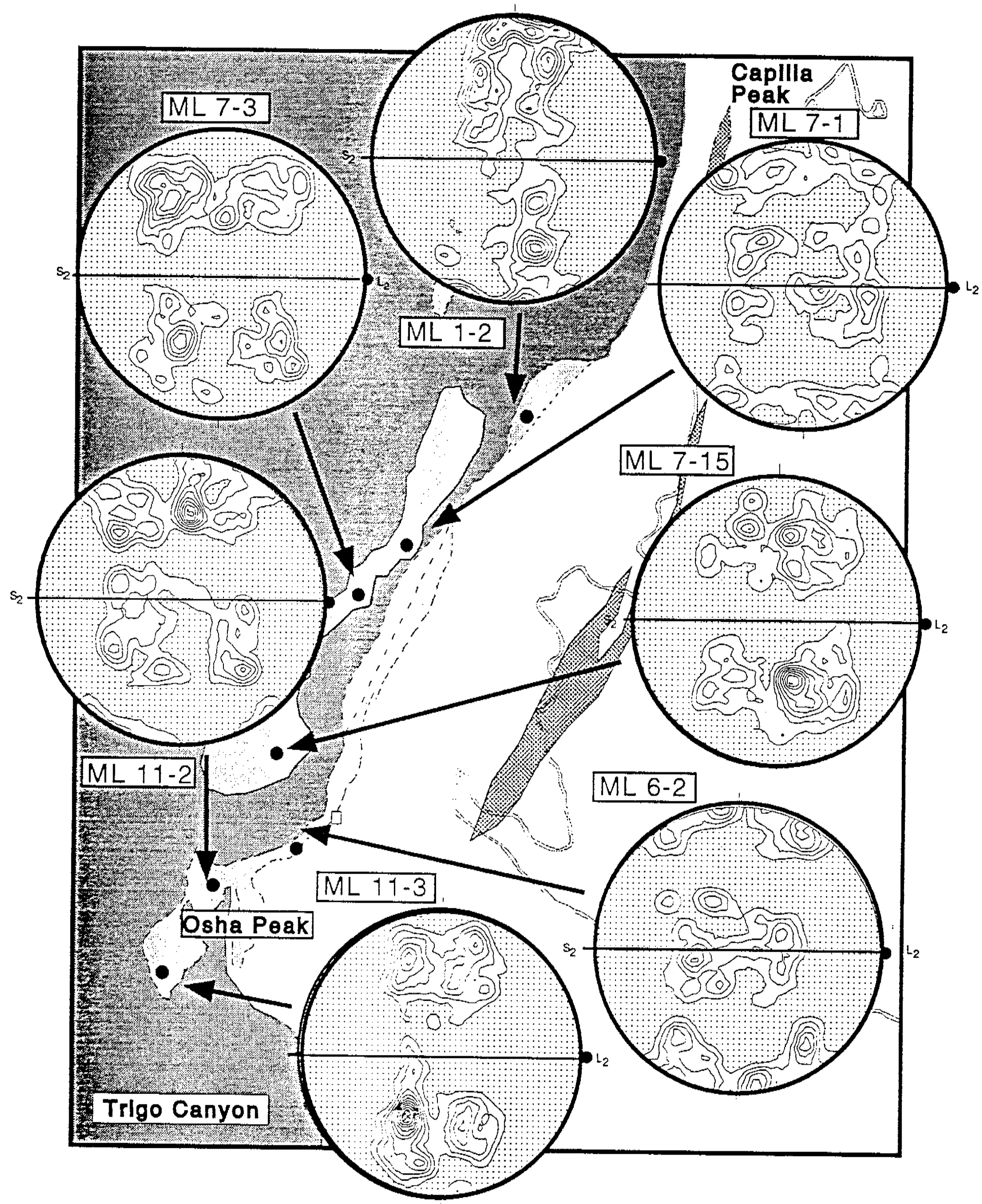

Figure 1-12. Geologic map of the study area showing the locations of quartz mylonite samples. Equal area, lower hemisphere plots of 200 quartz c- axes from each sample. Contours represent multiples of uniform distribution, from 1-10, area less than one multiple of uniform distribution is shaded (Starkey, 1977). S_2 is the trace of the main foliation and L_2 is the quartz mineral lineation on S_2. See figure 1-2 for map key.

C-axis patterns from samples ML 6-2, ML 7-1 and ML 11-2 (Fig 1-12) have a distribution of c-axis orientations that range from normal to the foliation to perpendicular to the lineation, within the foliation plane. The maxima in these three samples are relatively symmetric about the pole to the foliation, in both distribution and size. These plots are different from the first group of plots in that the maxima are located preferentially in the center and in the outer northern and southern portions of the plot.

Sample ML 1-2, (Fig. 1-12), has a different c-axis pattern than the other six samples. Maxima are located on both sides of the pole to the foliation as in the other samples, but they lie closer to the pole to the foliation and define a girdle approximately normal to the foliation.

DISCUSSION

The lithologic units in the study area each exhibit a different structural character on both the macroscopic and microscopic scales, as detailed in the previous sections. These differences in structural character are a result of different behavior during deformation. In a complexly deformed terrane with multiple lithologies, deformation will be accommodated in different ways. For example, a metarhyolite with a slightly higher percentage of phyllosilicates may appear to have accommodated more strain than a metarhyolite with fewer, even if the strain was the same. In the same scenario, a metarhyolite with a higher percentage of phyllosilicates may be easier to deform and hence accommodate more strain. With this in mind it is important to interpret the structural character in the context of the lithology and composition.

Microstructural studies are used to help interpret the deformational history by placing sense of shear, relative temperature and/or strain rate constraints on the main deformational event.

The quartz microstructures are relatively similar, even though they have been divided into three groups. These fabrics appear to be recording the transition from a coarser-grained microstructure characterized by monocrystalline quartz ribbons to a fine-grained roughly equigranular microstructure. Sample ML 11-2, for example, appears to have the entire range preserved within one thin section. Zones of monocrystalline quartz ribbons and zones with fine-grained equigranular microstructure co-exist (Fig. 1-13). This is interpreted to suggest that the polycrystalline quartz ribbon is a recrystallized monocrystalline quartz ribbon texture. The microstructures are consistent with those described by Hamner and Passchier (1991) and Simpson, (1985) as forming during upper greenschist to lower amphibolite facies conditions with slow strain rates. Assuming that the original grain-size and mineralogy of the quartz mylonite protolith was similar everywhere, and that temperatures were likely similar, the differences in microstructure observed are likely the result of either strain variations, strain rate variations, or variations in

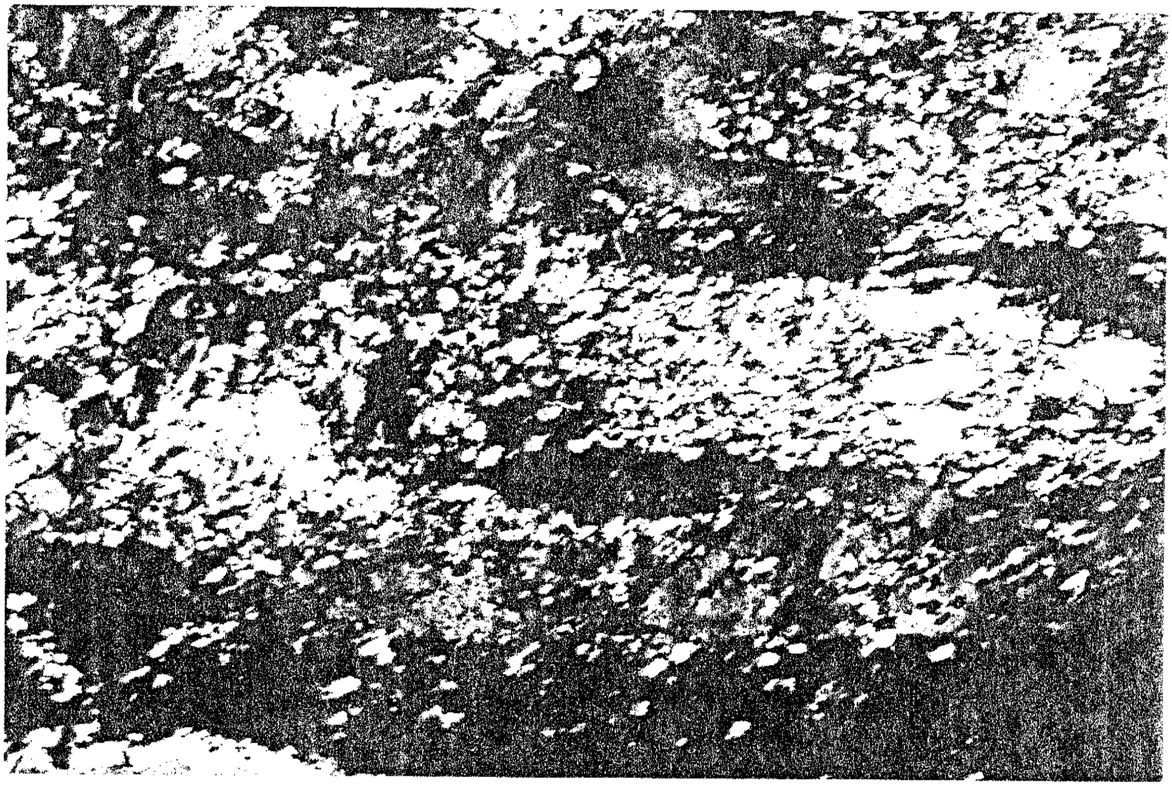

Figure 1-13. Photomicrograph of quartz mylonite sample ML 11-2, view is perpendicular to S_2 and L_2. Grain-shape preferred orientations ~45° from the C-surfaces (S_2) are consistent with an east-side-up sense of shear. The long dimension of the photo is approximately 6mm.

composition and/or water content (Kronenberg, 1981). Such local variations could also be controlled by deformation zone width, contrasting rheology with surrounding protolith or differences in the strain (cf. White et al., 1980).

The presence of predominantly delta-type porphyroclast systems within the metarhyolites, as opposed to sigma-type porphyroclast systems has been proposed to suggest that both, the strain (rotation) rate was high relative to the recrystallization rate and that there was a component of extensional shear (Hamner and Passchier, 1991). Based on the presence of asymmetric fabrics and porphyroclast systems and the nearly orthorhombic symmetry of most quartz mylonite fabrics and c-axis patterns, we interpret that the observed deformation formed during progressive general non-coaxial flow.

The majority of the kinematic indicators in the Capilla Peak area such as GSPO, shear bands and rare asymmetric porphyroclasts in the quartz mylonites and schists and asymmetric porphyroclast systems in the amphibolites and metarhyolites indicate an east-side-up sense of shear. A few (<5%) asymmetric porphyroclast systems indicate a west-side-up sense of shear; the geologic significance of this is unknown.

Interpretations from Crystallographic Preferred Orientations

The c-axis orientations of samples ML 11-3, ML 7-3 and ML 7-15 resemble small circle girdles about the pole normal to the foliation (Fig. 1-12). If these patterns are small circle girdles or possibly a transition to type 1 crossed girdles (Lister, 1977), then they suggest predominantly flattening strain (Law et al., 1984). In comparison with the c-axis distributions presented by Schmid and Casey (1986), the c-axis patterns from samples ML 7-3, ML 11-3 and ML 7-15 could suggest that slip occurred dominantly on the rhomb planes in the <a> direction. Quartz microstructures are consistent with formation during upper greenschist to lower amphibolite conditions. Amphibolite facies conditions are unambiguously indicated by the composition of syntectonic hornblende (Part 11). However at these conditions, slip should occur dominantly on the basal and prism systems (Fig. 1-14). As rhomb slip, in the absence of prism and basal slip, would only be expected under very specific conditions, such as properly oriented crystals, this scenario is probably unlikely (Fig. 1-14). An alternative and more plausible explanation would be that these patterns represent a combination of slip on the prism and basal planes. In such a situation where slip was accommodated by both the prism and basal systems, the c-axes may plot somewhere between the edge and the middle of the plot, giving the appearance of predominantly rhomb slip. An equal activation of both the prism and basal slip systems would place the samples in a temperature range consistent with that interpreted from the quartz mylonite microstructures.

It is not clear whether the CPO's from samples ML 6-2, ML 7-1 and ML 11-2 can be classified as either type 1 or type 2 fabrics of Lister (1977), however, they do not exhibit small circle girdles. c-axis maxima perpendicular

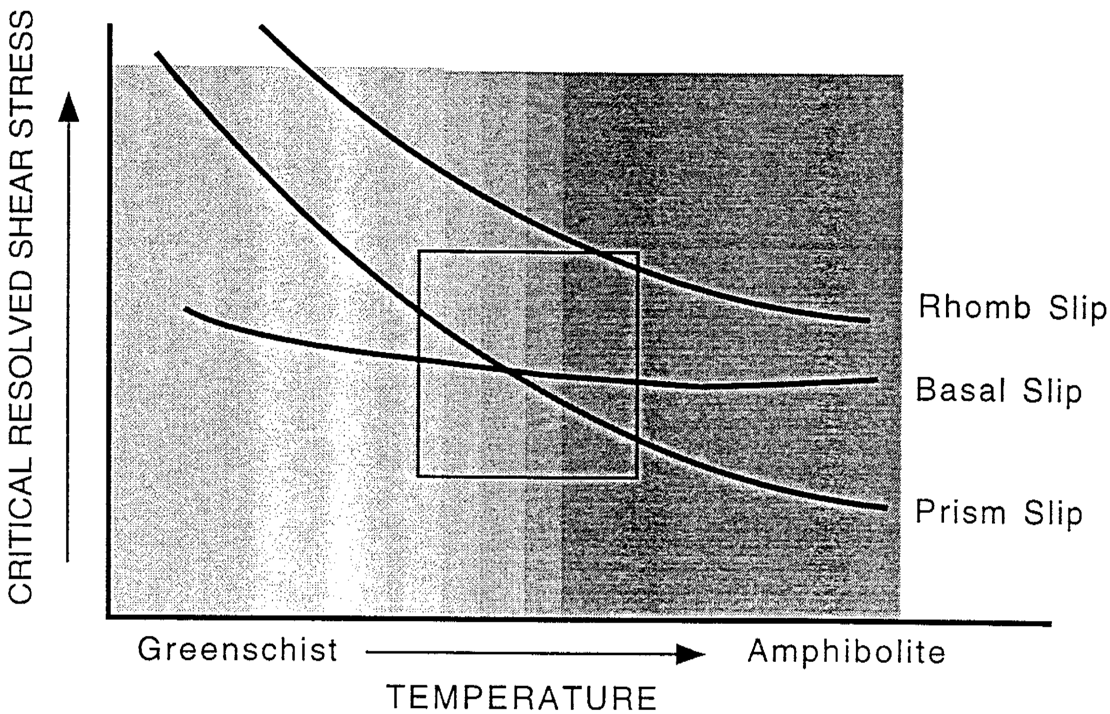

Figure 1-14. Plot of critical resolved shear stress against temperature for basal, prism and rhomb slip systems in quartz, modified from Hobbs (1985). Box represents proposed deformation conditions in the Capilla Peak area based on quartz mylonite c-axis patterns and other information (see text).

to the foliation plane in samples ML 6-2, ML 7-1 and ML 11-2, are consistent with basal slip; and c-axes sub-parallel to the foliation plane are consistent with prism slip (Schmid and Casey, 1986). These three plots lie somewhere between the flattening and plane strain field.

The crystallographic preferred orientations from the third group, sample ML 1-2, are different from those of the other groups. The c-axis distribution is relatively asymmetric with respect to S_2 and L_2 and is consistent with a larger component of non-coaxial flow than in the other samples (c.f. Schmid and Casey, 1986). This is consistent with the microstructure seen in thin section (Fig. 1-13) for example, Berthe et al. (1979) suggest that S-C fabrics are indicative of a large component of non-coaxial flow.

Slip dominantly on the basal systems is believed to be favored at low temperatures and is consistent with slip under greenschist facies conditions (Lister, 1978), while slip dominantly on the prism systems is proposed to occur at higher temperatures (Hobbs, 1972). Based on the c-axis preferred orientations, we interpret that slip occurred mainly along both the basal and prism planes compared to the other possible slip directions (Schmid and Casey, 1984). This is consistent with the inferred metamorphic grade of the deformation (c.f. Fig. 1-14).

A weak asymmetry in CPO's from ML 11-2, ML 1-2, ML 7-3, ML 7-15 and ML 6-2 is defined by the more populated NE-SW girdle suggesting a weak component of simple shear and an east-side-up sense of shear. In fabric ML

11-3, the NW-SE girdle has a higher population than the NE-SW girdle and is interpreted as west-side-up sense of shear.

CONCLUSIONS

The dominant NNE striking foliation (S_2) is observed in all lithologic units and overprints at least one older foliation. Deformation related to S_2 is preferentially preserved and partitioned into high and low strain zones. In low strain zones deformation is expressed as small scale folding and/or a poorly-defined crenulation cleavage. In high strain zones deformation is expressed as a strong planar foliation.

Microstructures such as grain-shape preferred orientations and S-C fabrics in the quartz mylonites and schists as well as asymmetric porphyroclast systems and hornblende growth in the metarhyolites and amphibolites record information about the character of deformation and metamorphism. From these microstructures the metamorphic grade, sense of shear and type of strain are inferred.

Constraints on metamorphic grade are based primarily on quartz mylonite microstructures and crystallographic fabrics and aligned mineral growth within the amphibolite layers (Part II). Quartz mylonite microstructures ranging from monocrystalline quartz ribbons to fine-grained equigranular foam textures are indicative of formation during an upper greenschist to lower amphibolite grade deformational event (c.f. Simpson, 1985). This interpretation is consistent with that inferred from the quartz c-axis fabrics. From the c-axis patterns it is inferred that strain was accommodated by a combination of basal and prism slip, again consistent with upper greenschist to lower amphibolite grade conditions. In the amphibolite layers, the foliation-forming euhedral hornblendes grew synchronous with S_2, the dominant NNE striking foliation observed in the Capilla Peak area, and are proposed in Part II to have grown at lower amphibolite grade conditions, probably around 500°C.

Microstructures within the Blue Springs Schist, quartz mylonites and Sevilleta Metarhyolite as well as outcrop scale structures in the amphibolite layers preserve evidence for sense of shear. In the schists, microscopic folds in the quartz layers and S-C surfaces preserve asymmetries consistent with east-side-up sense of shear. In the quartz mylonites, both east-side-up and west-side-up kinematic indicators such asymmetric porpyroclasts and asymmetric quartz crystallographic preferred orientations are present. However, five out of the seven quartz mylonite samples have microstructures and corresponding c-axis fabrics suggestive of an east-side-up sense of shear. In the amphibolite layers large sigmoidal shaped pods, and delta-type porphyroclast systems in the metarhyolites suggest east-side-up shear.

Delta-type porpyroclast sysems are dominant in the Sevilleta Metarhyolite and are interpreted to suggest that the strain rate is relatively high compared to the recystallization rate (c.f. bands Hammer and Passchier, 1991) and are interpreted to have formed during progressive general non-coaxial flow. General non-coaxial flow is probably more common than the dominantly simple shear deformation documented in many other studies (c.f. White et al., 1980).

It is proposed that the Proterozoic rocks currently exposed in the Manzano Mountains were all part of large ductile shear zone and that the Monte Largo Shear zone observed in Monte Largo Canyon is just one localized high strain zone within this larger deformation zone. This deformation occurred during lower amphibolite facies metamorphic conditions at ca. 1.4 Ga.

Part 2

STRUCTURAL AND $^{40}Ar/^{39}Ar$ CONSTRAINTS ON MIDDLE PROTEROZOIC DEFORMATION AND METAMORPHISM IN THE MANZANO MOUNTAINS, CENTRAL NEW MEXICO.

ABSTRACT

Rocks in the Capilla Peak area of the Manzano Mountains, New Mexico have been deformed at ca. 1660 Ma and again at 1440 Ma. $^{40}Ar/^{39}Ar$ geochronologic analyses on hornblende, actinolite, muscovite and biotite were conducted to constrain the timing of the observed deformational events. Actinolites are overgrown and crosscut by the well developed foliation-forming hornblendes. The hornblendes define the youngest tectonic fabric in the amphibolite. The actinolites yield complex $^{40}Ar/^{39}Ar$ age spectra characterized by age gradients increasing from ~200 Ma to 1600 Ma. These samples have total gas ages ranging from ~1110-1290 Ma. The hornblendes have less complex spectra and overall older ages. In particular, one sample yields a plateau age for 80% of the gas release of 1409 ± 10 Ma (2σ). Based on this result, it is proposed that temperatures at ca. 1400 Ma were sufficiently high to reset actinolite with respect to argon (at least 400°C), and that the amphibolites cooled through the hornblende closure temperature at ca. 1400 Ma.

Muscovite separates show variable age spectra with age gradients ranging from ~200 Ma to 1400 Ma. They record terminal ages ranging from ~1320 to 1400 Ma. The muscovite samples were collected over a vertical section of more than 1.5 km and show an age discordance with the highest being ~60 Ma older than the lowest sample. Assuming the samples within the traverse have similar argon T_C, the apparent ages have been interpreted to suggest a cooling rate of 0.3-1°C/Ma.

Biotites from similar structural levels yield plateau ages of 1276±6 Ma, 1379±4 and 1401±18 Ma respectively. This age discordance reflects a variation in biotite closure temperatures due to differences in grain-size coupled with apparent slow cooling.

Together, the geochronologic and structural data are interpreted to support a model of regional deformation, metamorphism and mineral growth at ca. 1400-1450 Ma. These data are interpreted to suggest that temperatures between 400 and 550°C existed ca. 1400 Ma and the rocks cooled to 200-300°C by at least ca. 1380 Ma, followed by a period of crustal stability and protracted cooling.

INTRODUCTION

Proterozoic rocks in the southwestern U.S. have experienced a complex deformational and thermal history related to cratonic assembly during the Yavapai and Mazatzal orogenies. Rocks in central New Mexico experienced only Mazatzal (1.65 Ga) and younger deformation. U-Pb dates on metamorphic zircons, crosscutting relationships between granitic plutons of known age and the regional foliations indicate that at least one deformational event occurred between 1.74 and 1.60 Ga (Bowring and Karlstrom, 1990; Karlstrom and Bowring, 1991; Bowring, 1991; Shastri and Bowring, 1992; Bauer and Williams, 1993). At that time, P-T conditions of 500-550°C and 3.5-4.5 kbar existed in structural levels currently exposed in northern New Mexico, with lower grade conditions in rocks exposed in central and southern New Mexico (Grambling, 1986; Bowring and Karlstrom, 1990). Abundant K-Ar, $^{40}Ar/^{39}Ar$ and Rb-Sr whole rock and mineral ages throughout the southwestern U.S. indicate that a period of metamorphism occurred ca. 1.4 Ga (Grambling, 1989; Bauer and Pollock, 1993). In the Manzano Mountains of New Mexico (Fig. 2-1), contact metamorphism and localized deformation were associated with emplacement of 1.4 Ga plutons (Thompson et al., 1996). The 1.4 Ga plutons were originally believed to be anorogenic since they were believed to be undeformed and additional evidence for orogenisis ca 1.4 Ga had not been documented.

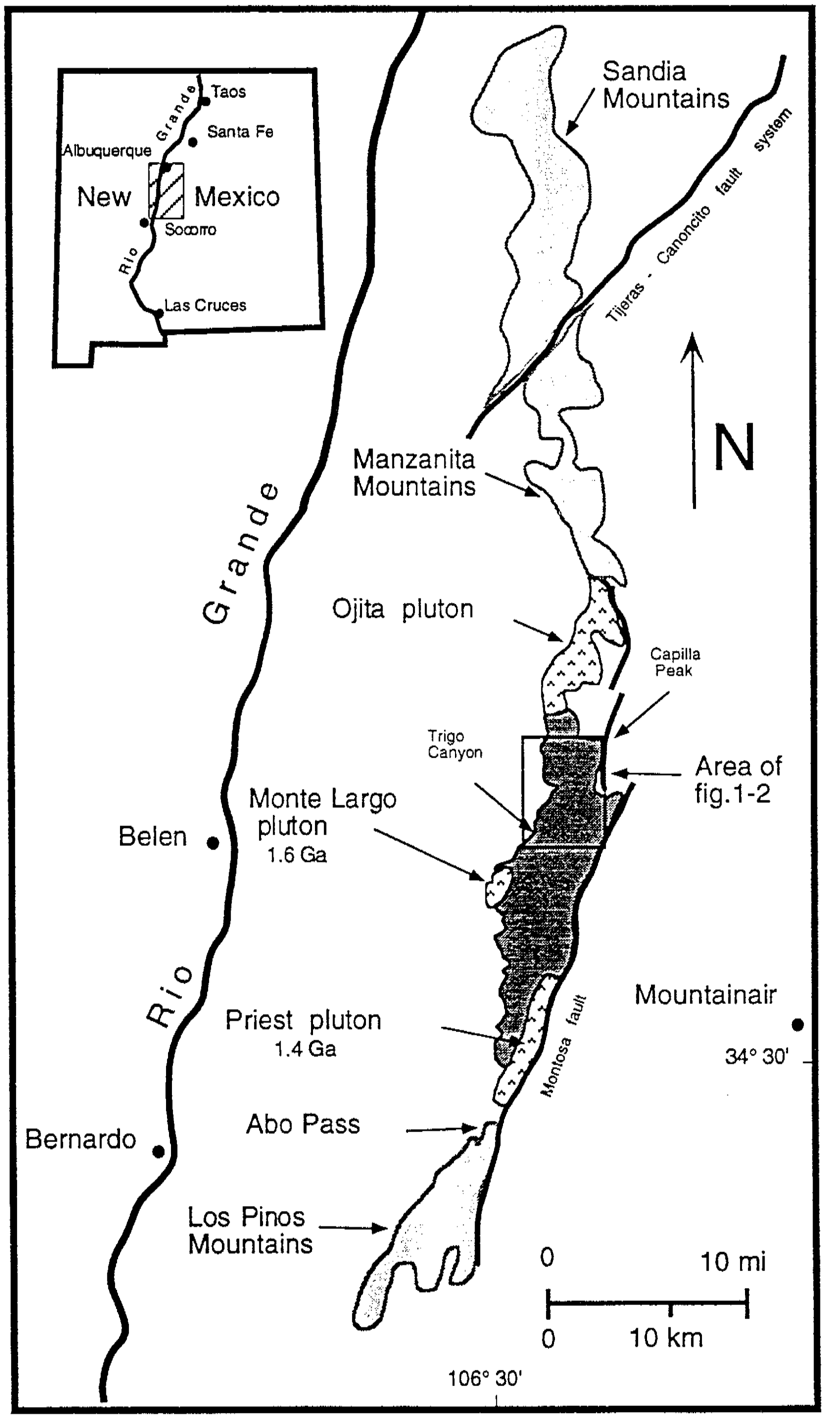

Figure 2-1. Geologic map of Proterozoic outcrops in central New Mexico showing the location of the study area and the plutonic rocks within the Manzano Mountains.

Two possible metamorphic and deformational models are proposed to explain the 1.4 Ga tectonism. The first model requires a metamorphic event at 1.4 Ga without regional deformation. This model was originally proposed to explain the absence of a pervasive tectonic foliation in 1.4 Ga plutons and the presence of 1.4 Ga mineral ages (Karlstrom and Bowring, 1993; Bauer and Williams, 1994; Karlstrom and Williams, 1995; Karlstrom et al. 1996 (in review)). The second model involves regional deformation and metamorphism at 1.4 Ga.

The purpose of this paper is to document a 1.4 Ga deformation event recorded by the Proterozoic rocks of the Manzano Mountains, and to further constrain the post-1.4 Ga thermal history of the area. We focus on petrography and chemistry of amphibolites and $^{40}Ar/^{39}Ar$ geochronology of amphiboles, biotites and muscovites located more than 10 km from the exposed margins of 1.4 Ga plutons (Fig. 2-1).

GEOLOGIC SETTING AND PREVIOUS WORK

The Manzano Mountains are an eastward tilted fault block of Proterozoic metasedimentary, metavolcanic, and plutonic rocks unconformably overlain by Paleozoic sedimentary rocks. The mountain range is approximately 60 km long and 15 km wide and defines the eastern margin of the Rio Grande rift between the Manzanita Mountains and Abo Pass (Fig. 2-1). The study area includes a steeply dipping structural sequence of muscovite schists, quartz mylonites, metarhyolites and amphibolite layers (Fig. 2-2).

Three phases of Proterozoic deformation have been recognized in the Manzano Mountains. Two phases of folding can be bracketed between 1.6 Ga and 1.4 Ga by crosscutting relationships with the 1656±10 Ma Monte Largo Pluton and the 1427±10 Ma Priest Pluton (Bauer et al., 1993) and evidence for one post-1.4 Ga phase of deformation can be found within the Priest Pluton (Heizler et al., 1996). Regional P-T conditions at ca. 1.4 Ga were estimated at 500-540°C and 4kb based on mineral assemblages, geothermometry and geobarometry (Grambling, 1989; Williams, 1990; Thompson et al., 1991).

Geochronologic data in the Manzano Mountains and the adjacent Los Pinos Mountains include: five U-Pb dates on zircons from metarhyolites in the Los Pinos Mountains and from the Priest and Monte Largo plutons (Shastri and Bowring, 1992; Shastri, 1993; Bauer et al., 1992; Bowring et al., 1983), three Rb-Sr dates from the Priest and Ojita plutons (Bolton, 1976; White, 1979; Brookins et al., 1980), and fourteen $^{40}Ar/^{39}Ar$ age spectra analyses of muscovite and biotite from in and around the Priest and Ojita plutons (Dallamyer et al., 1990; Thompson et al., 1991, 1996; Heizler et al., 1996). The U-Pb and Rb/Sr dates help constrain the ages of the plutons and the metarhyolite while the $^{40}Ar/^{39}Ar$ ages from in and around the plutons help constrain the timing of mineral growth associated with pluton emplacement. U-Pb zircon dates from the metarhyolites and Monte Largo Pluton range from 1656 to 1680 Ma while a U-Pb zircon from the Priest Pluton yields an age of 1427±10 Ma. Rb/Sr dates from

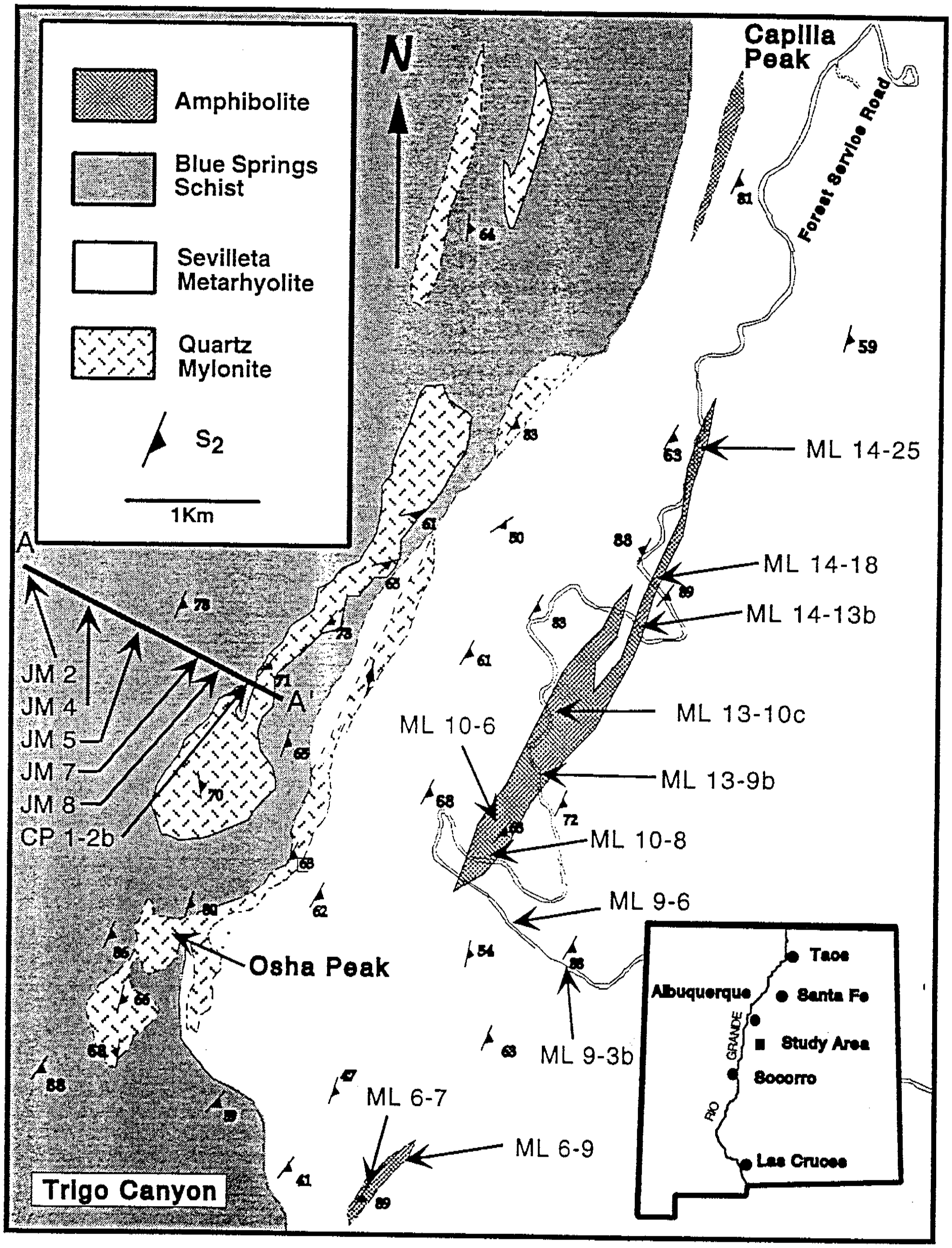

Figure 2-2. Generalized geologic map of the study area. Note the dominant NNE striking foliation and the various lithologies. A-A' marks the location of a sampling traverse across the Blue Springs schist. Amphibolite sample locations are noted.

the Manzano Mountains range from 1439 to 1569 Ma and all of the $^{40}Ar/^{39}Ar$ ages are between 1300 and 1450 Ma. The geochronologic data presented in this paper consist of $^{40}Ar/^{39}Ar$ data from the Capilla Peak area. The study area is more than 10 km from the plutonic rocks in the Manzano Mountains and ages will be used to help constrain the timing of deformation rather than pluton emplacement.

ANALYTICAL METHODS

Amphiboles and biotite from amphibolites within the Sevilleta Metarhyolite of Stark and Dapples (1946), and muscovite concentrates from the fine-grained Blue Springs Schist of Stark and Dapples (1946) were separated for $^{40}Ar/^{39}Ar$ age spectrum analysis (Fig. 2-2). All amphibolite samples contain both actinolite and a hornblende; these phases were separated from the 200-300 mesh size fraction along with a 60 mesh coarse amphibole (bulk amphibole) separate. Amphibole separates were purified using heavy liquids, the Franz magnetic separator and careful hand-picking based on color. All samples were ultrasonically cleaned for 5-10 minutes, rinsed in acetone, and dried at ~100°C. The mineral separates were packaged in Cu foil and placed in alternating positions around circular 6-hole irradiation trays with Fish Canyon Tuff sanidine [27.84 Ma] and Fe-mica biotite [307.3 Ma] flux monitors. Samples were irradiated in the L-67 position of the Ford reactor at the University of Michigan in three irradiations (NM-19, NM-29 and NM-42).

Analyses on all samples were performed at the New Mexico Geochronology Research Laboratory. The laboratory utilizes a MAP-215-50 mass spectrometer equipped with a Faraday and electron multiplier collector. The sensitivity is ~$3x10^{-17}$ mol/pA, and has a background at mass 36 of ~1×10^{-18} moles. The furnace blank is < 5×10^{-15} moles ^{40}Ar at temperatures below 1300°C. J-factors were determined by CO_2 laser total-fusion analysis of flux monitors to a precision of 0.25%. Unknown samples were incrementally heated, with seven minute heating steps, in a double vacuum Mo resistance furnace with an accuracy of 5-10°C, and a precision of ~±1C. The extracted gas was purified with SAES AP-10 and GP-50 getters for four minutes.

Due to the complexity of the age spectrum data, plateaus as defined by three or more contiguous steps, totaling more than 50% of the ^{39}Ar released that agree within analytical error at the 95% confidence level (Fleck et al., 1977), exist for only a few samples. Age determinations, when possible, are either integrated ages calculated for the relatively flat portion of the age spectra using ^{39}Ar as the weighting factor, or are the terminal ages defined by the high temperature steps of the age spectra.

All samples analyzed were examined petrographically. Back-scattered electron imaging, X-ray mapping and electron microprobe analyses of amphibolite samples ML 14-18 and ML 10-8 were performed on the University of New Mexico JEOL 733 electron microprobe and Arizona State University JEOL 8600 electron microprobe. Analyses were performed on doubly polished, carbon-coated thin-sections and standard ZAF calibration techniques were used. The amphiboles were analyzed for Na, Mg, Al, Si, Ca, Cl, K, Ti, Mn and Fe (Table 2-1). The locations of 35 spot chemical analyses were individually selected from the back-scattered electron images and obtained with a 10 μm beam. Numbers of ions are based on 23 oxygens and Fe is reported as Fe^{2+}.

Locations for microprobe spot analyses were carefully selected in order to avoid inclusions and intragranular impurities. Samples are probably not representative of the total actinolite and hornblende composition. In contrast, $^{40}Ar/^{39}Ar$ analyses were performed on multiple complete crystals, hence sampling the entire crystal. As a result, some variation in microprobe compositional data and the $^{40}Ar/^{39}Ar$ compositional data is expected.

SAMPLE DESCRIPTION

Amphibolites

Amphibolite samples were collected from a series of amphibolite layers believed to be early mafic dikes (Stark and Dapples, 1946) that cut the Sevilleta Metarhyolite. The amphibolite layers are 1-20 m in width, up to 400 m in length and are located more than 10 km from the Priest and Ojita plutons (Figs. 2-1 and 2-2). The amphibolite layers are highly foliated and aligned parallel to the regional foliation trend (Fig. 2-2).

	Hornblende	Actinolite
SiO_2	43.3 ±.13	53.0 ± 1.3
TiO_2	0.34 ±.05	0.07 ± .04
Al_2O_3	15.0 ± 1.5	3.8 ± 1.3
FeO	17.8 ±.68	3.8 ± 1.3
MnO	0.25 ±.05	0.23 ± .04
MgO	8.8 ± .90	15.5 ± .98
CaO	11.8 ±.16	12.2 ± .20
Na_2O	1.3 ± .11	0.39 ± .11
K_2O	0.4 ± .08	0.11± .06
Cl	0.01 ±.01	0.01 ± .01
Total	99.0	98.8

-numbers of ions based on 23 oxygens

- iron is reported as Fe^{2+}

Table 2-1. Average oxide weight percent derived from electron microprobe point analyses of amphibolites ML 14-18 and ML 10-8, showing two distinct amphibole phases. Hornblende data are averaged from 22 point analyses; actinolite data are from 13 point analyses.

The amphibolites are petrologically complex and contain two amphibole phases (Table 2-1), plagioclase, biotite, quartz, epidote, and minor amounts of magnetite and pyrite. Johnson (1986) reported that amphiboles from the Manzano Mountains were zoned, with blue-green hornblende cores surrounded by retrograde actinolite rims. This is contradicted by backscattered electron images, which show a sharp boundary between the amphibole phases, no compositional variation from rim to core, and distinct amphibole compositions. Actinolites occur as inclusion-rich 0.25-0.75 mm anhedral, equidimensional, cores overgrown by hornblende rims and crosscut by elongate hornblende crystals. Samples ML 10-8 and ML 14-18 have been characterized by transmitted light microscopy, electron mapping and electron microprobe analysis. Electron microprobe results from samples ML 10-8 and ML 14-18 are displayed in Table 2-1. Data from the two samples are not differentiated since compositions are identical within one standard deviation. The actinolite cores are typically relatively silica-rich and magnesium-rich with respect to the higher aluminum, lower iron ferro-tschermakitic hornblende rims (c.f. Yavuz, 1996) (Fig. 2-3, Table 2-1). Quartz inclusions and traces of cleavage planes within the actinolites are aligned nearly perpendicular to the dominant hornblende foliation. These inclusion trails are interpreted as recording an older, relict foliation.

Individual ferro-tschermakitic hornblende crystals are euhedral and bladed. These amphiboles define the well-developed foliation evident in the amphibolites (Fig. 2-4). The composition of the bladed hornblende is

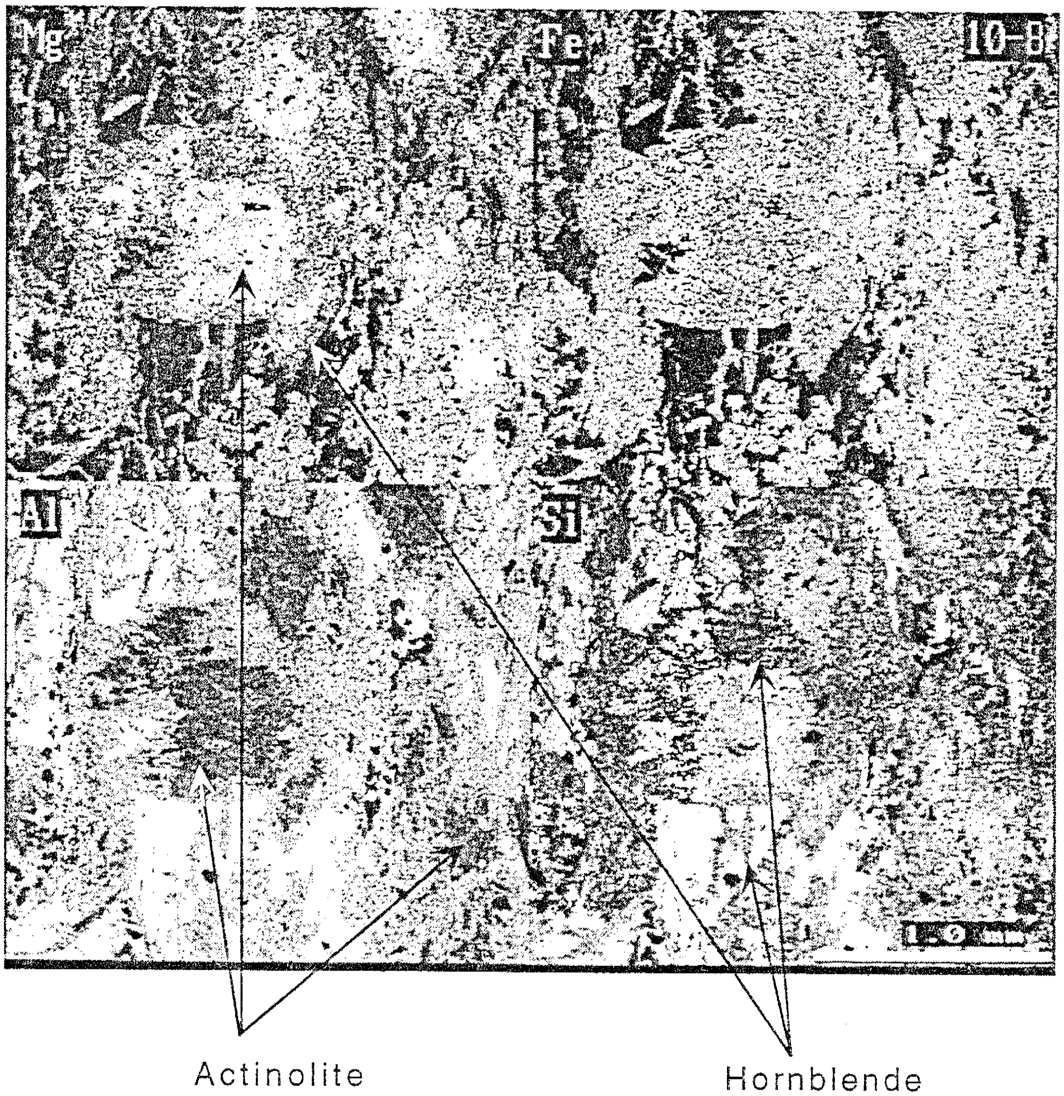

Figure 2-3. X-ray maps of ML 10-8 amphibolite showing distribution of Mg, Fe, Al, and Si. The brighter the area, the greater the amount of the labeled element. Note the high number of inclusions in the actinolite and the sharp boundary between the two distinct mineral phases.

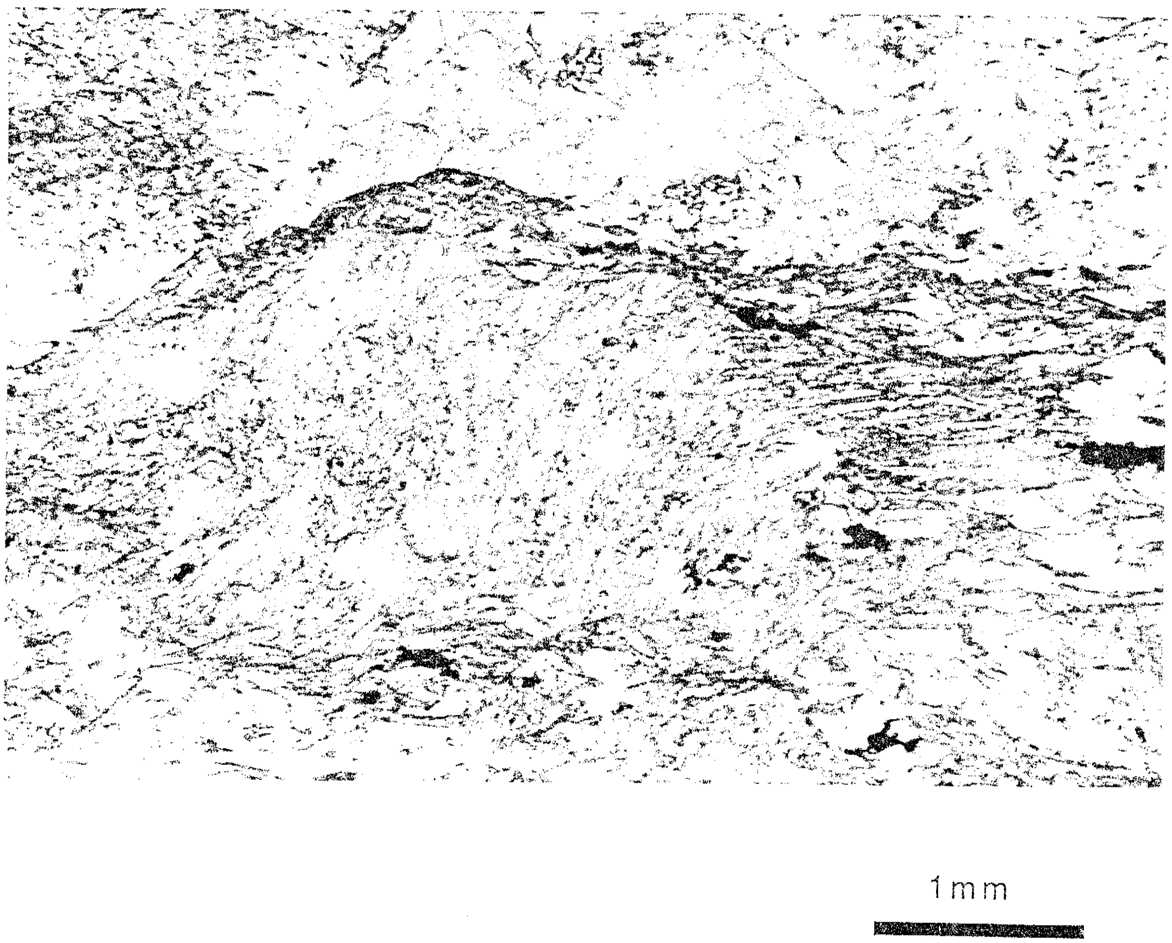

Figure 2-4. Photomicrograph of amphibolite sample ML 10-8. Long dimension of photo, ~6mm, is parallel to the dominant foliation. Note the abundant inclusion trails defining a relict foliation in the actinolite nearly perpendecular to the foliation-forming hornblende crystals.

indistinguishable from that of the hornblende rims around the actinolites (Table 2-1). Hornblende rims and individual euhedral hornblende crystals exhibit mutually cross-cutting relationships, indicating that they grew contemporaneously (Fig. 2-4).

Biotites occur locally within the amphibolite layers. The biotites are >0.25-0.75 mm in size and are aligned parallel to the dominant hornblende foliation.

Muscovite schists

The Blue Springs schist is intruded in the south by the Monte Largo pluton and trends NNE for approximately 17 km to where it is disconformably overlain by Pennsylvanian limestones in the north. The schist exposure is approximately 4 km wide, bounded on the west by overlying pediment gravels and on the east by the White Ridge quartzite (Fig. 2-2). Three dominant lithologies exist within the Blue Springs schist: metasiltstones, phyllites, and muscovite-chlorite schists (Stark 1956; Bauer 1982) (Fig. 2-2). The schist is highly foliated and crenulated and appears to be highly inhomogeneous with respect to composition and degree of deformation. Several generations of quartz veins are observed with varying thicknesses and frequency throughout the units. Also within the schist are 1-10 m-wide metasedimentary quartz mylonite layers (the "quartz reefs" of Stark and Dapples, 1946).

Six samples were collected along a traverse A-A' (Fig. 2-2) over a vertical section of greater than 1.5 km perpendicular to the regional NNE-striking foliation. The NNE-striking foliation is a crenulation cleavage in the schist (Fig. 2-5). It cuts an older foliation and becomes increasingly well developed with both increasing structural position in the traverse and increasing proximity to quartz-rich rocks. The spacing between cleavage planes decreases with increasing crenulation cleavage development. The schist contains abundant quartz and muscovite and minor amounts of biotite and chlorite. The muscovite grain size varies from 0.5 to 10 microns. The mean grain size decreases with increasing structural position and proximity to quartz-rich rocks, as the degree of crenulation cleavage development increases. The muscovites contain mineral inclusions and exhibit evidence of intra- and intergranular cataclasis (c.f. Goodwin and Wenk, 1990), particularly along crenulation cleavage planes (Fig. 2-5). In general there is a greater amount of intra- and intergranular cataclasis in the structurally higher samples than in the lower samples. In summary, the mechanisms by which the crenulation cleavage developed resulted in a decrease in muscovite grain size.

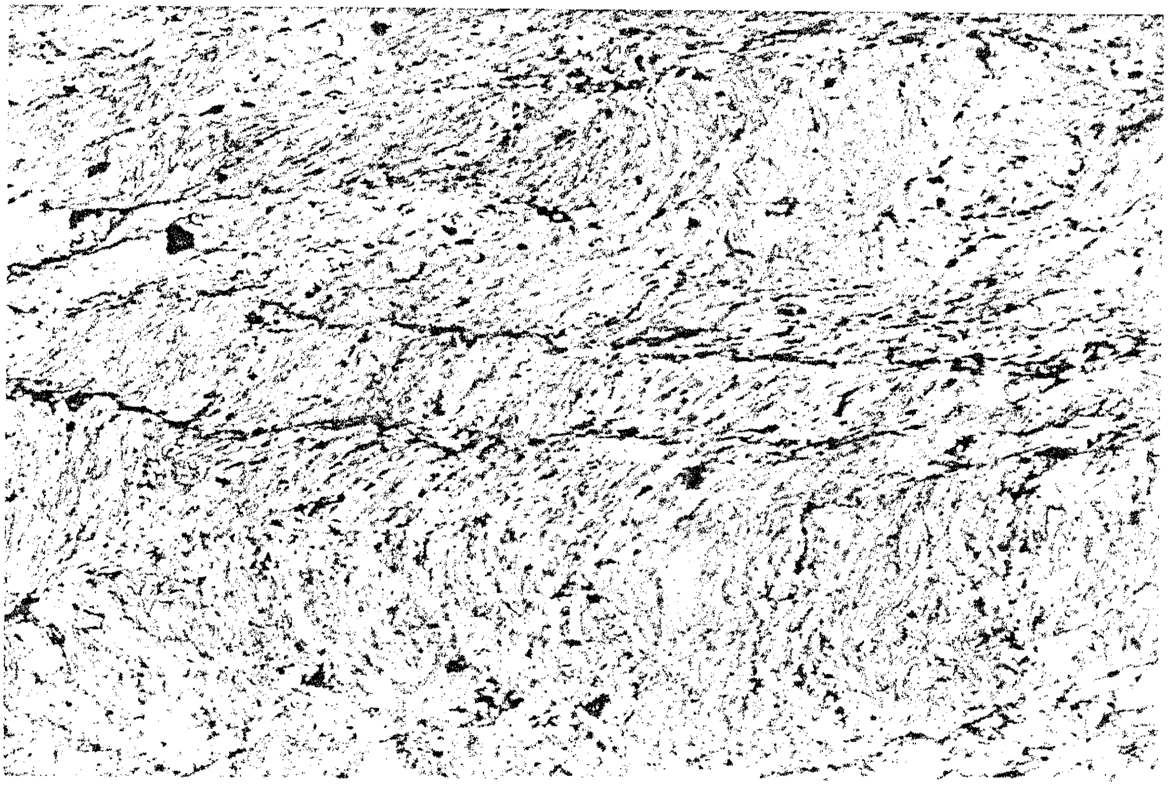

Figure 2-5. Photomicrograph of fine-grained muscovite schist from the Blue Springs schist. Long dimension of photo is 6mm. Note the older foliation is subparallel to the short dimension of the photo and is cut by a crenulation cleavage, parallel to the long dimension of the photo.

$^{40}Ar/^{39}Ar$ RESULTS

General Description

Eleven bulk amphibole separates from the amphibolite layers were step-heated and show complex age spectra. Eight finer grained actinolite and seven hornblende separates from the same hand samples were separated and heated from 500°C to 1700°C in 13 steps and have age spectra showing gradients from 200 Ma to 1500 Ma (Fig. 2-6). The hornblende age spectra tend to contain fewer low age steps than the more complex actinolite and the bulk amphibole age spectra. Age determinations, when possible, are either integrated ages calculated for the relatively flat portion of the age spectra weighting ^{39}Ar, or are the terminal ages defined by the high temperature steps of the age spectra. Interpretation of the $^{40}Ar/^{39}Ar$ age spectra are quite subjective and thus actual age assignment is also subjective. $^{40}Ar/^{39}Ar$ ages assigned in this paper reflect one possible interpretation of the data.

The K/Ca ratios are plotted above the corresponding age spectra (Figs. 2-6 - 2-12). Often the K/Ca plot is used to evaluate the age spectrum. In the hornblende and the actinolite samples a high K/Ca ratio is associated with the abundant young age steps in the early portions of the age spectra, and a relatively constant K/Ca ratio corresponds to the relatively flat portions of the age spectra. The K/Cl ratio is also plotted above the corresponding amphibole

Figure 2-6. $^{40}Ar/^{39}Ar$ spectra from bulk amphiboles (A, B), actinolites (C, D) and hornblendes (E, F) separated from samples ML 14-18. The actinolite age spectra are highly complex, showing age gradients and abundant young ages in the early portions of the spectra. The hornblende spectra are also complex; however, a significant portion of the age spectra yields an approximate age of 1400 Ma. Sample 14-18-1 (E) does not yield a true plateau age, but the flat portion of the age spectrum yields an integrated age of 1361 ± 8 Ma; while sample ML 14-18-2 (F) yields a true plateau age of 1409 ±10 Ma.

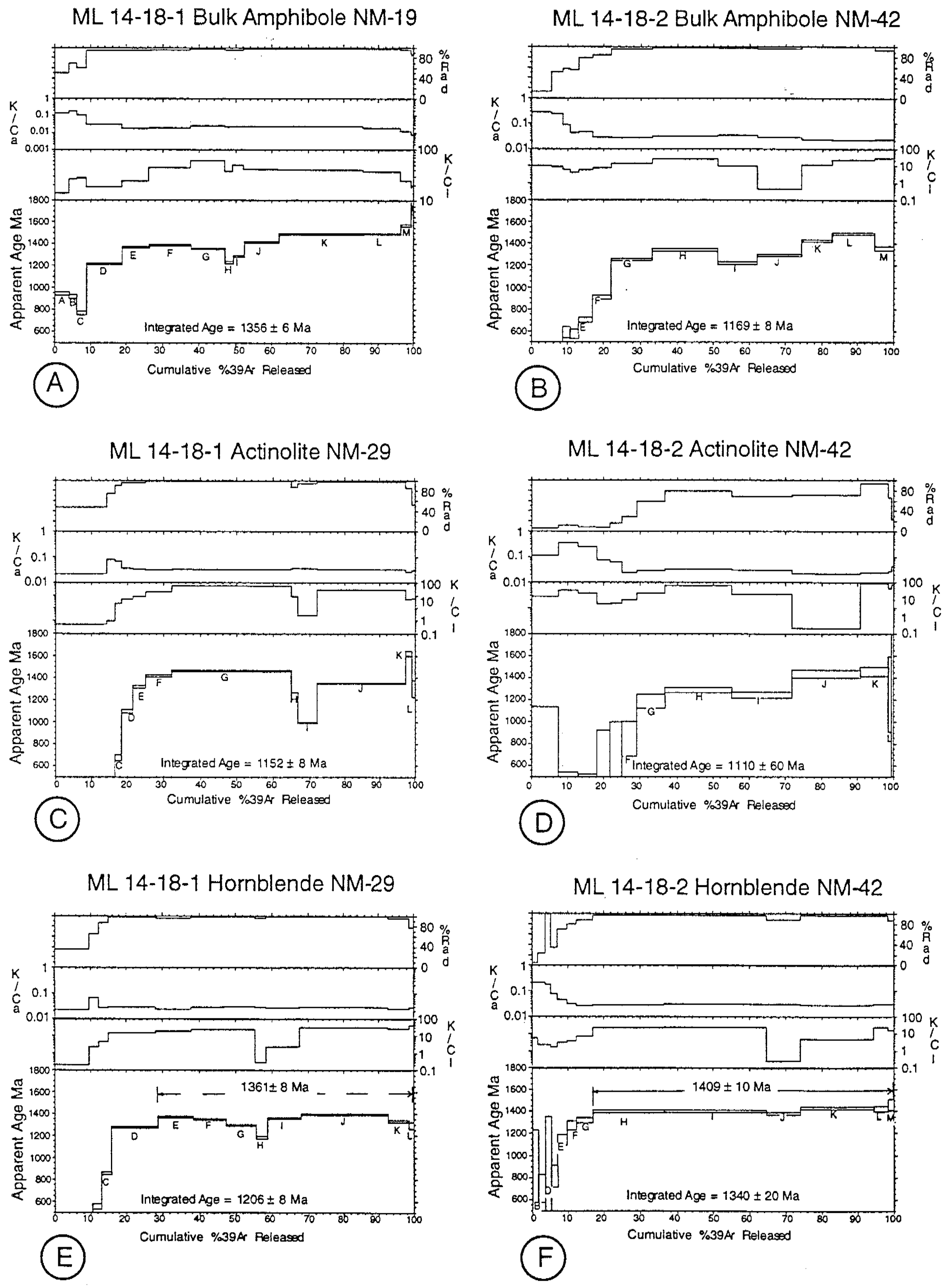
ML 14-18-1 Bulk Amphibole NM-19
Integrated Age = 1356 ± 6 Ma
Cumulative %39Ar Released
A
ML 14-18-2 Bulk Amphibole NM-42
Integrated Age = 1169 ± 8 Ma
Cumulative %39Ar Released
B
ML 14-18-1 Actinolite NM-29
Integrated Age = 1152 ± 8 Ma
Cumulative %39Ar Released
C
ML 14-18-2 Actinolite NM-42
Integrated Age = 1110 ± 60 Ma
Cumulative %39Ar Released
D
ML 14-18-1 Hornblende NM-29
1361± 8 Ma
Integrated Age = 1206 ± 8 Ma
Cumulative %39Ar Released
E
ML 14-18-2 Hornblende NM-42
1409 ± 10 Ma
Integrated Age = 1340 ± 20 Ma
Cumulative %39Ar Released
F
Apparent Age Ma
K/Ca
K/Cl
%Rad

Figure 2-6.

age spectra. In contrast to K/Ca, the forms of the K/Cl plot do not appear to be directly related to the age spectra. They are included as additional information.

Detailed description of age spectra

Samples presented in this paper have been irradiated in three separate irradiations (NM-19, NM-29 and NM-42) (Table 2-2). Irradiation NM-19 included eight bulk amphiboles, separated at a 60 mesh size fraction and two biotites. Irradiation NM-29 included two biotites, five hornblendes and six actinolites separated at a 200-300 mesh size fraction from the same sample as the bulk amphiboles from irradiation NM-19. The purpose for running NM-29 samples was to help understand the complex bulk amphibole spectrum observed from the NM-19 samples. Samples irradiated in NM-42 consisted of two bulk amphibole, two hornblende, two actinolite, one biotite and 10 muscovites. Detailed descriptions of amphibole age spectra are presented below.

Amphiboles

ML 14-18: Bulk amphibole, actinolite and hornblende were separated and analyzed from sample ML 14-18. Two sets of each were separated and irradiated in three different irradiations (NM-19, NM-29 and NM-42).

The general shape and values of the K/Ca and K/Cl relative to the age spectra for ML-14-18 bulk amphibole, actinolite and hornblende are similar for

Sample	Moles ^{39}Ar	Weight mg	J-factor	Moles $^{39}Ar/mg$	run
ML 9-3b Bulk	2.90E-15	2.6	0.01442337	7.73E-16	NM-19
ML 9-6 Bulk	3.40E-15	2.2	0.01445203	1.07E-15	NM-19
ML 13-9b Bulk	1.40E-14	2.9	0.01449799	3.33E-15	NM-19
ML 13-10c Bulk	1.80E-14	2.4	0.01450297	5.17E-15	NM-19
ML 14-18-1 Bulk	1.40E-14	3.4	0.01447063	2.85E-15	NM-19
ML 14-13b Bulk	4.00E-14	2.3	0.01444197	1.20E-14	NM-19
ML 6-7 Bulk	2.70E-14	2.8	0.01447585	6.66E-15	NM-19
ML 10-6 Bulk	2.80E-14	2.8	0.01451015	6.89E-15	NM-19
ML 10-8-1 Bulk	6.30E-14	3.8	0.01442939	1.15E-14	NM-19
ML 10-6 Act	4.10E-14	3.66	0.009526213	1.18E-14	NM-29
ML 13-9b Hbl	2.80E-14	2.08	0.009528751	1.41E-14	NM-29
ML 14-25 Act	1.60E-13	10.97	0.009518372	1.53E-14	NM-29
ML 9-3b Act	1.10E-14	1.58	0.009540874	7.30E-15	NM-29
ML 9-3b Hbl	1.00E-14	3.65	0.009543184	2.87E-15	NM-29
ML 9-6 Act	4.30E-15	1.89	0.009547693	2.38E-15	NM-29
ML 9-6 Hbl	1.00E-14	3.06	0.00954989	3.42E-15	NM-29
ML 6-7 Act	7.20E-15	1.11	0.009554171	6.79E-15	NM-29
ML 6-7 Hbl	1.50E-14	1.93	0.009556255	8.13E-15	NM-29
ML 14-18-1 Act	8.60E-15	1.99	0.009558301	4.52E-15	NM-29
ML 14-18-1 Hbl	8.80E-15	1.75	0.009560309	5.26E-15	NM-29
ML 14-18-2 Act	6.70E-16	0.51	0.01070469	1.23E-15	NM-42
ML 14-18-2 Hbl	2.10E-15	1.14	0.01073805	1.72E-15	NM-42
ML 14-18-2 Bulk	2.90E-15	1.04	0.01073225	2.60E-15	NM-42
ML 10-8-2 Act	7.80E-16	0.16	0.01071991	4.55E-15	NM-42
ML 10-8-2 Hbl	2.90E-15	0.6	0.01073843	4.50E-15	NM-42
ML 10-8-2 Bulk	1.40E-15	0.42	0.01077295	3.09E-15	NM-42

Table 2-2. Samples were irradiated in three separate irradiations (NM-19, NM-29 and NM-42). The moles $^{39}Ar/mg$ for each amphibole sample can be used to evaluate both the amount of gas derived from each sample, and the effectiveness of sample separation.

the majority of the bulk amphibole, actinolite and hornblende samples; exceptions will be noted. The K/Ca of the bulk amphiboles mirror the age spectra with high values corresponding to the low ages; the average K/Ca ratio around 0.02. Most resulting $^{40}Ar/^{39}Ar$ age spectra from the duplicate runs are somewhat reproducible especially for hornblende samples ML 14-18-1 and ML 14-18-2 (Fig. 2-6E,F).

The bulk amphibole age spectra are characterized by age gradients ranging from as low as 200 Ma in the first 25% of the ^{39}Ar released to 1300-1400 Ma for the intermediate temperature steps. The high temperature steps yield ages ranging from 1500-1600 Ma, with terminal ages as old as 1700 Ma (Figs. 2-6A, B). The K/Cl for actinolites and hornblendes ML 14-18-1 and ML 14-18-2 shows a direct correlation with the age spectra, including the distinctive dip in the age spectra around 1100°C, and steps H-I in ML 14-18-1 and I-J in ML 14-18-2 (Fig. 2-6); this is observed in nearly all amphibole samples analyzed.

The actinolite separates from ML 14-18 exhibit complex and non-reproducible age gradients (Fig. 2-6C, D). Terminal ages are between 1500 and 1600 Ma. The K/Ca ratios for the actinolites in ML 14-18-1 and 2 vary between 0.023 and 0.30, significantly higher than the 0.01 determined from electron microprobe analysis (Table 2-1).

The hornblende age spectra show age gradients similar to those observed for the bulk and actinolite samples for the first 20% of the ^{39}Ar release. The remainder of the hornblende age spectra are relatively flat and yield integrated ages calculated for the flat portions of the age spectra of 1361±8 and

1409±10 Ma respectively (Fig 2-6E, F). The average K/Ca for the hornblende samples is 0.04, similar to that determined from electron microprobe analyses.

ML 10-8: Two bulk amphibole splits, one actinolite and one hornblende were analyzed from this sample. $^{40}Ar/^{39}Ar$ age spectra from bulk amphiboles are reproducible in age and overall form (Fig. 2-7A, B). Bulk amphibole age spectra are characterized by age gradients from 800 to 1600 Ma; however, 50-70% of the cumulative ^{39}Ar released yields ages between 1300 and 1350 Ma. The actinolite age spectrum consists of an age gradient over 90% of the age spectrum with very old (>1800 Ma) initial and final steps (Fig. 2-7C). Steps H and I yield the oldest apparent ages of around 1240 Ma. The K/Ca ratios vary considerably for this sample and yield an undulatory pattern. The hornblende shows a complex age spectrum stepping from 300 Ma to 1340 Ma in the first 30% of the cumulative ^{39}Ar released. The final 60% of the age spectrum is relatively flat and yields an integrated age of 1329±10 Ma for steps G-K (Fig. 2-7D). Duplicate biotite analyses were also run from sample ML 10-8 biotite. The general shapes and ages of the flat portion of the two age spectra are similar. Biotite ML 10-8-1 has a large (~15% of the total gas) first step with an age of 220 Ma (Table 2-2). The sample yields an age gradient from 1100 to 1250 Ma (Fig. 2-7E). Biotite ML 10-8-2 has three young steps totaling less than 5% of the total ^{39}Ar released and a flat age spectrum from step E to K yielding an integrated age of 1276±6 Ma (Fig. 2-7 F). The forms of the two biotite age spectra are similar, but the total gas ages are very different.

Figure 2-7. $^{40}Ar/^{39}Ar$ spectra from bulk amphiboles (A, B), actinolites (C), hornblende (D) and biotites (E, F) separated from sample ML 10-8. The bulk amphiboles show age gradients from 800 to 1800 Ma. A significant portion of the age spectra from both ML 10-8-1 and ML 10-8-2 yield ages of 1.4 Ga. The actinolite age spectrum (C) is highly complex, showing an age gradient and a very old first step. The hornblende spectrum is also complex, however, a significant portion of the age spectra yields an approximate age of 1350 Ma. Biotite 10-8-1 (E) has a very large young (250 Ma) first step. Neither of the biotites yield plateau ages; however, biotite ML 10-8-2 (F) has fewer young ages and yields an integrated age from the flat portion of the age spectrum of 1276 ± 6 Ma; older than that from ML 10-8-1 biotite.

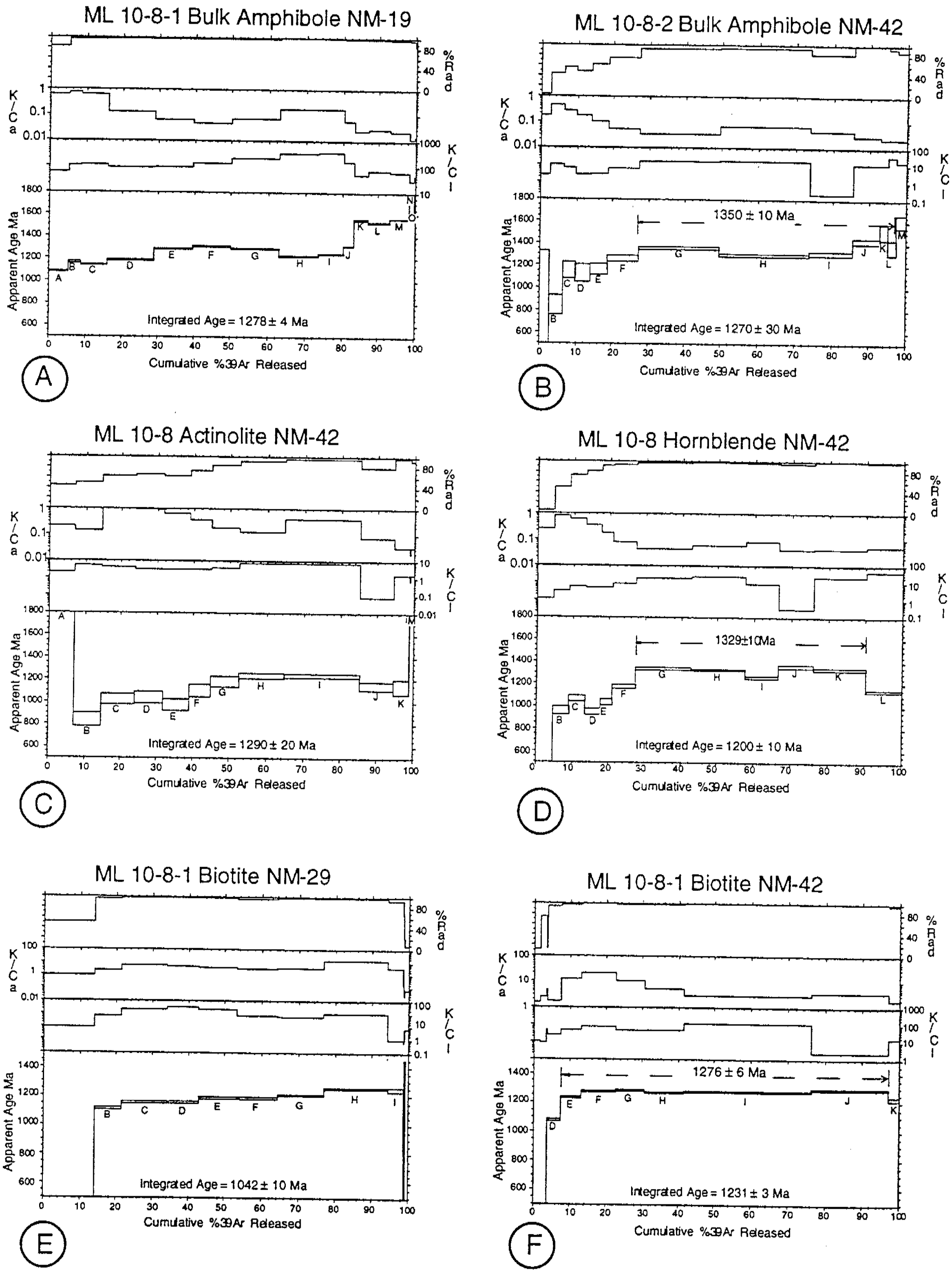
ML 10-8-1 Bulk Amphibole NM-19
% Rad
K/Ca
K/Cl
Apparent Age Ma
Integrated Age = 1278 ± 4 Ma
Cumulative %39Ar Released
A
ML 10-8-2 Bulk Amphibole NM-42
1350 ± 10 Ma
Integrated Age = 1270 ± 30 Ma
Cumulative %39Ar Released
B
ML 10-8 Actinolite NM-42
Integrated Age = 1290 ± 20 Ma
Cumulative %39Ar Released
C
ML 10-8 Hornblende NM-42
1329±10Ma
Integrated Age = 1200 ± 10 Ma
Cumulative %39Ar Released
D
ML 10-8-1 Biotite NM-29
Integrated Age = 1042 ± 10 Ma
Cumulative %39Ar Released
E
ML 10-8-1 Biotite NM-42
1276 ± 6 Ma
Integrated Age = 1231 ± 3 Ma
Cumulative %39Ar Released
F

Figure 2-7.

ML 6-7: A bulk amphibole, actinolite and hornblende were separated and analyzed from sample ML 6-7. $^{40}Ar/^{39}Ar$ age spectra from ML 6-7 bulk amphibole, actinolite and hornblende (Fig. 2-8A, C, E) show age gradients from 250 to 1400 Ma. The general shape of the three age spectra is the same with a large age gradient for the first 40% of the cumulative ^{39}Ar released and a relatively flat portion for the remainder of the spectra. The young ages in the early portions of the age spectra are associated with relatively high K/Ca. Integrated ages calculated over the flat portions of the bulk amphibole, actinolite and hornblende age spectra are 1411 ± 4, 1405 ± 6 and 1397 ± 6 respectively.

ML 9-6: A bulk amphibole, actinolite and hornblende were separated and analyzed from sample ML 9-6. The $^{40}Ar/^{39}Ar$ age spectrum from bulk amphibole (Fig. 2-8B) shows an age gradient from 600 to 1450 Ma. The actinolite has a complex age spectrum with 45% of the spectrum yielding an age of less than 500 Ma and a terminal age of 1450 Ma (Fig. 2-8). ML 9-6 hornblende also shows an age gradient but has a relatively flat portion between steps F and L, and an integrated age calculated from steps J and K of 1452±4 Ma (Fig. 2-8).

ML 9-3b: A bulk amphibole, actinolite and hornblende were separated and analyzed from sample ML 9-3b. In the case of sample bulk amphibole ML 9-3b, the K/Ca plot bears little resemblance to the age spectrum plot, and can not be used to explain the age variation. The bulk amphibole exhibits a highly complex age spectrum with the majority of steps having ages between 1250 and

Figure 2-8. $^{40}Ar/^{39}Ar$ spectra from ML 6-7 bulk amphiboles (A), actinolite (C) and hornblende (E). The bulk amphibole shows an age gradient from 700 to 1600 Ma. A significant portion of the age spectrum yields an age of 1.4 Ga. The actinolite age spectrum (C) and the hornblende spectrum (E) show more pronounced age gradients than the bulk amphibole. Samples ML 6-7 do not yield plateau ages; however, all three yield integrated ages, calculated from the flat portions of the age spectra, of 1.4 Ga. $^{40}Ar/^{39}Ar$ spectra from ML 9-6 bulk amphibole (B), actinolite (D) and hornblende (F) show highly complex age gradients. The hornblende yields a terminal age around 1450 Ma.

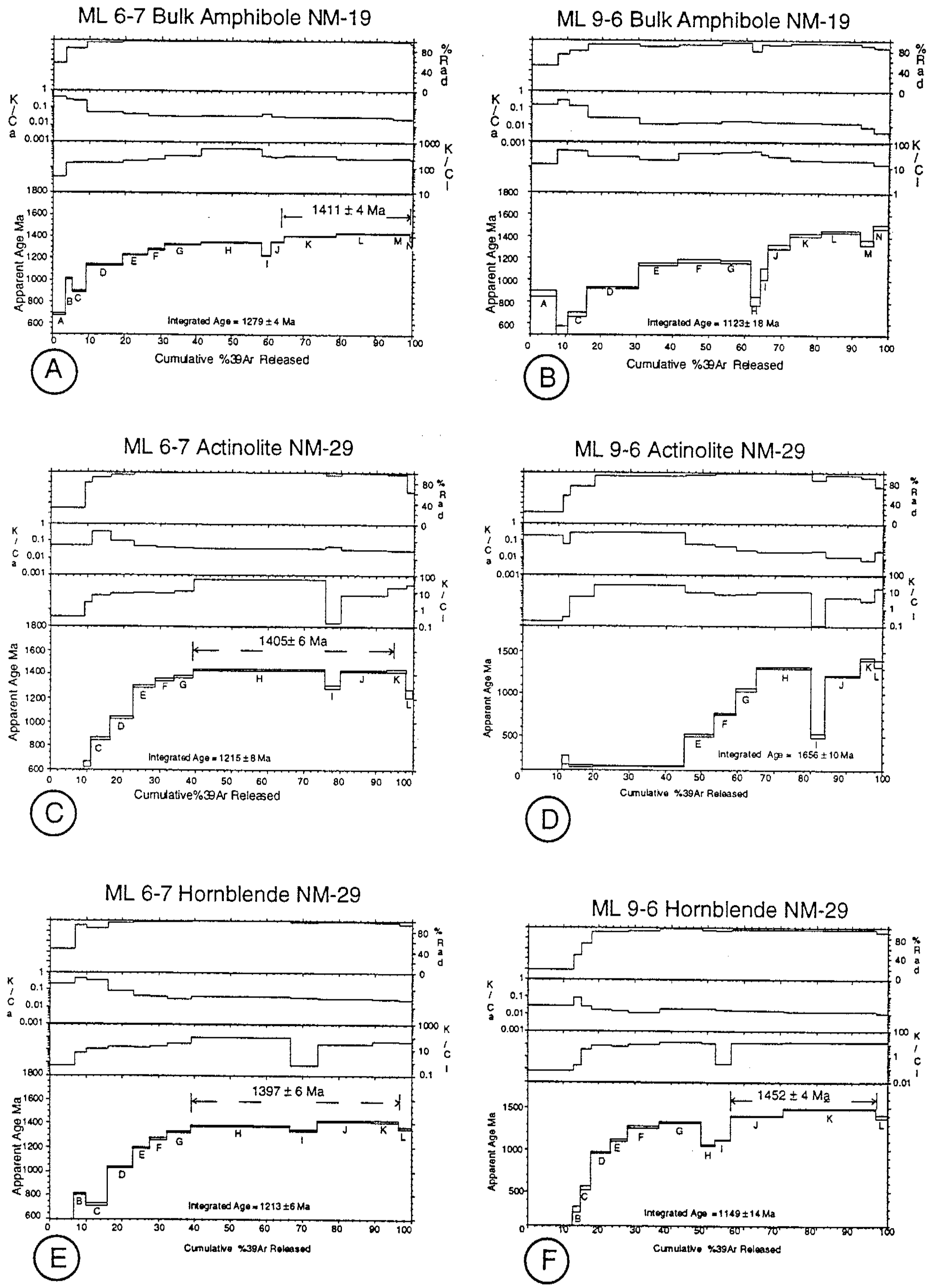
ML 6-7 Bulk Amphibole NM-19
1411 ± 4 Ma
Integrated Age = 1279 ± 4 Ma
Cumulative %39Ar Released
A
ML 9-6 Bulk Amphibole NM-19
Integrated Age = 1123± 18 Ma
Cumulative %39Ar Released
B
ML 6-7 Actinolite NM-29
1405± 6 Ma
Integrated Age = 1215 ± 8 Ma
Cumulative%39Ar Released
C
ML 9-6 Actinolite NM-29
Integrated Age = 1656 ± 10 Ma
Cumulative %39Ar Released
D
ML 6-7 Hornblende NM-29
1397 ± 6 Ma
Integrated Age = 1213 ±6 Ma
Cumulative %39Ar Released
E
ML 9-6 Hornblende NM-29
1452 ± 4 Ma
Integrated Age = 1149 ± 14 Ma
Cumulative %39Ar Released
F
Apparent Age Ma
K/Ca
K/Cl
% Rad

Figure 2-8.

1600 Ma (Fig. 2-9a). Both the K/Ca and K/Cl ratios are relatively flat for about 80% of the age spectrum and do not show the complexity of the age spectrum. ML 9-3b actinolite and hornblende age spectra are very different from the bulk amphibole. Both display an age gradient and maximum ages around 1400 Ma (Fig. 2-9C, E). Unlike the bulk amphibole, the shapes of the actinolite and hornblende age spectra appear to correspond to the shapes of the K/Ca and K/Cl plots.

ML 10-6: A bulk amphibole and actinolite were separated and analyzed from sample ML 10-6. $^{40}Ar/^{39}Ar$ age spectra from the bulk amphibole (Fig. 2-9b) show an age gradient from 1100 Ma to 1700 Ma. The actinolite separate yields a similar age spectrum form; however, the total gas ages differ by ~200 Ma, the terminal and initial ages are lower and the dip in the age spectrum at 1100°C is more pronounced(Fig. 2-9d).

ML 14-13b: A bulk amphibole was separated and analyzed from sample ML 14-13b. The $^{40}Ar/^{39}Ar$ age spectrum from the bulk amphibole (Fig. 2-9F) differs from the other bulk amphiboles in that 80% of the age spectrum is relatively flat at 1350 Ma.

ML 13-9b: A bulk amphibole and hornblende were separated and analyzed from sample ML 13-9b. $^{40}Ar/^{39}Ar$ age spectra from the bulk amphibole and hornblende have nearly identical age spectra and integrated ages (Fig. 2-10A, B). The age spectra are characterized by age gradients from 500-600 Ma to 1500 Ma.

Figure 2-9. $^{40}Ar/^{39}Ar$ spectra from ML 9-3b bulk amphibole (A), actinolite (C) and hornblende (E). The bulk amphibole shows a complex age spectrum with an old integrated age of 1.6 Ga, about 200 Ma older than the other amphibole integrated ages. The actinolite age spectrum (C) and the hornblende spectrum (E) are equally complex, and show more pronounced age gradients than the bulk amphibole. $^{40}Ar/^{39}Ar$ spectra from ML 10-6 bulk amphibole (B) and actinolite (D) show age gradients from 700 to 1600 Ma. $^{40}Ar/^{39}Ar$ spectra from ML 14-13b bulk amphibole (F) shows an age gradient from 1100 to 1700 Ma. The majority of the age spectrum yields an age of 1.35 Ga.

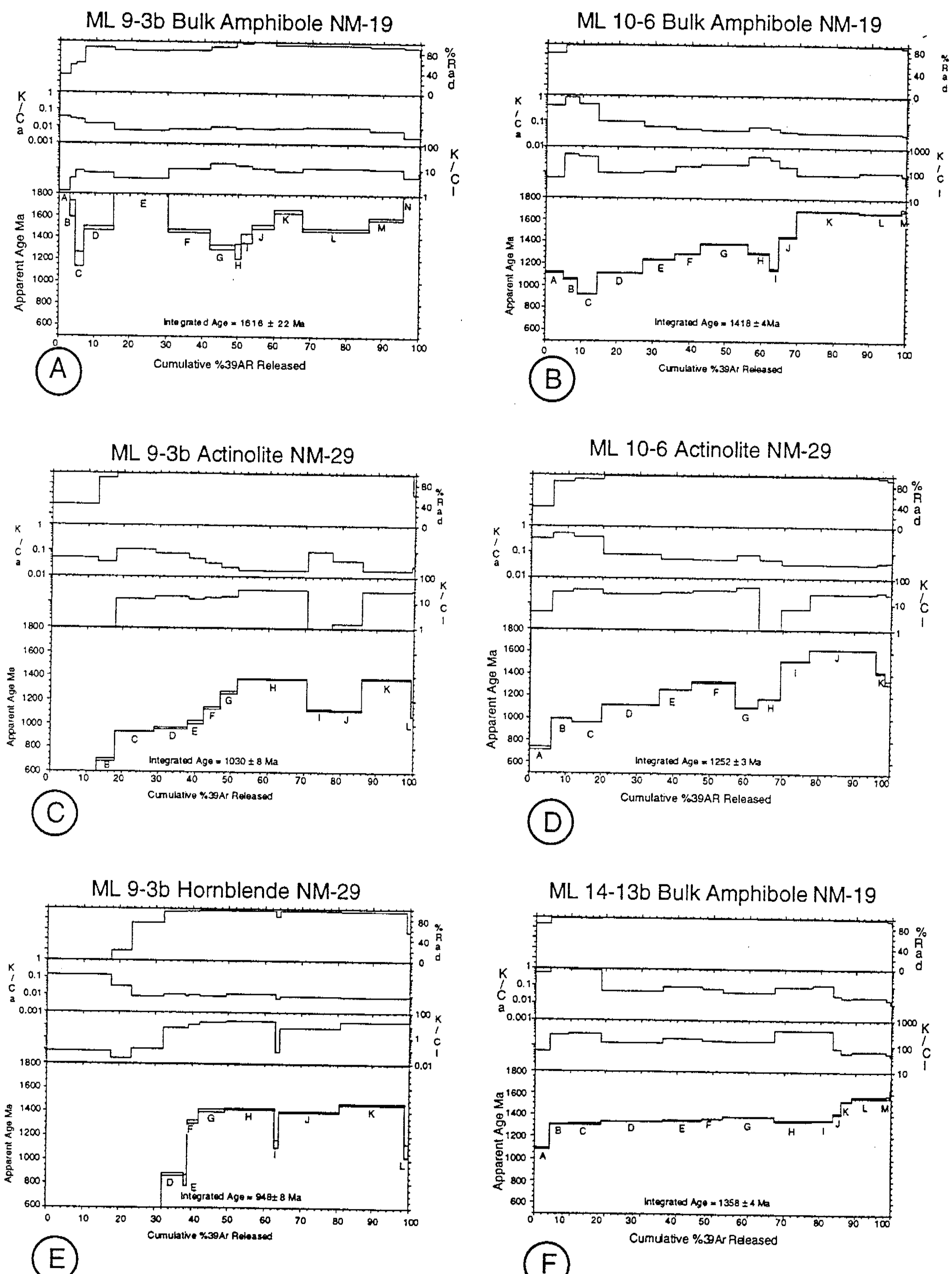
ML 9-3b Bulk Amphibole NM-19
Integrated Age = 1616 ± 22 Ma
Cumulative %39AR Released
A
ML 10-6 Bulk Amphibole NM-19
Integrated Age = 1418 ± 4Ma
Cumulative %39Ar Released
B
ML 9-3b Actinolite NM-29
Integrated Age = 1030 ± 8 Ma
Cumulative %39Ar Released
C
ML 10-6 Actinolite NM-29
Integrated Age = 1252 ± 3 Ma
Cumulative %39AR Released
D
ML 9-3b Hornblende NM-29
Integrated Age = 948± 8 Ma
Cumulative %39Ar Released
E
ML 14-13b Bulk Amphibole NM-19
Integrated Age = 1358 ± 4 Ma
Cumulative %39Ar Released
F
Apparent Age Ma
% Rad
K/Ca
K/Cl

Figure 2-9.

Figure 2-10. $^{40}Ar/^{39}Ar$ spectra from ML 13-9b bulk amphibole (A) and hornblende (B). The bulk amphibole and the hornblende age spectra show age gradients from 500 to 1500 Ma, and an integrated age of 1.0 Ga. The $^{40}Ar/^{39}Ar$ spectra from ML 14-25 actinolite (C) shows an age gradient from 1100 to 1400 Ma, with the majority of the spectrum yielding an integrated age of 1350 Ma. ML 13-10c bulk amphibole (D) shows a gentle age gradient with the majority of the age spectrum yielding an integrated age of 1350 Ma, and a terminal age of 1500 Ma. ML 6-10 biotite (E) and ML 10-2 biotite (F) show relatively flat age spectra, and yield ages of 1.4 Ga.

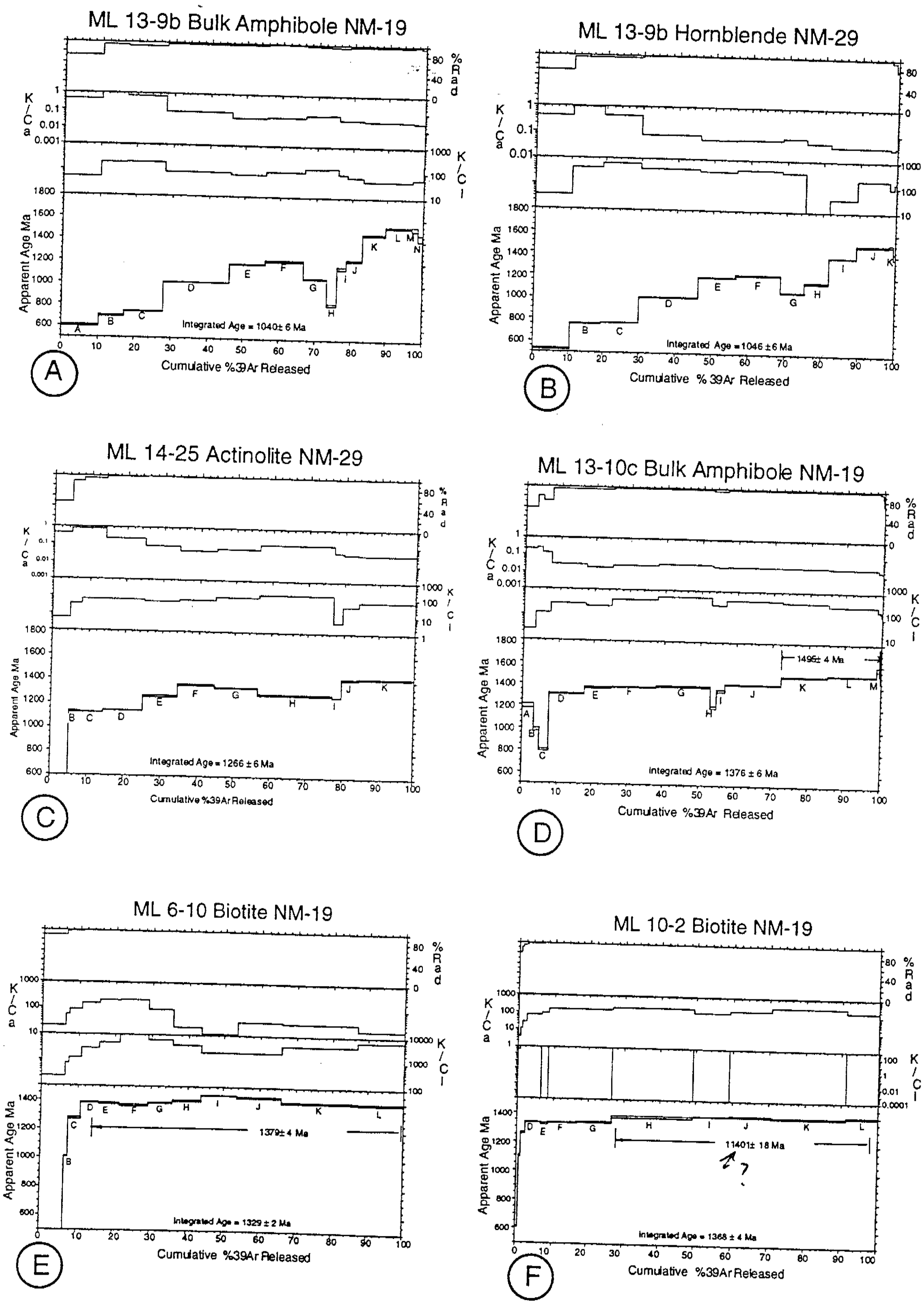
ML 13-9b Bulk Amphibole NM-19
Integrated Age = 1040± 6 Ma
Cumulative %39Ar Released
Apparent Age Ma
K/Ca
K/Cl
%Rad
A
ML 13-9b Hornblende NM-29
Integrated Age = 1046 ±6 Ma
Cumulative % 39Ar Released
B
ML 14-25 Actinolite NM-29
Integrated Age = 1266 ± 6 Ma
Cumulative %39Ar Released
C
ML 13-10c Bulk Amphibole NM-19
1495± 4 Ma
Integrated Age = 1376 ± 6 Ma
Cumulative %39Ar Released
D
ML 6-10 Biotite NM-19
1379± 4 Ma
Integrated Age = 1329 ± 2 Ma
Cumulative %39Ar Released
E
ML 10-2 Biotite NM-19
1140± 18 Ma
Integrated Age = 1368 ± 4 Ma
Cumulative %39Ar Released
F

Figure 2-10.

ML 14-25: An actinolite was separated and analyzed from sample 14-25. The $^{40}Ar/^{39}Ar$ age spectrum from the actinolite yields an age gradient from 1100 to 1400 Ma (Fig. 2-10C). About 60% of the age spectrum yields ages between 1350 and 1400 Ma with relatively flat corresponding K/Ca ratios. The sample yields a total gas age of 1266±6 Ma.

ML 13-10c: A bulk amphibole was separated and analyzed from sample 13-10c. The $^{40}Ar/^{39}Ar$ age spectrum from the bulk amphibole shows a gradual age gradient over 90% of the age spectrum from 1306 to 1568 Ma with a relatively flat corresponding K/Ca plot (Fig. 2-10D). An integrated age of 1495 Ma is observed for steps K-M (Fig. 2-10D).

ML 6-10 and ML 10-2 Biotite: A biotite was separated and analyzed from both samples ML 6-10 and ML 10-2. $^{40}Ar/^{39}Ar$ age spectra from the biotites yield relatively flat spectra for at least 90% of the ^{39}Ar released and total integrated ages of 1329±4 and 1368±2 Ma respectively (Fig. 2-10E). The K/Ca for ML 10-2 is nearly an order of magnitude larger and the K/Cl is much lower than that of ML 6-10 (Fig. 2-10E, F, Appendix A).

Muscovites

The muscovite separates collected from within the Blue Springs schist show variable age spectra with age gradients ranging from ~200 Ma to 1400 Ma. The total gas ages from the six samples are all different; however, ages derived from the portion of the age spectra between 20 and 90% of the argon released, yield similar ages. These micas record terminal ages ranging from

~1320 to 1400 Ma (Fig. 2-11, 2-12). Muscovite samples from the structurally highest samples generally yield an older age than the structurally lowest samples. The total age discordance between the lowest and highest sample is approximately 60 Ma (Fig. 2-12D).

JM 2, JM 4:a, JM 5, JM 7:a, JM 8:a and CP 1-2b:a: Six muscovites and duplicate splits JM 4:b, JM 7:b, JM 8:b and CP 1-2b:b yield relatively similar $^{40}Ar/^{39}Ar$ age spectra and K/Ca ratios. All muscovite samples exhibit age gradients and have been plotted relative to JM 2 muscovite (Figs. 2-11, 2-12). JM 2 is the structurally lowest sample and CP 1-2b is the structurally highest. It is difficult to assign an individual age to the muscovite samples since there are no plateaus and since the terminal ages are not always the oldest age on the age spectra. However, a general increase in age is observed from the lowest to the highest sample. Sample JM 2 and the adjacent JM 4 samples yield essentially identical age spectra (Fig. 2-11C, D). JM 2 plots increasingly further below JM 2 in each of the samples along the traverse from the structurally lowest to structurally highest position.

DISCUSSION

As discussed earlier, amphibolites exhibit complex microstructures (Fig. 2-13). Older anhedral actinolite grains display inclusion trails at a high angle to the main foliation. The main folaition is defined by euhedral hornblende

Figure 2-11. $^{40}Ar/^{39}Ar$ age spectra from muscovites JM 2 (A), JM 5 (C) and splits of JM 4 (B, D) and JM 7 (E, F). JM 2 is the structurally lowest sample and is plotted as a reference on B-F. Age spectra A-F show gradients ranging from 200 Ma to 1400 Ma. These micas record terminal ages ranging from 1320 to 1400 Ma. Muscovite samples from the structurally highest samples generally yield older ages than the structurally lowest samples.

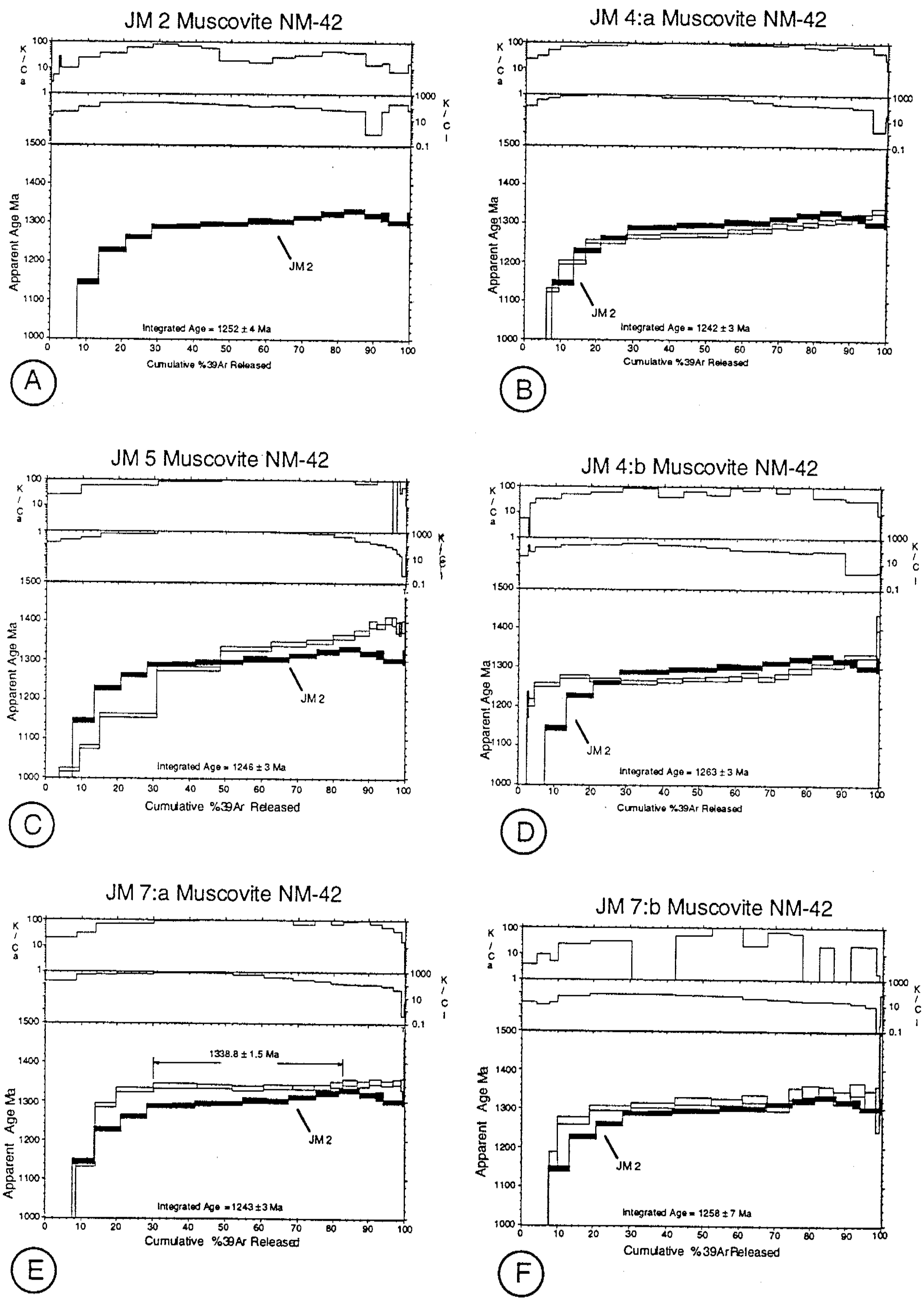
JM 2 Muscovite NM-42
Integrated Age = 1252 ± 4 Ma
JM 2
Cumulative %39Ar Released
A
JM 4:a Muscovite NM-42
Integrated Age = 1242 ± 3 Ma
JM 2
Cumulative %39Ar Released
B
JM 5 Muscovite NM-42
Integrated Age = 1246 ± 3 Ma
JM 2
Cumulative %39Ar Released
C
JM 4:b Muscovite NM-42
Integrated Age = 1263 ± 3 Ma
JM 2
Cumulative %39Ar Released
D
JM 7:a Muscovite NM-42
1338.8 ± 1.5 Ma
Integrated Age = 1243 ± 3 Ma
JM 2
Cumulative %39Ar Released
E
JM 7:b Muscovite NM-42
Integrated Age = 1258 ± 7 Ma
JM 2
Cumulative %39ArReleased
F
Apparent Age Ma
K/Ca
K/Cl

Figure 2-11.

Figure 2-12. $^{40}Ar/^{39}Ar$ age spectra from splits of muscovites JM 8 (A, B) and CP 1-2b (C, D). JM 2 is the structurally lowest sample and is plotted as a reference on B-F. Age spectra A-D show gradients ranging from 200 Ma to 1400 Ma. These micas record terminal ages ranging from 1320 to 1400 Ma. JM 8 shows a plateau age of 1333 $\pm$1.9. Muscovite samples from the structurally highest samples generally yield older ages than the structurally lowest samples. CP 1-2b (D) is the structurally highest sample. The age discordance between JM 2 and CP 1-2b is about 60 my and is interpreted to have resulted from slow cooling along an average geothermal gradient.

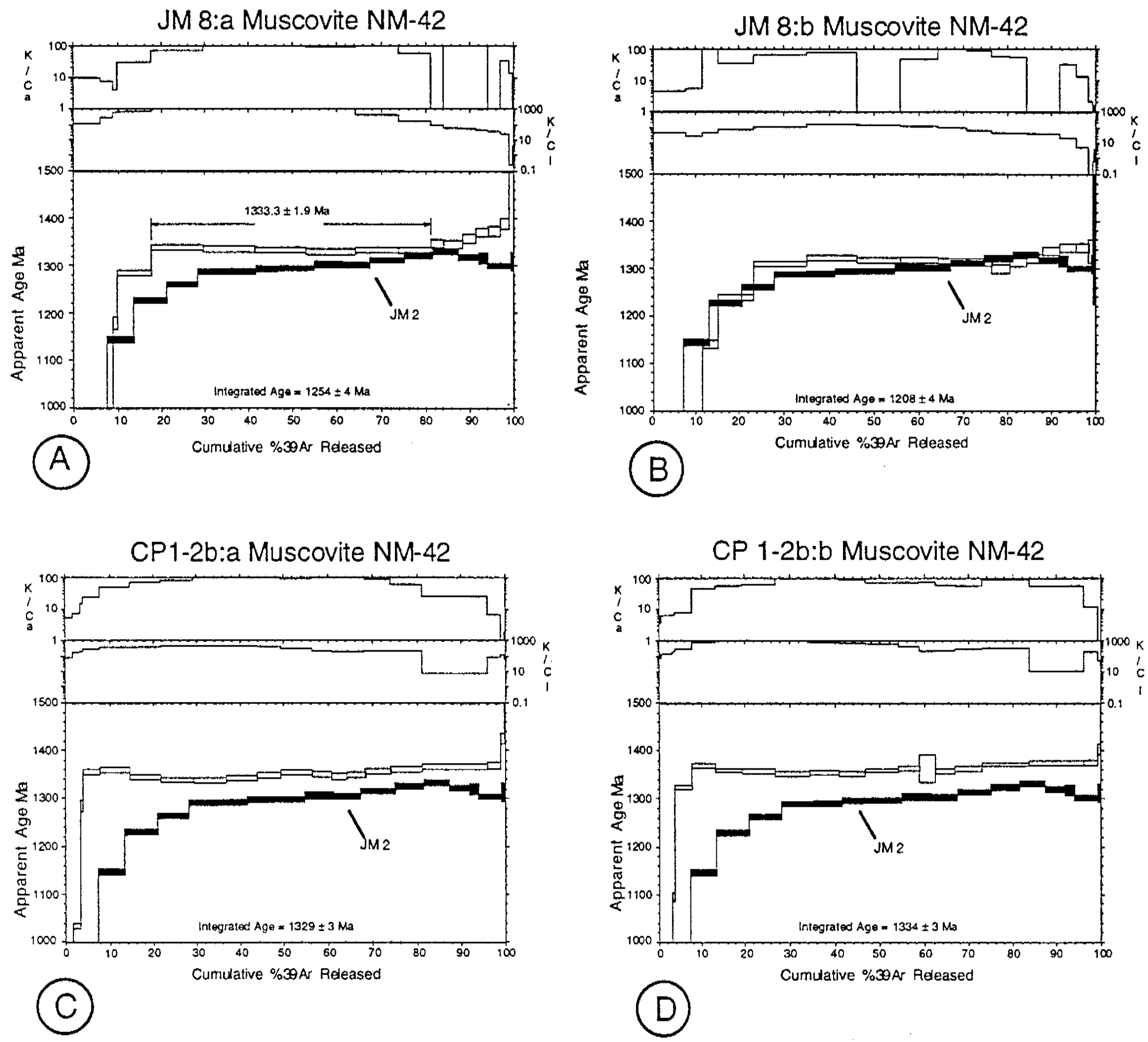
JM 8:a Muscovite NM-42
1333.3 ± 1.9 Ma
JM 2
Integrated Age = 1254 ± 4 Ma
A
JM 8:b Muscovite NM-42
JM 2
Integrated Age = 1208 ± 4 Ma
B
CP1-2b:a Muscovite NM-42
JM 2
Integrated Age = 1329 ± 3 Ma
C
CP 1-2b:b Muscovite NM-42
JM 2
Integrated Age = 1334 ± 3 Ma
D
K/Ca
K/Cl
Apparent Age Ma
Cumulative %39Ar Released

Figure 2-12.

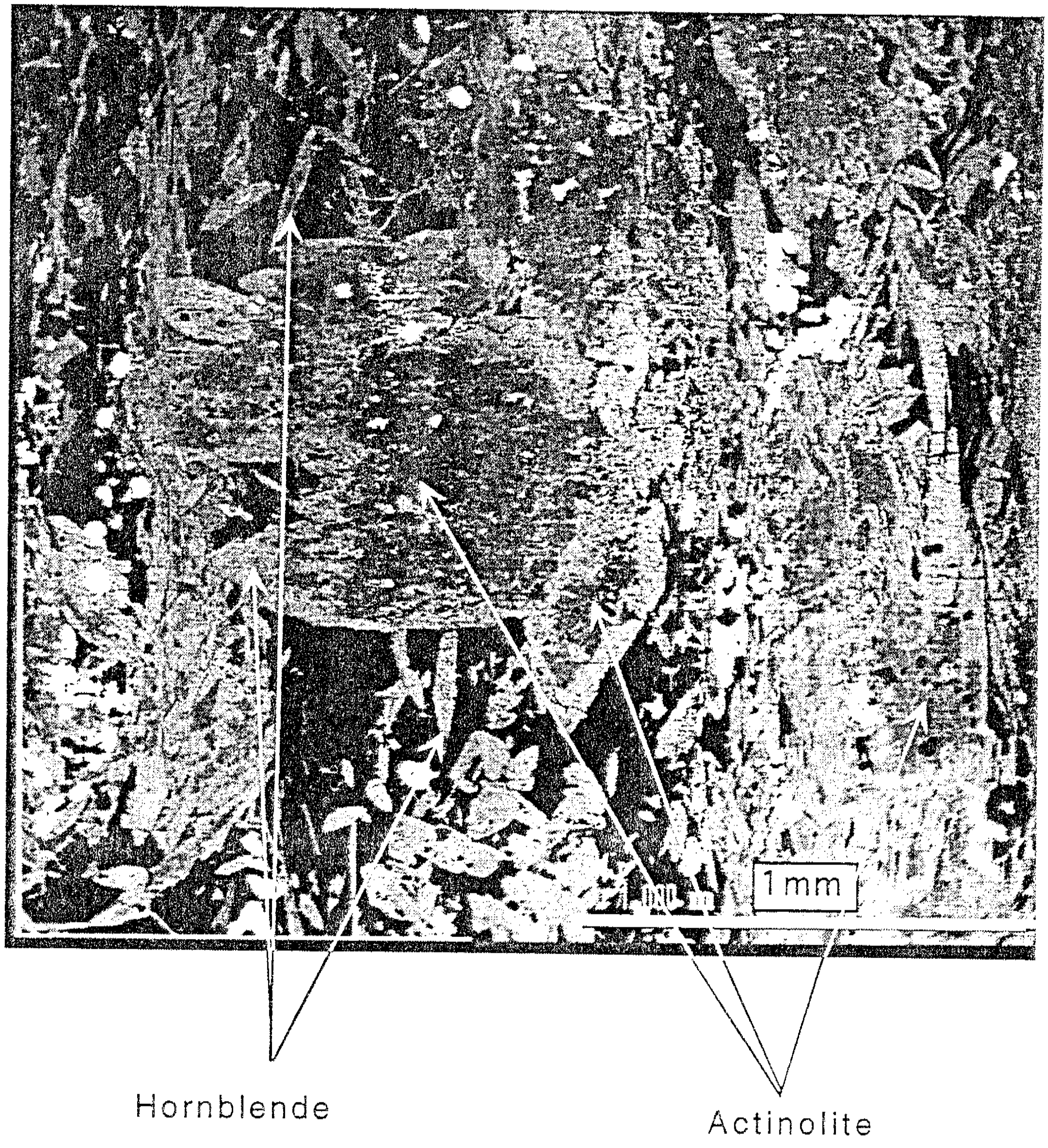

Figure 2-13. Backscattered electron image of ML 10-8 amphibolite showing the relationship between actinolite (dark) and hornblende (light). Note the high number of inclusions in the actinolite, the sharp boundary between the actinolite cores and the hornblende rims and the mutually cross-cutting relationship between the hornblende rims and bladed crystals.

grains. Hornblende also rims the actinolite grains. Hornblende rims and euhedral hornblende grains exhibit mutually crosscutting relationships, indicating contemporaneous growth (Fig. 2-13). Two different foliation orientations defined by 1) inclusion trails in the actinolites and 2) the nearly perpendicular hornblende crystals suggest that mineral growth occurred during two separate tectonic events. A miscibility gap is inconsistent with the structural and chemical data (c.f. Klein, 1968) and can not explain the sharp boundary between actinolite and hornblende of this particular composition. The chemical compositions of the ferro tschermakitic hornblendes and actinolites analyzed are inconsistent with those expected to co-exist and are not likely to be equilibrium pairs (Klein, 1968). Spear (1981) demonstrates that amphibole composition varies with temperature: typically amphiboles that form during a higher-grade metamorphic event have a higher Al and lower Si composition than observed in amphiboles formed during lower-grade metamorphic events. The hornblende studied here contains a significantly higher amount of Al and a lesser amount of Si then does the actinolite (Table 2-1). The hornblende compositions indicate formation under amphibolite facies conditions, while the actinolites record greenschist facies conditions (c.f. Spear, 1981). The structural and chemical relationships therefore indicate that the hornblende is younger than the actinolite and suggest two distinct periods of growth rather than simple prograde amphibole growth.

These data place constraints on the relative age of, and the metamorphic conditions during, amphibole growth. The $^{40}Ar/^{39}Ar$ data is used to further constrain the timing of mineral growth. The K/Ca ratio can be obtained from both microprobe analyses and from the $^{37}Ar/^{39}Ar$ ratio measured during the $^{40}Ar/^{39}Ar$ step-heating experiment. Comparing these values can give an indication of how meaningful the $^{40}Ar/^{39}Ar$ ages are. The microprobe and argon results yield nearly identical K/Ca ratios for the hornblende samples. Amphibole separates have elevated K/Ca ratios (calculated from the $^{37}Ar/^{39}Ar$ ratio) for the first few low temperature steps (Appendix 1). These high K/Ca ratios are common in amphiboles and may be related to exsolution features (Harrison and Fitzgerald, 1986; McDougall and Harrison, 1988) or degassing of fine-grained alteration phases (Onstott and Peacock, 1987). The average hornblende K/Ca derived from microprobe data is 0.036 and that derived from averaging the K/Ca from the flat portions of the hornblende age spectra is 0.04. This suggests that the gas derived during these steps is probably not contaminated by fine-grained K-rich phases and therefore may yield meaningful apparent ages.

In contrast, the actinolite K/Ca ratio from the microprobe data is 0.01 and from the age spectra varies from approximately 0.02 to 0.23 (Appendix 1). The high K/Ca ratios in the actinolite age spectra are interpreted to suggest that the actinolite separates are contaminated by varying amounts of fine-grained K-rich phases throughout the age spectra. The low temperature steps with young apparent ages and high K/Ca ratios are likely a result of degassing of fine-grained K-rich phases within the amphiboles. Several samples exhibit low K/Ca in the first 5 to 15% of the age spectra and corresponding young age steps, (e.g. ML 14-18-1 actinolite and hornblende, Fig. 2-10). This behavior is not well understood and is clearly not a result of a fine-grained K-bearing phases; it may be related to argon loss by chemical re-equlibrium as observed in complexly zoned amphiboles (Wartho, 1995). Samples with low K/Ca ratios in the early portions of the age spectra, as mentioned earlier, are all samples irradiated in irradiation NM-29. This problem is addressed below.

It is possible to evaluate both the amount of gas derived from each sample and the effectiveness of sample separation by examining the moles ^{39}Ar/mg for each amphibole sample with respect to irradiation number (Table 2-2). Samples from NM-29 have abundant young ages in the early portions of the age spectrum, without the corresponding rise in K/Ca seen in samples from NM-19 and NM-42. A zero age high-potassium contaminant could explain the low ages and low K/Ca ratios in the early portion of the age spectra. In this scenario, contamination must have occurred after separation, since only NM-29 samples are contaminated.

Fine-grained (300 mesh-size) actinolite and hornblende crystals were hand-picked under a binoculor low-power microscope. Considering the microstructural complexity of the two amphiboles, it is nearly impossible to obtain pure separates of each phase. The effectiveness of sample separation can be evaluated by comparing the hornblende: actinolite ratio of K_2O contents from the probe data, with the hornblende: actinolite ratio of moles ^{39}Ar/mg derived from $^{40}Ar/^{39}Ar$ analyses from the same sample (Table 2-2). A ratio of 3.6 is calculated from the microprobe data. Ratios between 0.3 and 1.2 are obtained for amphibole pairs analyzed from NM-29 and NM-42. For example, samples ML 9-6 and ML 6-7 have ratios of 1.4 and 1.2 respectively, indicating that the actinolite and the hornblende were somewhat concentrated but are not pure separates. Sample ML 9-3b has a ratio less than one probably indicating that the separates are not pure, and possibly that ML 9-3b actinolite is as much as 50% hornblende and vice-versa. The effect of the samples being concentrates rather than pure separates is a more complex age spectra. For example, the young ages observed early in the hornblende age spectra could be explained by a small percentage of actinolite in the hornblende concentrate since in general the actinolite age spectra show more young apparent ages than the hornblende spectra. As a result, age spectra interpretations are somewhat speculative since the relative contribution of each different age mineral is unknown.

A much higher percentage of ^{39}Ar released yields young ages in the actinolite spectra compared to the higher ages in the hornblende age spectra. This is likely a result of mineral inclusions, possibly feldspar and biotite (Fig. 2-13). These inclusions are probably the source for the excess argon released in the first steps of the actinolite age spectra in ML 10-8, thus explaining the anonymously old ages. However, in most cases the first 10-60% of the actinolite age spectra show young ages which correspond to a two order of magnitude smaller radiogenic yield and an elevated K/Ca. Due to the low radiogenic yields, high K/Ca ratios and abundant inclusions, limited geologic information can be derived from the actinolite age spectra. Since the bulk amphiboles consist of an unknown percentage of actinolite, hornblende and other minerals, both the bulk amphibole and the actinolite age spectra will not be used to constrain the thermochronology. The hornblende age spectra are also complex and probably related to the hornblendes being concentrates rather than pure separates; however, the majority have relatively flat portions of the age spectra around 1400 Ma with a flat corresponding K/Ca plot. For example, approximately 80%, 65% and 60% of the ^{39}Ar released for hornblende separated from ML 14-18, ML 10-8 and ML 6-7 respectively, yield apparent cooling ages of 1409 ± 10 Ma, 1329 ± 10 and 1397 ± 6 Ma with a constant K/Ca ratio for each step (Figs. 2-6E, F; 2-7D; 2-8C). However, several samples have a highly complex structure with a flat corresponding K/Ca (e.g., ML 9-3b, Fig. 2-9A). The fact that several samples have complex forms for the entire spectra suggests that the flat portions of the age spectra observed in the majority of samples are not a result of a simple homogenization of the $^{40}Ar/^{39}Ar$ ratio. Much of the hornblende age spectra complexity is probably related to the variable amounts of actinolite within each hornblende concentrate. Despite the overall age spectra complexity, the frequency of this recurring age between 1350 and 1410 Ma is more than coincidence, and at least suggests that this 1350-1400 Ma is a minimum time of closure for the hornblendes.

The flat portions of the hornblende age spectra clearly do not define rigorous plateau ages; however between 50 and 70% of the cumulative ^{39}Ar released consistently yields cooling ages of between 1330 and 1450 Ma (Figs. 2-6E, F; 7D, E, F). These relatively flat portions of the $^{40}Ar/^{39}Ar$ age spectra suggest that the foliation-forming hornblende cooled through its closure temperature ca. 1400 Ma; in particular, ML 14-18-2 hornblende exhibits a true plateau of 1409 ± 10 Ma. The last 5-10% of the gas released yields terminal ages up to ~1450 Ma and is may be the best estimate for the age of hornblende growth; this conclusion is consistent with that of Thompson et al., (1991). The variation in ages recorded by the flat portion of the age spectra is likely a result of differences in closure temperature of the hornblendes, which could be caused by either fine-grained intergrowths (Onstott and Peacock, 1987) or a variation in Mg and Fe content (O'Nions et al., 1969). The first of these options is the most likely, since fine-grained intergrowths have been postulated to have a greater affect on closure temperatures in high-grade metamorphic hornblendes (Onstott and Peacock, 1987). The probe data show little Mg and Fe variation between samples suggesting that composition is not the main variable controlling closure temperature, consistent with the studies of Harrison, (1981). If regional temperatures were high enough (450-550°C) to grow the tschermakitic hornblende prior to 1400 Ma, than temperatures should be high enough to reset the older actinolites with respect to argon. If so, one would not expect to see through the amphibolite facies event, and the older actinolites should yield younger or similar $^{40}Ar/^{39}Ar$ apparent ages.

The hornblende age spectra therefore record a period of cooling through the variable hornblende closure temperatures at ca. 1400 Ma, as well as a minimum age of mineral growth. Petrographic observations of amphibolites suggest syn-tectonic hornblende growth. The age of the hornblende growth can be further constrained by U-Pb ages from the 1.4 Ga Priest Pluton. Since the Priest Pluton (Fig. 2-1) is not highly deformed, syn-tectonic hornblende growth most likely occurred prior to emplacement, dated at 1427± 10 Ma (U-Pb zircon) (Bauer et al., 1993). The Priest Pluton is postulated to have been emplaced in the late stages of regional deformation (this manuscript) or in the absence of deformation (Karlstrom et al. 1996; Thompson et al., 1996; Karlstrom and Williams, 1995; Bauer and Williams, 1994; Karlstrom and Bowring, 1993). Hence, the age of hornblende growth is best constrained to 1440-1450 Ma (Fig. 2-8F), pre-dating emplacement of the Priest Pluton and corresponding to the terminal $^{40}Ar/^{39}Ar$ hornblende ages.

Two scenarios can explain the microstructural and $^{40}Ar/^{39}Ar$ data in the context of the regional tectonic history (Fig. 2-14). In the first model, the data are explained in the context of a non-deformational heating event ca. 1400 Ma; the second model involves regional deformation and metamorphism ca. 1400 Ma.

Model one requires no deformation at 1.4 Ga. Hornblende would grow syntectonically at ca. 1650 Ma (Mazatzal orogeny), and possibly undergo enlargement by overgrowth of hornblende with an identical composition during metamorphism at ca. 1400 Ma. If this is the case, an earlier deformation and metamorphic event (pre-1650 Ma) would have to be called upon to produce the older actinolites. Additionally, a younger deformational event, post-1400 Ma, would also be needed.

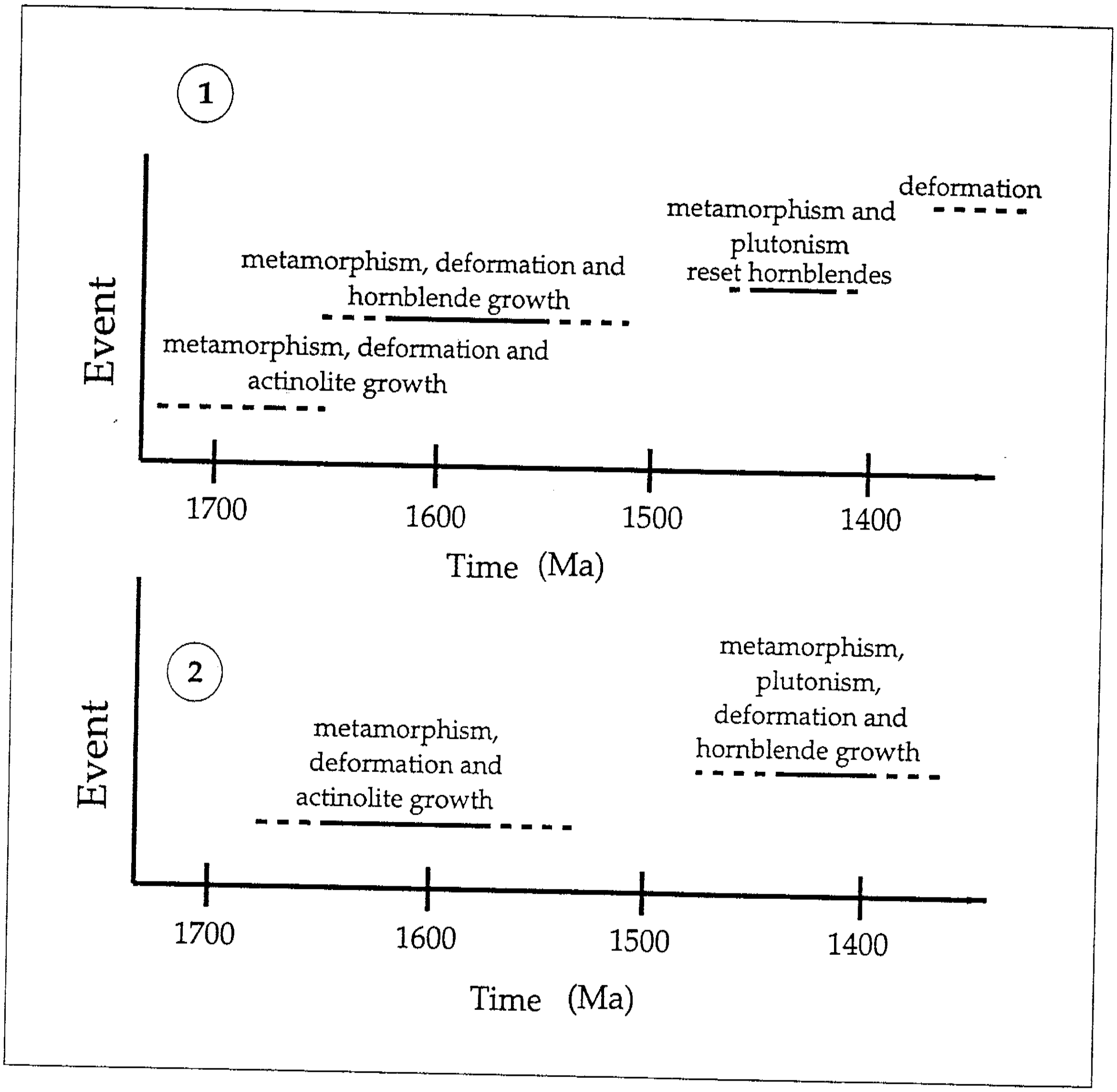

Figure 2-14. Schematic plots illustrating approximate timing of deformation and metamorphism using models 1 and 2. Model 1 requires three distinct events to explain the observed data in the context of 1.4 Ga static heating, whereas model 2 requires two metamorphic and deformational events at 1.6 and 1.4 Ga.

If metamorphism was not accompanied by deformation ca. 1400 Ma, then later deformation must be involved to produce the observed microstructures. The available microstructural data do not support a post 1400 Ma event as needed in model one; for example, microstructures in the Blue Springs schist and the adjacent quartz mylonites (see Part I) show no evidence of annealing. Monocrystalline quartz ribbons (Fig. 1-19), fine-grained muscovite and intracrystalline cataclasite, would be expected to recrystallize during the 500° C static reheating event that previous workers (Thompson et al., 1991) have suggested occurred at 1400 Ma. Although possible, there is no evidence to support a pre-1600 Ma regional deformational event or a post-1400 Ma event in the Capilla Peak area. The absence of a well-developed tectonic foliation in the Priest Pluton is therefore the result of emplacement during the late stages of deformation.

The second scenario is more consistent with the observed data: $^{40}Ar/^{39}Ar$ ages from foliation-forming hornblende and micas whose microstructures suggest that they grew syn-tectonically, probably at ca. 1440-1450 Ma, and cooled through their closure temperatures between 1330 and 1400 Ma.

THERMAL HISTORY

The thermal history for the Manzano Mountains from 1.65 Ga to the present can be evaluated from a combination of microstructural, electron microprobe and $^{40}Ar/^{39}Ar$ age spectra data. Figure 2-15 is a schematic diagram showing two different thermal histories. Number 1 is consistent with model 1 (discussed earlier), and number 2 is consistent with model 2, the metamorphic and deformational history of the Capilla Peak area proposed here.

Thermal history number 1 includes amphibolite grade metamorphic conditions around 1.6 Ga (Grambling, 1988). Data constraining regional temperatures between 1600 and 1400 Ma are limited. However, Karlstrom et al. (1996) proposed that amphibolite facies conditions existed around 1600 Ma, and a period of slow cooling followed. Abundant $^{40}Ar/^{39}Ar$, Rb-Sr and K-Ar ages indicate that a reheating event occurred around 1400-1450 Ma. Thompson et al. (1996) suggest that temperatures adjacent to the Priest pluton of 500-550°C existed at 1438 Ma, and Karlstrom et al. (1996) suggest that crustal temperatures remained relatively constant between 1400 and 1300 Ma.

Data presented in this paper are consistent with thermal history number 2 (Fig. 2-15).

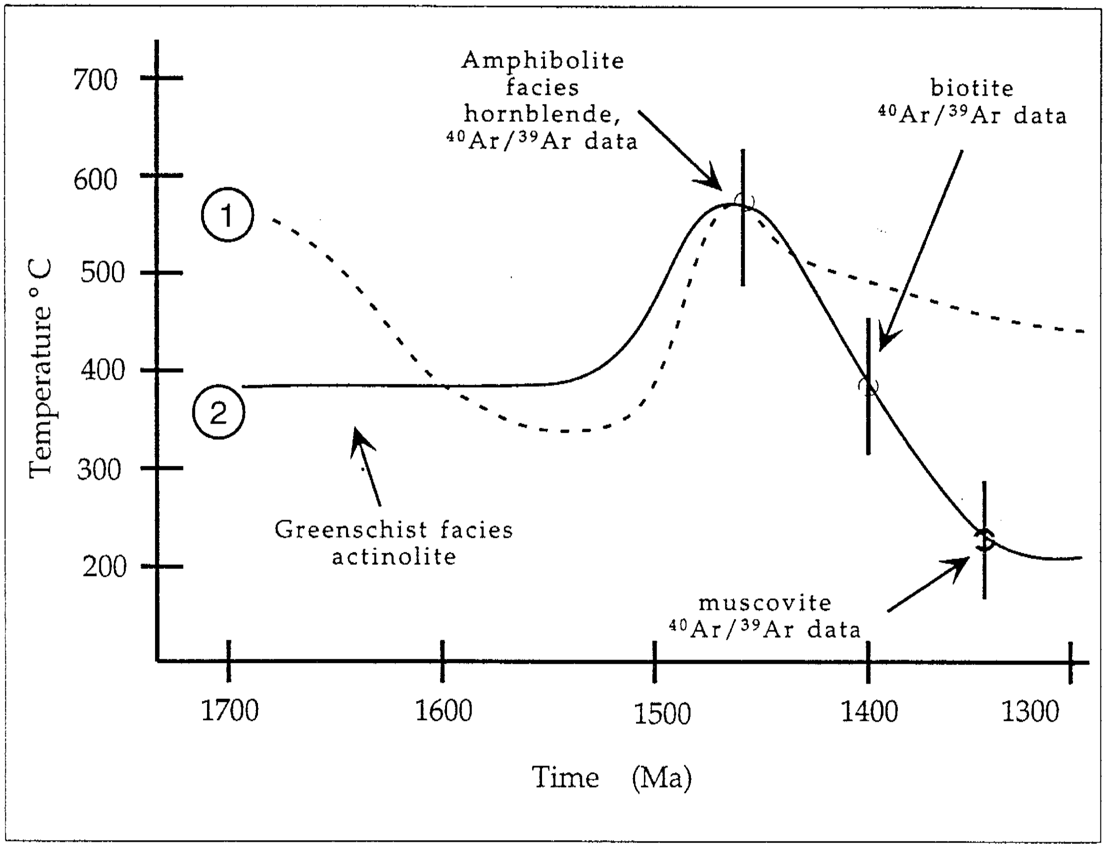

Figure 2-15. Schematic temperature-time plots for models 1 and 2. Model 1 is based on data from other workers, from around the Priest Pluton. Model 2 is based on geochronology and probe data from the Capilla Peak area. Points represent locations on the curves that are constrained by geochronology, with error bars representing approximate proposed temperature range.

Amphiboles

As mentioned earlier, evidence for the age of the actinolites is weak. However, based on 1.6 Ga terminal ages from bulk amphibole and actinolites (e.g. ML 10-6, Fig. 2-9 B and D), and the fact that the actinolites are older than the 1.4 Ga hornblendes, it is proposed that actinolites formed at 1.6 Ga. Contrary to the conclusions of Marcoline et al. (1995), Bauer and Williams (1994) and Grambling (1988), syntectonic growth of pre-1450 Ma actinolites (probably 1600-1650 Ma) suggest that local conditions were greenschist facies, with temperatures around 300-450°C, instead of amphibolite facies conditions. Thompson (1996) and Bowring and Karlstrom (1990), suggest that crustal temperatures in the Manzano Mountains remained constant at around 300°C until 1450 Ma. Amphibole mineral stabilities (Spear, 1981) and closure temperatures suggest that metamorphic conditions at 1.45 Ga were amphibolite facies.

Biotites

Concordant ca. 1400 Ma hornblende and biotite age spectra are interpreted to suggest that regional temperatures dropped rapidly (>10° C/Ma) from ca. 500-550° C (hornblende closure temperature) through 300-350°C (biotite closure temperature) around or shortly after 1400 Ma (Fig. 2-10E, F). However a third biotite (ML 10-8) from the same area as this hornblende-biotite pair yields an age of 1276 ± 6 Ma (Fig. 2-7F), ~130 Ma younger than ML 10-2 and ML 6-10 biotites. This younger biotite has a much smaller grain-size than the other two biotites, and in turn would be expected to have a lower closure temperature. The result of ML 10-8 biotite having a lower closure temperature than ML 10-2 and ML 6-10 biotites would be an amplification of any age discordance.

Muscovites

Inboard thermal effects of the Grenville Orogeny have been recorded in muscovites from discrete shear zones within the Priest Pluton (Heizler et al., 1996) and in northern New Mexico (Karlstrom et al., 1996). The muscovite age spectra from the Blue Springs schist may have experienced inboard thermal effects of the Grenville Orogeny however, do not preserve an 1100 Ma signature. The muscovites do, however, appear to be affected by later thermal events contributing to the abundant young ages early in the age spectra, probably related to late Paleozoic burial.

As indicated previously, muscovites were sampled from the base to the ridge of the Manzano Mountains within the Blue Springs schist (Fig. 2-2) in order to investigate the spatial variability of ages. The muscovites yield age gradients and terminal ages between 1320 and 1400 Ma (Fig. 2-11, 2-12). The muscovites have grain sizes ranging from 0.5 to 10 microns. These muscovite age spectra are similar in form and slightly younger in age to those observed in deformed muscovites near the Priest Pluton (Heizler et al., 1996). Different mechanisms proposed to explain well defined age gradients in muscovite are summarized in Heizler et al. (1996). However, in this case the young ages are most likely related to late Paleozoic burial, and the age gradients to a mixed grain size population.

Grain size reduction is observed in the muscovites in the form of intragranular cataclasite and recrystallization. Even though this deformation has reduced the grain size to ~0.5 microns within the cataclasite zones (c.f. Goodwin and Wenk, 1990), and essentially reduced the effective diffusion radii, associated argon loss appears to be negligible. If grain-size reduction were responsible for the observed age gradients we would expect to see more pronounced age gradients in the structurally higher positions where, in general, there is a greater amount of intra- and intergranular cataclasis.

The muscovite ages show a generally increasing age trend of 60 m.y. from the structurally lowest sample (JM-2) to the structurally highest sample (CP 1-2b). The observed age discordance is not related to grain size, either by different muscovite closure temperatures or by recoil. If the observed age discordance were related to different closure temperatures, assuming the sub-micron to 10 micron grain size is the controlling factor for muscovite closure with respect to argon, then we would expect the oldest sample to have the coarsest grain size, and the youngest the finest grain size. However, the structurally highest samples have about an order of magnitude smaller grain size than the structurally lowest samples. For example, Table 2-3 shows the relationship between grain-size and closure temperature; the closure temperature of a 0.5 micron muscovite is 217° C while a 10 micron muscovite

grain-size µm	T_c A	T_c B
0.05	159	170
0.5	203	217
1.0	219	233
1.5	228	244
2.0	236	250
2.5	241	257
3.0	246	262
3.5	250	265
4.0	253	269
4.5	256	273
5.0	259	276
5.5	262	278
6.0	264	281
6.5	266	283
7.0	268	285
7.5	270	287
8.0	272	289
8.5	274	291
9.0	275	293
9.5	277	294
10.0	278	296
20.0	299	317
50.0	328	349

Table 2-3. Chart showing the relationship between grain-size in muscovite and closure temperature (°C). Column A gives the Tc calculated using a cooling rate of 0.3°C/Ma and B is calculated using 1°C/Ma; all calculations used an E of 40 Kcal/mole and a D_o of 6 X 10^{-7} cm^2/s.

would be expected to have a closure temperature of 296° C. In this situation we would expect that the age of the fine-grained muscovites from the structurally highest position would be on the order of 30 Ma younger than the age of a muscovite from the structurally lowest position (assuming 1°C/Ma cooling), and 75 Ma younger if the samples were at the same structural level. Since the entire range of grain-sizes are observed in all samples (in varying amounts) and since the grain-size model predicts the opposite age trend of that observed, we interpret that this grain size distribution is not responsible for the observed age discordance; and actually would have the effect of minimizing the observed age discordance. However the grain-size probably is responsible for the age gradients observed in the muscovite age spectra since the fine-grained material would be expected to degas first (West et al., 1993).

The age spectra do not resemble those interpreted to have been affected by recoil (Harrison and Fitzgerald, 1986), hence, the phenomenon of older ages related to the recoil of ^{39}Ar into cataclasite (as observed by Goodwin and Renne, 1991) is unlikely; rather the data support a simple cooling model. Assuming an average geothermal gradient (25-30°C/m.y.) slow cooling on the order of 0.3 - 1°C/Ma would be consistent with the area undergoing uplift and erosion, explaining the observed muscovite age trend. Muscovite data, in conjunction with hornblende and biotite data, therefore are interpreted to suggest that a period of early (1450-1350 Ma) rapid and late (1350-?) slow cooling occurred.

CONCLUSIONS

The combination of $^{40}Ar/^{39}Ar$ age spectra, field observations and microstructures indicate that at least two episodes of regional deformation, metamorphism and mineral growth occurred in the Manzano Mountains. Deformation and mineral growth accompanied both amphibolite grade metamorphism at 1400-1450 Ma, and an older period of greenschist-facies metamorphism. There is no direct way to date the early event; however, the presence of inclusion trails in actinolites that are nearly perpendicular to the hornblende tectonic foliation is interpreted to suggest that the actinolite formed syntectonically during a prior lower grade metamorphic and deformational event, probably at 1650 Ma.

Amphibole compositional data suggest that regional temperatures reached 550-650°C (cf. Spear, 1981) at 1450 Ma and cooled to between 400 and 550°C by 1400 Ma. Muscovite and biotite $^{40}Ar/^{39}Ar$ data are interpreted to suggest that regional temperatures cooled rapidly to 200-300°C by about 1350 Ma. Discordant muscovite $^{40}Ar/^{39}Ar$ age spectra from different structural levels indicate that a period of protracted slow cooling occurred after 1350 Ma.

COMBINED REFERENCES

Bauer, P. W., 1988, Geology of the Precambrian rocks of the southern Manzano Mountains, New Mexico, New Mexico Bureau of Mines and Mineral Resources Open-file Report 339, 145 p.

Bauer, P. W., Callender, J. F., Grambling, J. A., Wells, S. C., 1982, Precambrian geology and tectonics of the southern Manzano Mountains, Central New Mexico: New Mexico Geological Society, Guidebook to 33rd Field Conference, pp. 211-216.

Bauer, P. W., Karlstrom, K. E., Bowring, S. A., Smith, A. G., and Goodwin, L. B., 1993, Proterozoic plutonism and regional deformation - new constraints from the southern Manzano Mountains, Central New Mexico. New Mexico Geology, v.15, no. 3, pp. 49-56.

Bauer, P. W. and Pollock, T., 1993, Compilation of Precambrian isotope ages in New Mexico: New Mexico Bureau of Mines and Mineral Resources Open-file Report 389, 130 p.

Bauer, P. W., and Williams, M. L., 1994, The age of Proterozoic orogenesis in New Mexico, U.S.A.: Precambrian Research v. 67, pp. 349-356.

Berthe, D., Choukroune, P., and Jegouzo, P., 1979, Orthogneiss, mylonite and non-coaxial deformation of granites: the example of the South Armoricain shear zone: Journal of Structural Geology, v. 1, pp. 31-42.

Blumenfeld, P., Mainprice, D., Bouchez, J. L., 1896, C-slip in Quartz from subsolidus deformed granite. Tectonophysics, v. 127, pp. 97-115.

Blumenfeld, P., and Bouchez, J. L., 1988, Shear criteria in granite and migmatite deformed in the magmatic and solid states. Journal of Structural Geology, v. 10, No. 4, pp. 361-372.

Bolton, W. R., 1976, Precambrian geochronology of the Sevilleta Metarhyolite and the Los Pinos, Sepultura, and Priest plutons of the southern Sandia uplift, New Mexico [MS Thesis]: Socorro, New Mexico Institute of Mining and Technology, 45 p.

Bowring, S. A., Kent, S. C., and Sumner, W., 1983, Geology and U-Pb geochronology of Proterozoic rocks in the vicinity of Socorro, New Mexico: New Mexico Geological Society, Guidebook 34, pp. 137-142.

Bowring, S. A. 1991, Early Proterozoic lithospheric growth, stabilization, and reactivation in New Mexico and Arizona (abs.): Geological Society of America, Abstracts with programs, v. 23, no. 5, p. 58.

Bowring, S. A., and Karlstrom, K. E., 1990, Growth, stabilization, and reactivation of Proterozoic lithosphere in the southwestern United States: Geology, v. 18, pp. 1203-1206.

Brookins, D. G., Bolton, W. R. and Condie, K. C., 1980, Rb-Sr isochron ages of four Precambrian igneous rock units from south-central New Mexico: Isochron/West, no. 29, pp. 31-37.

Cosca, M. A., and O'Nions, K. R., 1994, A re-examination of the influence of composition on argon retentivity in metamorphic calcic amphiboles. Chemical Geology, v. 112, p. 39-56.

Culshaw, N. G., and Fyson, W. K., 1984, Quartz ribbons in high grade granite gneiss: modifications of dynamically formed quartz c-axis preferred orientation by oriented grain growth. Journal of Structural Geology, v. 6, no. 6, pp. 663-668.

Dallameyer, R. D., Grambling, J. A. and Thompson, A. G., 1990, Age and character of Proterozioc polymetamorphism in New Mexico:

Geological Society of America, Abstracts with Programs ,v. 22, no. 7, p. 113.

Dell'angelo, L. N., and Tullis, J., 1989, Fabric development in experimentally sheared quartzites. Tectonophysics, v. 169, pp. 1-21.

Fleck, R. J., Sutter, J. F., Elliot, D. H., 1977, Interpretation of discordant $^{40}Ar/^{39}Ar$ age spectra of Mesozoic tholeiites from Antarctica: Geochim Cosmochim Acta, v. 41, pp. 15-32.

Gapais, D. and Barbbarin, B., 1986, Quartz fabric transition in a cooling syntectonic granite (Hermitage Massif, France). Tectonophysics, v. 125, pp. 357-370.

Goodwin, L. B. and Wenk, H., 1990, Intracrystalline folding and cataclasis in biotite of the Santa Rosa mylonite zone: HVEM and TEM observations. Tectonophyiscs, v. 172, pp. 201-214.

Goodwin, L. B. and Renne, P. R., 1991, Effects of progressive mylonitization on Ar retention in biotites from the Santa Rosa mylonite zone, California, and thermochronologic implications: Contributions to Mineralogy and Petrology, v. 108, pp. 283-297.

Grambling, J. A., 1982, Precambrian structures in Cañon del Trigo, Manzano Mountains, central New Mexico: New Mexico Geological Society, Guidebook to 33rd Field Conference, pp. 217-220.

Grambling, J. A., 1986, Crustal thickening during Proterozoic metamorphism and deformation in New Mexico: Geology, v. 14, pp. 149-152.

Grambling, J. A., Williams, M. L., Mawer, C. K., 1988, The Proterozoic tectonic assembly of New Mexico: Geology, v. 16, pp. 724-727.

Grambling, J. A., Williams, M. L., Smith, R. F., and Mawer, C. K., 1989, Metamorphism and deformation of Kyanite - andalusite - sillimanite and sillimanite-K-feldspar rocks in New Mexico, in Grambling, J. A., and Tewksbury, B. J., eds., Proterozoic Geology of the central and southern Rocky Mountains: Geological Society of America Special Paper 235, pp. 111-118.

Hanmer, J., and Passchier, C., 1991, Shear sense indicators: A review. Geological Survey of Canada Paper 90-17.

Harrison, T. M., and Fitzgerald J. D., 1986, Exsollution in hornblende and its consequences for $^{40}Ar/^{39}Ar$ age spectra and closure temperature. Geochim Cosmochim Acta 50: pp. 247-253.

Harrison, T. M., and McDougall, I., 1981, Excess ^{40}Ar in metamorphic rocks from Broken Hill, New South Wales: implications for $^{40}Ar/^{39}Ar$ age spectra and the thermal history of the region: Earth and Planetary Science Letters. v. 55, pp. 123-149.

Harrison, T. M., 1981, Diffusion of ^{40}Ar in hornblende: Contributions to Mineralogy and Petrology, v. 78, pp. 324-331.

Heizler, M. T., Ralser, S, and Karlstrom, K. E., 1996, Late Proterozoic deformation in central New Mexico: Consequences for muscovite 40Ar/39Ar age spectra and Grenville Orogenesis: Precambrian Research, in press.

Hobbs, B. E., 1972, Deformation of Non-Newtonian materials in simple shear in flow and fracture of rocks: American Geophys. Union, Geophys. Monogram, no. 16, pp. 243-258.

Hobbs, B. E., 1985, The Geological significance of microfabric analysis, Wenk ed. Preferred orientation in deformed metals and rocks: An introduction to modern texture analysis. pp. 463-484. Academic Press Orlando, Florida.

Johnson, S. E., 1986, Structural analysis and reinterpretation of an apparent Precambrian angular unconformity, central Manzano Mountains, New Mexico. New Mexico Geology, v.8, no. 3, pp. 45-50.

Karlstrom, K. E., and Bowring, S. A. 1991, Styles and timing of Early Proterozoic deformation in Arizona-constraints on tectonic models (abs.) Geological Society of America, Abstracts with programs, v. 23, no. 4, p. 37.

Karlstrom, K. E. and Bowring, S. A., 1993, Proterozoic orogenic history of Arizona, in Precambrian: Conterminous U.S., Decade of North American Geology, v. C-2, J. C. Read, Jr. et al., (eds), Geological Society of America, Boulder, Colorado, pp. 188-211.

Karlstrom, K. E., Dallameyer, R. D. and Grambling, J. A., 1996, Mesoproterozoic (1.42-1.35 Ga) regional metamorphism in New Mexico and implications for thermal evolution of lithosphere in the southwestern U.S.A.: Evidence from 40Ar/39Ar ages, In press Journal of Geology.

Karlstrom, K. E. and Williams, M. L., 1995, The case for simultaneous deformation, metamorphism and plutonism: an example from Proterozoic rocks in central Arizona: Journal of Structural Geology, v. 17, pp. 59-81.

Klein, C., Jr., 1968, Coexisting amphiboles: Journal of Petrology, v. 9, pp. 282-330.

Kronenberg, A., 1981, Quartz preferred orientations within a deformed pebble conglomerate from New Hampshire, U.S.A., Tectonophysics, v. 79, pp. T7-T15.

Law. R.D., 1990, Crystallographic fabrics: a selective review of their applications to research in structural geology. in Knipe, R. J., and Rutter, E. H., eds., Deformation mechanisms rheology and tectonics: Geological Society Special Publication 54, pp. 335-348.

Lister, G. S., 1977, Discussion; crossed-girdle c-axis fabrics in quartzites plastically deformed by plane strain and progressive simple shear: Tectonophysics, v. 39, no. 1-3, pp. 51-54.

Lister, G. S., and Dornseipen, U. F., 1982, Fabric transitions in the Saxony granulite terrain: Journal of Structural Geology, v. 4, no. 1, pp. 81-93.

Lister, G. S., and Hobbs, B. E., 1980, The simulation of fabric development during plastic deformation and its application to quartzite: the influence of deformational history. Journal of Structural Geology, v. 2, no. 3, pp. 355-370.

Lister, G. S., and Williams, P. F., 1979, Fabric development in shear zones: theoretical controls and observed phenomena. Journal of Structural Geology, v. 1, no. 4, pp. 283-297.

Mainprice, D., Bouchéz, J. L., Blumenfeld, P., Tabia, J. M., 1986, Dominant c slip in naturally deformed quartz: Implications for dramatic plastic softening at high temperatures. Geology, v. 14, pp. 819-822.

Marcoline, J. R., Ralser, S. and Heizler, M. T., 1995, Monte Largo shear zone, Manzano Mountains, New Mexico: Tectonic significance and argon geochronology: New Mexico Geology, v. 17, p.26.

Marcoline, J. R., Ralser, S. and Heizler, M. T., Goodwin, L. B., 1995, Middle Proterozoic regional deformation: Evidence from the Monte Largo shear zone, Manzano Mountains, central New Mexico, Geological Society of America, Abstracts with Programs, v. 27, no. 6, p. 162.

McDougall, I. and Harrison, T. M., 1988, *Geochronology and thermochronology by the 40Ar/39Ar method.*. Oxford University Press.

Myres, D. A., and McKay, E. J., 1972, Geologic map of the Capilla Peak quadrangle, Torrance and Valencia Counties, New Mexico: U.S. Geological Survey, Geologic Quadrangle map GQ-1008, scale 1:24,000.

Northrup, C. J., 1991, *Thermal, chemical, and structural characteristics of fluid migration and fluid-rock interaction in a Mid-Proterozoic shear zone, Manzano Mountains, New Mexico.* M.S. thesis, University of Arizona, 121 p.

O'nions, R. K., Smith, D. G. W., Baadsgaard, H., Morton, R. D., 1969, Influence of chemical composition on argon retentivity in metamorphic calcic amphiboles from south Norway: Earth and Planetary Science Letters, v. 5, no. 5, pp. 339-345.

Onstott, T. C., and Peacock, M. W., 1987, Argon retentivity of hornblendes: A field experiment in a slowly cooled metamorphic terrane: Geochimica et Cosmochimica Acta, v. 51, pp. 2891-2903.

Passchier, C. W., and Simpson, C., 1986, Porphyroclast systems as kinematic indicators. Journal of Structural Geology, v. 8, pp. 831-843.

Ralser, S, 1990, Shear zones in an experimentally deformed quartz mylonite. Journal of Structural Geology, v. 12, no. 8, pp. 1033-1045.

Reiche, P., 1949, Geology of the Manzanita and north Manzano Mountains, New Mexico, Geol. Soc. Am. Bull., v. 60, pp. 1183-1212.

Shastri, L. L., and Bowring, S. A., 1992, Timing of Proterozoic deformation, plutonism, and metamorphism in the Los Pinos Mountains, central New Mexico (abs.): Geological Society of America, Abstracts with programs, v. 24, no. 7, p. A117.

Shastri, L. L., 1993, Proterozoic geology of the Los Pinos Mountains [MS Thesis]: Albuquerque, University of New Mexico, 82 p.

Simpson, C., 1985, Deformation of granitic rocks across the brittle-ductile transition. Journal of Structural Geology, v. 7, pp. 503-511.

Schmid, S. M., and Casey, M., 1986. Complete texture analysis of commonly observed quartz c-axis patterns. Hobbs, H. C. and Heard, H. C., eds., Mineral and rock deformation: Laboratory studies. pp. 263-386. Am. Geophys. Union Monogr. 36.

Spear, F. S., 1981, An experimental study of hornblende stability and compositional variability in amphibole. AJS, v. 28, pp. 697-734.

Stark, J. T., and Dapples, E. C., 1946, Geology of the Los Pinos Mountains, New Mexico. Geological Society of America Bulletin. v. 57, pp. 1121-1172.

Stark, J. T., 1956, Geology of the south Manzano Mountains, New Mexico: *New Mexico Bureau of Mines And Mineral Resources Bulletin*, 34, pp. 1-47.

Starkey, J., 1977, The contouring of orientation data represented in spherical projection. Canadian Journal of Earth Sciences. v. 14, pp. 268-277.

Thompson, A. G., Grambling, J. A., and Dallmeyer, R. D., 1991, Proterozoic tectonic history of the Manzano Mountains, central New Mexico. *New Mexico Bureau of Mines And Mineral Resources Bulletin*, 137, pp. 71-77.

Thompson, A. G., Grambling, J. A., and Karlstrom, K. E., and Dallmeyer, R. D., 1996, Thermal evolution of the Proterozoic middle crust during the following 1.4 Ga pluton emplacement, Manzano Mountains, New Mexico: Journal of Geology.

Tullis, J., Christie, J. M., Griggs, D. T., 1973, Microstructures and preferred orientations of experimentally deformed quartzites. Geol. Soc. America Bulletin, v. 84, pp. 297-314.

van der Pluijm, B. A., Mezger, K., Cosca, M. A. Essene, E. J., 1994, Determining the significance of high-grade shear zones by using temperature- time paths, with examples from the Grenville orogen. Geology. v. 22, no. 8, pp. 743-746.

Wartho, J., 1995, Apparent argon diffusive loss $^{40}Ar/^{39}Ar$ age spectra in amphiboles: Earth and Planetary Science Letters, v. 134, pp. 393-407.

West, D. P., and Lux, D. R., 1993, Dating mylonitic deformation by the $^{40}Ar/^{39}Ar$ method: An example from Norumbega Fault Zone, Maine: Earth and Planetary Science Letters, v. 120, pp. 221-237.

Williams, P. F. and Price, G. P., 1990, Origin of kink bands and shear-band cleavage in shear zones: an experimental study: Journal of Structural Geology, v. 12, n. 2, pp. 145-164.

Williams, M. L., 1990, Proterozoic geology of northern New Mexico: recent advances and ongoing questions. N. M. Geol. Soc. Guidebook., v. 41, pp. 151-159.

Williams, P. F., Goodwin, L. B. and Ralser, S., 1994, Ductile deformation processes, in Hancock, P. L. eds., Continental deformation. pp. 1-27. Pergamon Press, New York.

White, D. L., 1979, RB-SR age and isotopic data of some Precambrian plutons in central New Mexico, USA: The Mountain Geologist, no. 4, pp. 131-147.

White, S.H.., Burrows, S. E., Carreras, J., Shaw, N. D., and Humphreys, F. J., 1980, On mylonites in ductile shear zones: Journal of Structural Geology, v. 2, pp. 175-187.

Yavuz, F., 1996, AMPHCAL: A quickbasic program for determining the amphibole name from electron microprobe analysis using the IMA rules; Computers and Geoscience, V. 22. 2, pp. 101-107.

Appendix 2-1. Appendix 2-1 is a table containing all of the $^{40}Ar/^{39}Ar$ data organized by irradiations NM-19, NM-29 and NM-42. The run ID # is the lab sample number with the adjacent capital letter representing each successive heating step. For each heating step at the given temperature a value of $^{40}Ar/^{39}Ar$, $^{37}Ar/^{39}Ar$, ^{36}Ar, ^{39}Ar, ^{39}Ar moles, K/Ca, Cl/K, % $^{40}Ar^{*}$, % ^{39}Ar and age is given.

Run ID#	Temp	$^{40}Ar/^{39}Ar$	$^{37}Ar/^{39}Ar$	$^{36}Ar/^{39}Ar$	^{39}Ar moles	K/Ca	Cl/K	$\%^{40}Ar^*$	$\%^{39}Ar$	Age	± Err
MH-9-3b Bulk Amphibole, JM, J=0.01442337					**NM-19**		**2.6 mg**				
2216-01A	700	809.484	14.900	1.8064	8.9E-17	0.034	0.7953	34.1	3.11	2895	56
2216-01B	800	195.392	17.879	0.3127	4.9E-17	0.029	0.2511	52.7	4.82	1642	37
2216-01C	900	113.061	22.331	0.1659	7.2E-17	0.023	0.1246	56.6	7.35	1180	33
2216-01D	1000	98.916	36.844	0.0387	2.4E-16	0.014	0.1564	88.4	15.67	1472.1	7.3
2216-01E	1040	170.375	88.551	0.1018	4.3E-16	0.006	0.2705	82.3	30.65	1995.8	7.3
2216-01F	1070	101.787	73.743	0.0552	3.3E-16	0.007	0.1098	83.9	42.24	1448.8	7.5
2216-01G	1100	81.992	50.294	0.0293	2.0E-16	0.010	0.0626	89.4	49.24	1302	10
2216-01H	1130	65.229	67.298	-0.0184	4.8E-17	0.008	0.0746	108.3	50.93	1267	33
2216-01I	1160	81.823	59.032	0.0065	8.7E-17	0.009	0.0774	97.6	53.98	1383	19
2216-01J	1190	88.802	66.073	-0.0012	1.7E-16	0.008	0.0971	100.4	59.93	1491.4	9.2
2216-01K	1220	107.104	59.485	0.0186	2.3E-16	0.009	0.1258	94.9	67.85	1627.9	7.6
2216-01L	1250	92.056	50.923	0.0172	5.4E-16	0.010	0.0907	94.4	86.75	1466.2	4.4
2216-01M	1280	103.370	76.700	0.0249	2.6E-16	0.007	0.1005	92.9	95.91	1567.7	6.1
2216-01N	1350	155.104	193.623	0.0500	1.1E-16	0.003	0.2295	90.5	99.81	1996	11
2216-01O	1700	307.758	196.068	0.2585	5.4E-18	0.003	0.1529	75.2	100.00	2647	162
	total gas age			n=15	2.9E-15	0.010	0.0094			1613	11
MH-9-6 Bulk Amphibole, JM, J=0.01445203					**NM-19**		**2.2 mg**				
2217-01A	700	85.519	3.352	0.1456	2.5E-16	0.152	0.0760	49.7	7.32	863	14
2217-01B	800	32.986	1.828	0.0317	1.2E-16	0.279	0.0216	71.5	10.81	529	19
2217-01C	900	39.257	3.977	0.0266	1.8E-16	0.128	0.0236	79.9	16.22	674	10
2217-01D	1000	49.048	19.220	0.0110	5.0E-16	0.027	0.0372	93.3	30.84	916.0	4.0
2217-01E	1040	68.309	43.930	0.0267	3.7E-16	0.012	0.0542	88.4	41.60	1131.9	5.9
2217-01F	1070	68.700	40.851	0.0195	4.0E-16	0.012	0.0307	91.6	53.42	1166.6	5.7
2217-01G	1100	65.876	28.754	0.0110	2.9E-16	0.018	0.0258	95.0	61.88	1162.3	6.4
2217-01H	1130	48.011	32.115	0.0319	9.1E-17	0.016	0.0246	80.3	64.58	799	20
2217-01I	1160	58.700	36.446	0.0138	6.9E-17	0.014	0.0314	93.0	66.62	1049	26
2217-01J	1190	79.594	34.364	0.0224	2.0E-16	0.015	0.0377	91.7	72.61	1298.9	8.5
2217-01K	1220	86.634	35.441	0.0167	3.0E-16	0.014	0.0544	94.3	81.40	1406.4	5.9
2217-01L	1250	89.469	39.657	0.0166	3.7E-16	0.013	0.0575	94.5	92.40	1440.2	4.7
2217-01M	1280	84.558	63.269	0.0274	1.3E-16	0.008	0.0583	90.4	96.14	1342	11
2217-01N	1350	102.653	131.754	0.0487	1.3E-16	0.004	0.0842	86.0	99.85	1483	11
2217-01O	1700	238.371	214.083	0.5818	5.2E-18	0.002	0.1395	27.9	100.00	1214	318
	total gas age			n=15	3.4E-15	0.041	0.0784			1120.0	8.6
MH-13-9b Bulk Amphibole, JM, J=0.01449799					**NM-19**		**2.9 mg**				
2218-01A	700	36.405	1.216	0.0322	1.4E-15	0.419	0.0190	73.8	10.36	593.8	2.3
2218-01B	800	33.939	0.475	0.0063	9.6E-16	1.075	0.0052	94.4	17.23	688.6	2.3
2218-01C	900	36.876	0.778	0.0080	1.5E-15	0.656	0.0047	93.5	27.81	731.6	1.8
2218-01D	1000	52.443	5.868	0.0044	2.6E-15	0.087	0.0112	97.5	46.25	1000.6	1.8
2218-01E	1040	64.694	11.537	0.0061	1.4E-15	0.044	0.0145	97.2	56.11	1168.8	2.6
2218-01F	1070	66.668	10.983	0.0044	1.5E-15	0.046	0.0112	98.0	66.69	1202.5	2.3
2218-01G	1100	55.734	8.304	0.0047	9.2E-16	0.061	0.0078	97.5	73.27	1047.9	2.4
2218-01H	1130	41.519	7.301	0.0063	4.1E-16	0.070	0.0074	95.5	76.21	819.4	5.1
2218-01I	1160	65.399	12.902	0.0133	3.5E-16	0.040	0.0125	93.9	78.74	1149.1	4.8
2218-01J	1190	67.882	13.305	0.0058	6.2E-16	0.038	0.0166	97.5	83.16	1213.3	3.6
2218-01K	1220	87.425	16.016	0.0074	9.1E-16	0.032	0.0227	97.5	89.63	1451.4	3.3
2218-01L	1250	93.942	16.653	0.0075	1.0E-15	0.031	0.0229	97.6	96.95	1525.5	3.0
2218-01M	1280	92.241	17.942	0.0034	2.4E-16	0.028	0.0184	98.9	98.64	1520.1	9.0
2218-01N	1350	87.684	17.739	0.0129	1.6E-16	0.029	0.0180	95.6	99.75	1435	14
2218-01O	1700	83.577	20.882	0.0579	3.5E-17	0.024	0.0054	79.5	100.00	1217	64
	total gas age			n=15	1.4E-14	0.226	0.3059			1039.2	2.9
ML-13-10c Bulk Amphibole, JM, J=0.01450297					**NM-19**		**2.4 mg**				
2219-01A	700	109.045	2.477	0.1511	5.7E-16	0.206	0.0364	59.0	3.20	1189.5	7.7
2219-01B	800	60.748	2.047	0.0373	2.9E-16	0.249	0.0086	81.8	4.80	979.2	6.3
2219-01C	900	52.075	3.883	0.0469	4.7E-16	0.131	0.0091	73.4	7.44	795.3	6.0
2219-01D	1000	76.850	18.522	0.0120	1.8E-15	0.028	0.0042	95.4	17.59	1306.5	2.4
2219-01E	1040	81.610	25.759	0.0137	1.3E-15	0.020	0.0052	95.0	25.02	1359.5	3.5
2219-01F	1070	80.758	18.784	0.0077	2.3E-15	0.027	0.0029	97.1	37.78	1370.7	2.2
2219-01G	1100	81.164	16.555	0.0063	2.7E-15	0.031	0.0022	97.7	53.07	1380.8	2.2
2219-01H	1130	68.643	19.251	0.0112	2.7E-16	0.027	0.0038	95.2	54.57	1202.3	6.3
2219-01I	1160	79.749	20.744	0.0097	4.5E-16	0.025	0.0041	96.4	57.09	1351.0	4.1
2219-01J	1190	83.978	19.126	0.0071	2.7E-15	0.027	0.0028	97.5	72.39	1412.0	2.0
2219-01K	1220	90.426	20.066	0.0069	2.3E-15	0.025	0.0031	97.7	85.29	1488.1	2.1
2219-01L	1250	91.978	21.577	0.0081	2.4E-15	0.024	0.0038	97.4	98.76	1501.7	2.2
2219-01M	1280	100.484	30.605	0.0167	1.3E-16	0.017	0.0058	95.1	99.52	1568.5	9.3
2219-01N	1350	111.096	31.540	0.0550	5.2E-17	0.016	0.0065	85.4	99.81	1561	26
2219-01O	1700	126.476	33.249	0.1164	3.4E-17	0.015	0.0084	72.8	100.00	1530	41
	total gas age			n=15	1.8E-14	0.038	0.0749			1376.1	2.9
ML-14-18-1 Bulk Amphibole, JM, J=0.01447063					**NM-19**		**3.4 mg**				
2220-01A	700	96.331	3.808	0.1656	5.6E-16	0.134	0.0719	49.2	4.12	941.7	8.0

Run ID#	Temp	$^{40}Ar/^{39}Ar$	$^{37}Ar/^{39}Ar$	$^{36}Ar/^{39}Ar$	^{39}Ar moles	K/Ca	Cl/K	$\%^{40}Ar^*$	$\%^{39}Ar$	Age	± Err
2220-01B	800	66.933	2.787	0.0678	3.1E-16	0.183	0.0384	70.0	6.36	934.0	7.3
2220-01C	900	60.239	4.521	0.0796	3.7E-16	0.113	0.0360	60.9	9.07	768.4	8.2
2220-01D	1000	70.766	17.990	0.0153	1.3E-15	0.028	0.0568	93.6	18.94	1212.7	2.6
2220-01E	1040	82.736	29.319	0.0176	1.0E-15	0.017	0.0437	93.7	26.32	1357.2	3.1
2220-01F	1070	82.355	25.873	0.0105	1.5E-15	0.020	0.0236	96.2	37.61	1377.9	2.6
2220-01G	1100	79.194	18.873	0.0078	1.3E-15	0.027	0.0170	97.1	47.00	1349.2	2.4
2220-01H	1130	70.223	22.865	0.0102	3.1E-16	0.022	0.0274	95.7	49.26	1225.3	5.3
2220-01I	1160	74.246	20.988	0.0090	4.1E-16	0.024	0.0208	96.4	52.29	1282.2	3.7
2220-01J	1190	84.502	21.272	0.0085	1.3E-15	0.024	0.0253	97.0	61.93	1411.2	2.3
2220-01K	1220	90.769	22.063	0.0084	3.2E-15	0.023	0.0262	97.3	85.64	1484.9	2.2
2220-01L	1250	91.472	27.430	0.0098	1.5E-15	0.019	0.0274	96.8	96.32	1488.2	2.4
2220-01M	1280	100.277	41.276	0.0157	3.9E-16	0.012	0.0435	95.4	99.17	1567.1	5.0
2220-01N	1350	127.848	64.567	0.0497	3.7E-17	0.008	0.0596	88.5	99.44	1750	35
2220-01O	1700	126.349	63.087	0.0616	7.6E-17	0.008	0.0548	85.6	100.00	1699	19
	total gas age		n=15		1.4E-14	0.033	0.0534			1355.2	3.3
ML-14-13b Bulk Amphibole, JM,		J=0.01444197		NM-19		2.3 mg					
2221-01A	700	64.848	0.890	0.0270	1.7E-15	0.573	0.0175	87.7	4.32	1081.3	2.4
2221-01B	800	74.885	0.326	0.0061	2.1E-15	1.563	0.0039	97.6	9.61	1299.5	2.0
2221-01C	900	75.256	0.605	0.0059	3.7E-15	0.844	0.0035	97.7	18.87	1305.1	2.1
2221-01D	1000	76.667	9.797	0.0048	6.9E-15	0.052	0.0079	98.1	36.06	1327.0	2.0
2221-01E	1040	77.035	5.548	0.0030	4.4E-15	0.092	0.0052	98.8	46.95	1338.1	2.0
2221-01F	1070	78.249	7.484	0.0031	2.4E-15	0.068	0.0066	98.8	52.92	1352.7	2.2
2221-01G	1100	80.400	12.443	0.0048	5.8E-15	0.041	0.0072	98.2	67.23	1373.0	1.8
2221-01H	1130	76.820	5.480	0.0023	4.2E-15	0.093	0.0027	99.1	77.75	1337.9	1.8
2221-01I	1160	77.786	4.025	0.0035	2.4E-15	0.127	0.0026	98.7	83.69	1345.6	1.9
2221-01J	1190	83.785	18.038	0.0074	9.5E-16	0.028	0.0124	97.4	86.04	1404.5	2.7
2221-01K	1220	93.867	23.174	0.0077	1.2E-15	0.022	0.0185	97.6	89.12	1520.3	2.5
2221-01L	1250	97.149	22.429	0.0079	3.8E-15	0.023	0.0170	97.6	98.49	1555.8	2.0
2221-01M	1280	99.586	32.487	0.0155	4.4E-16	0.016	0.0206	95.4	99.58	1558.1	4.7
2221-01N	1350	104.863	48.527	0.0250	8.6E-17	0.011	0.0258	92.9	99.79	1585	18
2221-01O	1700	122.183	48.192	0.0550	8.4E-17	0.011	0.0286	86.7	100.00	1674	19
	total gas age		n=15		4.0E-14	0.236	0.4377			1357.5	2.1
ML-6-7 Bulk Amphibole, JM,		J=0.01447585		NM-19		2.8 mg					
2222-01A	700	57.573	1.281	0.0881	1.0E-15	0.398	0.0231	54.8	3.74	678.2	4.7
2222-01B	800	61.181	1.714	0.0333	4.9E-16	0.298	0.0073	83.9	5.53	1002.4	4.5
2222-01C	900	53.092	2.092	0.0312	1.0E-15	0.244	0.0070	82.6	9.26	886.8	3.0
2222-01D	1000	62.316	10.163	0.0076	2.8E-15	0.050	0.0071	96.4	19.49	1128.5	1.8
2222-01E	1040	68.781	11.717	0.0061	1.9E-15	0.044	0.0056	97.3	26.26	1222.5	2.3
2222-01F	1070	72.375	16.077	0.0068	1.3E-15	0.032	0.0051	97.2	31.04	1266.8	2.7
2222-01G	1100	76.031	16.269	0.0062	2.8E-15	0.031	0.0038	97.6	41.35	1316.1	2.1
2222-01H	1130	77.399	14.424	0.0046	4.6E-15	0.035	0.0021	98.2	58.27	1339.0	1.9
2222-01I	1160	68.468	11.275	0.0065	7.3E-16	0.045	0.0037	97.2	60.93	1217.0	2.5
2222-01J	1190	78.583	16.971	0.0077	9.5E-16	0.030	0.0043	97.1	64.40	1342.2	2.5
2222-01K	1220	82.157	17.499	0.0056	4.0E-15	0.029	0.0037	98.0	78.90	1393.6	1.9
2222-01L	1250	84.726	18.508	0.0056	4.2E-15	0.028	0.0050	98.0	94.35	1424.2	1.9
2222-01M	1280	85.293	20.769	0.0081	1.3E-15	0.025	0.0046	97.2	99.25	1422.2	2.5
2222-01N	1350	84.748	22.787	0.0181	1.5E-16	0.022	0.0052	93.7	99.81	1380	11
2222-01O	1700	103.985	22.084	0.0830	5.3E-17	0.023	-0.0004	76.4	100.00	1381	32
	total gas age		n=15		2.7E-14	0.060	0.1201			1278.5	2.3
ML-10-6 Bulk Amphibole, JM,		J=0.01451015		NM-19		2.8 mg					
2223-01A	700	84.678	1.633	0.0734	1.4E-15	0.312	0.0453	74.4	4.81	1171.0	3.7
2223-01B	800	62.125	0.752	0.0114	1.1E-15	0.678	0.0159	94.5	8.88	1112.0	2.6
2223-01C	900	54.921	1.333	0.0185	1.5E-15	0.383	0.0173	90.0	14.30	975.4	2.2
2223-01D	1000	64.212	6.786	0.0055	3.6E-15	0.075	0.0369	97.5	27.12	1165.6	1.8
2223-01E	1040	73.636	10.679	0.0052	2.5E-15	0.048	0.0344	97.9	35.90	1291.4	1.9
2223-01F	1070	78.033	12.791	0.0056	2.0E-15	0.040	0.0274	97.9	43.07	1345.4	2.2
2223-01G	1100	85.630	13.541	0.0053	3.7E-15	0.038	0.0244	98.2	56.17	1438.5	2.2
2223-01H	1130	78.715	10.738	0.0050	1.7E-15	0.048	0.0173	98.1	62.20	1355.9	2.2
2223-01I	1160	67.242	12.254	0.0051	6.9E-16	0.042	0.0198	97.8	64.67	1208.3	3.5
2223-01J	1190	92.180	16.099	0.0071	1.4E-15	0.032	0.0278	97.7	69.61	1507.9	2.6
2223-01K	1220	113.927	16.450	0.0064	4.8E-15	0.031	0.0396	98.3	86.79	1741.4	2.1
2223-01L	1250	112.918	17.192	0.0064	3.3E-15	0.030	0.0348	98.3	98.55	1731.2	2.1
2223-01M	1280	115.885	19.046	0.0117	3.2E-16	0.027	0.0399	97.0	99.67	1745.4	5.1
2223-01N	1350	145.586	22.018	0.0606	4.8E-17	0.023	0.0566	87.7	99.85	1891	28
2223-01O	1700	171.604	26.263	0.1293	4.3E-17	0.019	0.0566	77.7	100.00	1943	35
	total gas age		n=15		2.8E-14	0.100	0.1893			1416.9	2.4
ML-10-8-1 Bulk Amphibole, JM,		J=0.01442939		NM-19		3.8 mg					
2224-01A	700	68.189	0.877	0.0410	3.3E-15	0.582	0.0173	82.2	5.24	1069.1	2.5
2224-01B	800	64.237	0.710	0.0077	2.2E-15	0.719	0.0092	96.4	8.68	1152.0	2.1
2224-01C	900	61.710	0.839	0.0051	4.6E-15	0.608	0.0088	97.5	16.02	1127.9	1.8
2224-01D	1000	64.218	3.870	0.0026	8.2E-15	0.132	0.0114	98.8	29.18	1172.3	1.6

Run ID#	Temp	$^{40}Ar/^{39}Ar$	$^{37}Ar/^{39}Ar$	$^{36}Ar/^{39}Ar$	^{39}Ar moles	K/Ca	Cl/K	$\%^{40}Ar^{*}$	$\%^{39}Ar$	Age	± Err
2224-01E	1040	72.247	7.899	0.0033	6.6E-15	0.065	0.0110	98.6	39.68	1275.7	1.9
2224-01F	1070	74.138	10.648	0.0038	6.5E-15	0.048	0.0080	98.5	50.14	1298.0	2.0
2224-01G	1100	72.176	7.000	0.0024	8.1E-15	0.073	0.0050	99.0	63.13	1278.3	1.6
2224-01H	1130	67.015	3.105	0.0013	6.6E-15	0.164	0.0030	99.4	73.74	1215.1	2.0
2224-01I	1160	68.319	3.060	0.0014	4.3E-15	0.167	0.0030	99.4	80.69	1232.0	1.7
2224-01J	1190	75.162	8.816	0.0042	1.8E-15	0.058	0.0071	98.3	83.51	1309.3	2.2
2224-01K	1220	95.510	19.838	0.0064	2.4E-15	0.026	0.0206	98.0	87.29	1541.9	2.2
2224-01L	1250	93.243	17.718	0.0056	3.8E-15	0.029	0.0140	98.2	93.29	1519.2	2.1
2224-01M	1280	96.754	21.310	0.0076	3.2E-15	0.024	0.0170	97.7	98.35	1551.8	2.3
2224-01N	1350	126.384	41.245	0.0183	8.9E-16	0.012	0.0358	95.7	99.77	1821.9	3.5
2224-01O	1700	120.002	33.723	0.0560	1.5E-16	0.015	0.0229	86.2	100.00	1648	11
	total gas age		n=15		6.3E-14	0.173	0.2422			1277.6	2.0
ML-10-2 Biotite, JM,		J=0.01439601			NM-19		1.2 mg				
2225-01A	600	34.986	0.143	0.0239	1.9E-15	3.578	0.0028	79.7	76.83	609.1	2.2
2225-01B	650	63.891	0.047	0.0182	1.4E-15	10.957	0.0007	91.6	132.41	1102.3	2.5
2225-01C	700	72.951	0.020	0.0093	3.5E-15	25.510	0.0000	96.2	272.15	1259.7	2.0
2225-01D	750	76.680	0.007	0.0022	1.3E-14	70.059	0.0000	99.1	802.90	1333.5	1.7
2225-01E	800	75.710	0.006	0.0005	6.2E-15	90.802	0.0000	99.8	1051.44	1327.7	2.0
2225-01F	870	76.197	0.003	0.0004	2.4E-14	152.651	0.0001	99.8	2024.58	1334.3	1.7
2225-01G	920	76.724	0.003	0.0003	3.1E-14	146.705	0.0000	99.8	3269.09	1340.9	1.9
2225-01H	1000	79.823	0.002	0.0002	6.9E-14	208.842	0.0000	99.9	6031.10	1379.3	3.0
2225-01I	1050	80.813	0.004	0.0002	3.1E-14	128.577	0.0000	99.9	7259.82	1391.4	1.9
2225-01J	1100	80.982	0.003	0.0001	3.5E-14	171.312	0.0000	99.9	8655.82	1393.5	2.1
2225-01K	1200	80.594	0.002	0.0001	6.4E-14	284.048	0.0000	99.9	11223.83	1389.0	2.5
2225-01L	1700	81.461	0.003	0.0002	2.7E-14	170.285	0.0000	99.9	12304.12	1399.0	2.0
	total gas age		n=12		2.5E-15	0.010	0.0095			1599	11
ML-6-10 Biotite, JM,		J=0.01455661			NM-19		2.0 mg				
2226-01A	600	18.366	0.026	0.0064	2.2E-14	19.955	0.0041	89.6	432.30	387.6	1.0
2226-01B	650	53.155	0.009	0.0057	3.5E-15	57.022	0.0014	96.8	500.42	1008.5	1.6
2226-01C	700	71.659	0.006	0.0035	1.2E-14	86.877	0.0008	98.5	735.96	1275.3	1.9
2226-01D	750	79.816	0.004	0.0013	1.7E-14	145.496	0.0004	99.5	1061.45	1386.1	2.0
2226-01E	800	78.863	0.002	0.0006	1.9E-14	211.151	0.0002	99.7	1436.83	1376.8	2.0
2226-01F	870	78.122	0.002	0.0005	2.7E-14	223.305	0.0001	99.8	1970.93	1368.2	1.8
2226-01G	920	79.494	0.005	0.0004	2.3E-14	94.187	0.0002	99.8	2418.11	1385.4	1.9
2226-01H	1000	81.068	0.026	0.0004	2.7E-14	19.380	0.0002	99.8	2948.97	1404.5	2.1
2226-01I	1050	84.263	0.044	0.0003	3.4E-14	11.547	0.0005	99.9	3622.48	1442.7	1.9
2226-01J	1100	83.068	0.016	0.0002	4.3E-14	31.982	0.0005	99.9	4453.05	1429.0	2.1
2226-01K	1200	80.589	0.018	0.0002	7.3E-14	28.770	0.0003	99.9	5881.77	1399.3	2.5
2226-01L	1700	80.044	0.029	0.0003	4.5E-14	17.367	0.0002	99.9	6763.21	1392.5	2.0
	total gas age		n=10		5.1E-15	0.030	0.0912			1334.0	9.9
ML-10-6 Actinolite, JM,		J=0.009526213			NM-29		0.175 mg				
2496-01A	700	142.173	1.547	0.3054	2.4E-15	0.330	0.2238	36.6	#REF!	726.8	7.1
2496-01B	800	89.215	0.972	0.0411	2.4E-15	0.525	0.0366	86.4	#REF!	994.3	2.2
2496-01C	900	80.615	1.343	0.0234	3.5E-15	0.380	0.0295	91.5	#REF!	961.0	2.2
2496-01D	1000	91.517	6.365	0.0067	6.5E-15	0.080	0.0435	98.3	#REF!	1120.7	2.2
2496-01E	1040	107.001	9.430	0.0085	3.6E-15	0.054	0.0386	98.3	#REF!	1258.4	2.1
2496-01F	1070	114.836	10.099	0.0072	4.9E-15	0.051	0.0300	98.8	#REF!	1328.7	2.4
2496-01G	1100	89.367	6.322	0.0071	2.7E-15	0.081	0.0215	98.2	#REF!	1099.5	2.4
2496-01H	1150	97.918	9.563	0.0084	2.5E-15	0.053	1.1475	98.2	#REF!	1178.8	2.3
2496-01I	1200	140.211	14.356	0.0123	3.2E-15	0.036	0.1558	98.2	#REF!	1521.9	2.3
2496-01J	1250	153.487	14.837	0.0099	7.6E-15	0.034	0.0396	98.8	#REF!	1624.1	2.4
2496-01K	1400	129.308	13.016	0.0196	1.0E-15	0.039	0.0347	96.3	#REF!	1419.8	3.5
2496-01L	1700	124.195	12.397	0.0402	6.1E-16	0.041	0.0418	91.2	#REF!	1328.4	6.3
	total gas age		n=12		4.1E-14	0.125	0.1689			1250.7	2.7
ML-13-9b Hornblende, JM,		J=0.009528751			NM-29		02.08 mg				
2497-01A	700	51.020	1.169	0.0522	2.9E-15	0.437	0.2639	69.9	10.45	528.2	2.5
2497-01B	800	57.470	0.536	0.0093	2.4E-15	0.952	0.0230	95.2	19.13	757.5	1.8
2497-01C	900	57.895	1.152	0.0073	3.0E-15	0.443	0.0155	96.4	29.86	769.8	1.7
2497-01D	1000	78.482	6.238	0.0057	4.6E-15	0.082	0.0254	98.4	46.21	998.5	1.7
2497-01E	1040	98.503	9.223	0.0068	2.9E-15	0.055	0.0314	98.7	56.40	1188.1	1.8
2497-01F	1070	101.205	8.681	0.0059	3.5E-15	0.059	0.0261	98.9	68.75	1213.9	2.1
2497-01G	1100	84.686	7.235	0.0065	1.8E-15	0.071	0.0305	98.4	75.30	1058.2	2.2
2497-01H	1150	94.529	10.708	0.0084	1.9E-15	0.048	1.1666	98.2	81.96	1149.8	2.2
2497-01I	1200	122.649	14.459	0.0123	2.1E-15	0.035	0.3089	97.9	89.46	1386.0	2.3
2497-01J	1250	135.867	14.629	0.0104	2.5E-15	0.035	0.0553	98.6	98.24	1494.0	2.2
2497-01K	1400	143.669	16.244	0.0326	3.5E-16	0.031	0.1156	94.1	99.48	1505.4	6.2
2497-01L	1700	159.663	15.096	0.1282	1.5E-16	0.034	0.0679	77.0	100.00	1409	14
	total gas age		n=12		2.8E-14	0.216	0.2835			1044.8	2.1
ML-10-8 Biotite, JM,		J=0.00951019			NM-29		0.2 mg				
2694-01A	650	27.190	0.618	0.0450	8.2E-16	0.825	1.1374	51.2	13.82	224.4	3.4

Run ID#	Temp	$^{40}Ar/^{39}Ar$	$^{37}Ar/^{39}Ar$	$^{36}Ar/^{39}Ar$	^{39}Ar moles	K/Ca	Cl/K	$\%^{40}Ar^*$	$\%^{39}Ar$	Age	± Err
2694-01B	750	93.134	0.217	0.0125	4.4E-16	2.346	0.1676	96.0	21.30	1110.4	4.5
2694-01C	850	95.718	0.098	0.0069	7.6E-16	5.213	0.0503	97.9	34.09	1149.3	3.3
2694-01D	920	95.482	0.117	0.0050	5.0E-16	4.349	0.0316	98.4	42.56	1152.1	3.4
2694-01E	1000	98.740	0.139	0.0048	6.2E-16	3.680	0.0505	98.6	53.06	1182.0	3.2
2694-01F	1075	102.204	0.169	0.0162	6.4E-16	3.026	0.1357	95.3	63.94	1182.8	3.5
2694-01G	1120	101.352	0.149	0.0049	7.6E-16	3.417	0.1810	98.6	76.71	1204.9	2.7
2694-01H	1180	106.254	0.035	0.0042	1.0E-15	14.678	0.0962	98.8	94.09	1249.1	2.8
2694-01I	1210	110.446	0.130	0.0210	2.5E-16	3.917	9.5346	94.4	98.38	1242.6	7.1
2694-01J	1250	118.180	2.617	0.1312	1.4E-17	0.195	15.9333	67.4	98.63	1018	110
2694-01K	1300	142.132	18.976	0.3753	4.9E-18	0.027	11.4380	23.0	98.71	494	478
2694-01L	1700	215.801	6.989	0.6773	7.7E-17	0.073	1.4011	7.5	100.00	259	71
	total gas age		n=12		5.9E-15	5.198	3.9572			1042	5
ML-14-25 Actinolite, JM, J=0.009518372				NM-29		10.97 mg					
2695-01A	700	81.615	1.127	0.1416	7.7E-15	0.453	0.1879	48.8	4.85	580.3	3.8
2695-01B	800	105.449	0.596	0.0407	4.9E-15	0.856	0.0292	88.6	7.90	1148.2	2.5
2695-01C	900	98.849	0.599	0.0183	1.0E-14	0.852	0.0160	94.6	14.15	1148.5	1.9
2695-01D	1000	95.799	2.168	0.0037	1.7E-14	0.235	0.0159	99.0	24.99	1161.9	1.6
2695-01E	1040	107.558	5.923	0.0038	1.5E-14	0.086	0.0185	99.4	34.55	1269.7	1.8
2695-01F	1070	118.217	10.507	0.0065	1.6E-14	0.049	0.0160	99.0	44.56	1357.8	2.0
2695-01G	1100	115.279	8.335	0.0034	1.9E-14	0.061	0.0102	99.7	56.61	1338.5	1.8
2695-01H	1160	110.003	4.182	0.0017	3.3E-14	0.122	0.0066	99.8	77.15	1293.4	2.0
2695-01I	1200	108.410	10.660	0.0054	4.3E-15	0.048	0.2419	99.3	79.83	1279.1	2.1
2695-01J	1250	124.606	13.274	0.0054	7.1E-15	0.038	0.0284	99.5	84.31	1415.3	2.2
2695-01K	1400	125.005	15.300	0.0060	2.5E-14	0.033	0.0153	99.5	99.97	1419.8	2.0
2695-01L	1750	132.289	11.341	0.1947	4.0E-17	0.045	0.0351	57.2	100.00	984	50
	total gas age		n=12		1.6E-13	0.181	0.3109			1265.5	2.1
ML-9-3b Actinolite, JM, J=0.009540874				NM-29		1.58 mg					
2698-01A	700	29.747	10.117	0.0624	1.4E-15	0.050	24.1362	40.6	12.95	197.9	3.7
2698-01B	800	58.128	13.688	0.0198	5.2E-16	0.037	19.2022	91.7	17.88	747.7	5.3
2698-01C	900	73.490	4.837	0.0033	1.2E-15	0.105	0.0761	99.1	28.94	954.6	2.7
2698-01D	1000	76.039	6.619	0.0030	9.6E-16	0.077	0.0589	99.5	38.02	983.7	3.1
2698-01E	1040	80.592	10.630	0.0045	4.8E-16	0.048	0.0771	99.3	42.55	1029.6	5.3
2698-01F	1070	90.373	15.910	0.0035	4.9E-16	0.032	0.0688	100.2	47.17	1132.7	4.9
2698-01G	1100	104.000	22.613	0.0103	4.7E-16	0.023	0.0603	98.7	51.63	1246.4	3.9
2698-01H	1150	115.831	29.435	0.0137	2.0E-15	0.017	0.0344	98.4	70.66	1347.8	2.6
2698-01I	1200	91.510	5.387	0.0056	7.3E-16	0.095	1.5878	98.6	77.58	1123.7	3.3
2698-01J	1250	90.586	11.732	0.0068	8.9E-16	0.043	0.6886	98.8	85.98	1120.1	2.8
2698-01K	1400	116.897	28.892	0.0141	1.4E-15	0.018	0.0379	98.3	99.34	1354.9	3.3
2698-01L	1700	150.978	19.148	0.2086	6.9E-17	0.027	0.0326	60.1	100.00	1137	30
	total gas age		n=12		1.1E-14	0.048	0.0297			1028.8	3.6
ML-9-3b Hornblende, JM, J=0.009543184				NM-29		3.65 mg					
2699-01A	700	21.469	3.575	0.0742	1.8E-15	0.143	11.3050	-0.9	18.18	-3.4	3.6
2699-01B	800	15.629	16.474	0.0471	5.8E-16	0.031	41.3690	18.9	23.94	50.6	5.4
2699-01C	900	40.399	64.990	0.0547	8.8E-16	0.008	7.7156	72.3	32.74	462.1	4.7
2699-01D	1000	70.169	46.557	0.0260	5.8E-16	0.011	0.1675	94.1	38.56	905.1	4.7
2699-01E	1040	64.297	60.550	0.0251	9.8E-17	0.008	0.2006	95.7	39.53	862	20
2699-01F	1070	110.267	53.223	0.0280	3.1E-16	0.010	0.1031	96.2	42.63	1296.2	5.5
2699-01G	1100	119.116	56.595	0.0271	7.1E-16	0.009	0.0658	96.9	49.71	1378.6	4.2
2699-01H	1150	121.295	45.028	0.0222	1.4E-15	0.011	0.0511	97.4	63.45	1393.1	3.0
2699-01I	1200	100.091	78.445	0.0663	1.1E-16	0.007	13.6127	86.4	64.60	1133	14
2699-01J	1250	118.535	56.231	0.0280	1.7E-15	0.009	0.1678	96.6	81.25	1370.8	3.0
2699-01K	1400	126.383	65.025	0.0330	1.8E-15	0.008	0.0561	96.2	99.06	1435.4	2.5
2699-01L	1700	147.024	55.577	0.2300	9.4E-17	0.009	0.0549	56.7	100.00	1088	26
	total gas age		n=12		1.0E-14	0.035	0.0386			940.3	4.1
ML-9-6 Actinolite, JM, J=0.009547693				NM-29		1.89 mg					
2700-01A	700	36.685	2.792	0.0981	4.9E-16	0.183	4.8841	21.5	11.31	131.4	7.1
2700-01B	800	35.386	7.923	0.0568	9.0E-17	0.064	3.2136	54.2	13.41	305	22
2700-01C	900	20.975	1.887	0.0196	3.0E-16	0.270	0.1897	72.9	20.27	246.3	6.3
2700-01D	1000	16.558	1.642	0.0042	1.1E-15	0.311	0.0405	93.1	45.73	248.1	1.7
2700-01E	1040	38.946	7.870	0.0079	3.4E-16	0.065	0.1118	95.5	53.75	550.9	4.6
2700-01F	1070	56.988	11.237	0.0086	2.6E-16	0.045	0.1481	97.0	59.89	769.8	5.3
2700-01G	1100	80.481	17.239	0.0100	2.4E-16	0.030	0.1270	98.0	65.41	1021.8	6.5
2700-01H	1150	104.834	22.980	0.0110	6.5E-16	0.022	0.0986	98.6	80.42	1253.0	3.5
2700-01I	1200	43.113	19.155	0.0253	1.7E-16	0.027	9.6192	86.1	84.27	553.4	9.1
2700-01J	1250	96.476	45.008	0.0256	4.2E-16	0.011	0.2262	95.7	93.97	1167.7	4.2
2700-01K	1400	121.708	62.118	0.0524	1.6E-16	0.008	0.3183	91.2	97.77	1345.1	8.8
2700-01L	1700	148.641	20.455	0.1408	9.6E-17	0.025	0.0593	73.1	100.00	1297	19
	total gas age		n=12		4.3E-15	0.136	0.1055			651.8	5.2
ML-9-6 Hornblende, JM, J=0.00954989				NM-29		3.06 mg					
2701-01A	700	53.009	17.296	0.1494	1.3E-15	0.029	14.9900	19.2	12.98	169	24

Run ID#	Temp	$^{40}Ar/^{39}Ar$	$^{37}Ar/^{39}Ar$	$^{36}Ar/^{39}Ar$	^{39}Ar moles	K/Ca	Cl/K	$\%^{40}Ar^*$	$\%^{39}Ar$	Age	± Err
2701-01B	800	60.632	5.854	0.1101	2.3E-16	0.087	5.0300	47.0	15.20	436	13
2701-01C	900	64.022	20.072	0.0709	3.0E-16	0.025	0.2669	69.7	18.12	647.7	8.2
2701-01D	1000	83.610	30.562	0.0290	5.8E-16	0.017	0.1459	92.5	23.78	1014.7	4.6
2701-01E	1040	97.406	34.613	0.0305	4.8E-16	0.015	0.1696	93.4	28.42	1149.3	5.1
2701-01F	1070	113.041	43.149	0.0354	8.7E-16	0.012	0.1134	93.7	36.87	1288.5	4.5
2701-01G	1100	114.883	26.926	0.0133	1.2E-15	0.019	0.0734	98.4	48.70	1338.5	3.5
2701-01H	1150	89.353	27.375	0.0183	4.0E-16	0.019	0.0965	96.3	52.54	1097.6	4.5
2701-01I	1200	96.801	30.050	0.0256	4.4E-16	0.017	3.7777	94.5	56.77	1151.1	4.4
2701-01J	1250	124.585	32.492	0.0215	1.5E-15	0.016	0.0798	96.9	71.25	1405.6	3.5
2701-01K	1400	133.384	39.479	0.0218	2.6E-15	0.013	0.0789	97.4	96.86	1484.0	2.5
2701-01L	1700	131.120	46.164	0.0523	3.2E-16	0.011	0.0736	90.9	100.00	1402.9	7.1
total gas age			n=12		1.0E-14	0.019	0.0208			1147.0	6.7
ML-6-7 Actinolite, JM, J=0.009554171					NM-29		1.11 mg				
2702-01A	700	54.953	9.504	0.1333	6.7E-16	0.054	2.8326	29.6	9.26	262.3	6.7
2702-01B	800	62.295	9.691	0.0439	1.4E-16	0.053	0.4382	80.3	11.20	709	10
2702-01C	900	73.987	1.542	0.0238	3.8E-16	0.331	0.1558	90.6	16.47	894.0	4.6
2702-01D	1000	87.240	5.706	0.0189	4.6E-16	0.089	0.1139	94.1	22.80	1047.5	4.2
2702-01E	1040	109.337	11.408	0.0096	4.4E-16	0.045	0.1050	98.2	28.85	1280.8	4.1
2702-01F	1070	115.428	11.957	0.0100	3.8E-16	0.043	0.1141	98.2	34.16	1331.9	4.7
2702-01G	1100	117.746	13.426	0.0088	3.9E-16	0.038	0.0880	98.6	39.49	1355.8	4.0
2702-01H	1150	123.145	14.403	0.0063	2.7E-15	0.035	0.0183	99.4	76.11	1406.9	2.2
2702-01I	1200	113.019	11.142	0.0221	3.0E-16	0.046	6.2966	94.9	80.26	1280.3	5.5
2702-01J	1250	123.106	15.950	0.0091	9.3E-16	0.032	0.1412	98.8	93.03	1402.0	3.1
2702-01K	1400	124.821	17.450	0.0150	3.7E-16	0.029	0.0519	97.5	98.13	1403.6	5.0
2702-01L	1700	162.123	17.279	0.2090	1.4E-16	0.030	0.0320	62.7	100.00	1235	15
total gas age			n=12		7.2E-15	0.057	0.0841			1214.0	4.0
ML-6-7 Hornblende, JM, J=0.009556255					NM-29		1.93 mg				
2703-01A	700	39.134	2.343	0.0715	1.0E-15	0.218	1.8463	46.4	6.80	289.2	3.9
2703-01B	800	69.938	1.112	0.0202	5.0E-16	0.459	0.1803	91.6	10.17	861.9	3.6
2703-01C	900	65.904	1.577	0.0309	8.9E-16	0.324	0.0886	86.3	16.14	783.9	3.0
2703-01D	1000	86.077	6.158	0.0126	1.0E-15	0.083	0.0559	96.2	23.05	1055.2	2.9
2703-01E	1040	100.309	11.702	0.0093	7.0E-16	0.044	0.0646	98.1	27.72	1203.4	3.1
2703-01F	1070	107.861	13.488	0.0096	7.2E-16	0.038	0.0522	98.3	32.53	1271.0	3.3
2703-01G	1100	113.187	17.774	0.0091	9.8E-16	0.029	0.0301	98.8	39.10	1323.1	3.0
2703-01H	1150	118.452	13.495	0.0061	4.1E-15	0.038	0.0104	99.3	66.76	1368.6	1.9
2703-01I	1200	116.471	14.889	0.0129	1.1E-15	0.034	1.6507	97.7	74.39	1337.5	2.7
2703-01J	1250	123.292	16.542	0.0082	2.2E-15	0.031	0.0345	99.0	89.31	1406.5	2.9
2703-01K	1400	124.800	17.829	0.0150	1.1E-15	0.029	0.0196	97.5	96.59	1404.1	3.2
2703-01L	1700	123.372	18.864	0.0308	5.1E-16	0.027	0.0247	93.8	100.00	1356.0	4.4
total gas age			n=12		1.5E-14	0.082	0.1435			1211.6	2.8
ML-14-18-1 Actinolite, JM, J=0.009558301					NM-29		1.99 mg				
2704-01A	700	43.759	22.573	0.0836	1.2E-15	0.023	18.5475	47.4	14.20	331.4	3.8
2704-01B	800	41.137	6.493	0.0379	2.0E-16	0.079	10.9178	74.0	16.53	462	13
2704-01C	900	55.361	7.403	0.0196	1.6E-16	0.069	0.4391	90.6	18.37	709	11
2704-01D	1000	88.158	14.634	0.0151	2.7E-16	0.035	0.2043	96.2	21.50	1079.2	7.0
2704-01E	1040	110.290	15.922	0.0183	3.2E-16	0.032	0.1158	96.2	25.17	1273.2	5.9
2704-01F	1070	118.689	16.146	0.0103	6.0E-16	0.032	0.0559	98.5	32.17	1364.0	4.5
2704-01G	1100	123.621	16.026	0.0081	2.8E-15	0.032	0.0209	99.0	64.89	1408.8	2.2
2704-01H	1150	112.081	14.876	0.0499	1.7E-16	0.034	0.1289	87.8	66.85	1206	10
2704-01I	1200	79.730	14.665	0.0188	4.6E-16	0.035	3.7327	94.4	72.24	985.9	3.8
2704-01J	1250	112.479	15.879	0.0125	2.2E-15	0.032	0.0381	97.8	97.38	1306.5	2.7
2704-01K	1400	167.331	19.082	0.0879	1.6E-16	0.027	0.2126	85.3	99.29	1567	11
2704-01L	1700	200.088	16.549	0.3271	6.1E-17	0.031	0.1601	52.3	100.00	1262	33
total gas age			n=12		8.6E-15	0.033	0.0171			1151.9	4.0
ML-14-18-1 Hornblende, JM, J=0.009560309					NM-29		1.75 mg				
2705-01A	700	39.770	22.474	0.0920	8.6E-16	0.023	5.0212	36.0	9.72	234.7	4.8
2705-01B	800	56.627	7.568	0.0665	2.3E-16	0.067	0.4293	66.3	12.32	556	11
2705-01C	900	72.072	18.425	0.0358	2.4E-16	0.028	0.2128	87.3	15.02	858.3	7.8
2705-01D	1000	110.750	18.371	0.0177	1.2E-15	0.028	0.0664	96.5	28.19	1282.0	3.3
2705-01E	1040	122.678	21.808	0.0218	8.5E-16	0.023	0.0557	96.1	37.86	1376.3	3.5
2705-01F	1070	118.850	17.237	0.0160	8.0E-16	0.030	0.0446	97.1	46.90	1353.0	3.3
2705-01G	1100	111.953	16.408	0.0117	7.3E-16	0.031	0.0444	98.0	55.13	1304.9	3.6
2705-01H	1150	101.567	17.301	0.0211	2.9E-16	0.029	3.6909	95.2	58.41	1191.1	5.9
2705-01I	1200	119.402	18.651	0.0127	8.1E-16	0.027	0.4227	98.0	67.57	1367.5	3.5
2705-01J	1250	123.224	18.167	0.0114	2.2E-15	0.028	0.0328	98.4	92.52	1401.0	2.6
2705-01K	1400	118.256	20.650	0.0211	5.3E-16	0.025	0.0353	96.0	98.57	1340.1	4.4
2705-01L	1700	139.389	17.306	0.1064	1.3E-16	0.029	0.0248	78.4	100.00	1302	14
total gas age			n=12		8.8E-15	0.028	0.0118			1205.7	4.0
ML 14-18-2 Actinolite, JM, J=0.01070469					NM-42		0.51 mg				
5897-01A	700	843.093	4.546	2.7029	5.0E-17	0.112	0.3414	5.3	7.54	707	214

Run ID#	Temp	$^{40}Ar/^{39}Ar$	$^{37}Ar/^{39}Ar$	$^{36}Ar/^{39}Ar$	^{39}Ar moles	K/Ca	Cl/K	$\%^{40}Ar^{*}$	$\%^{39}Ar$	Age	± Err
5897-01B	800	200.127	1.503	0.6032	3.6E-17	0.340	0.2023	11.0	12.95	381	81
5897-01C	900	219.633	2.072	0.6824	3.5E-17	0.246	0.2643	8.3	18.16	320	101
5897-01D	950	441.414	6.670	1.3932	2.6E-17	0.076	0.7058	6.8	22.00	508	209
5897-01E	1000	273.586	8.239	0.7789	2.1E-17	0.062	0.6843	16.1	25.16	700	150
5897-01F	1040	196.395	20.052	0.4837	2.7E-17	0.025	0.5074	28.0	29.19	844	80
5897-01G	1080	147.235	17.847	0.2123	5.0E-17	0.029	0.2735	58.3	36.68	1187	31
5897-01H	1120	122.327	15.181	0.0911	1.3E-16	0.034	0.1291	78.9	55.35	1290	11
5897-01I	1160	134.490	16.268	0.1500	1.1E-16	0.031	0.2842	68.0	71.95	1241	14
5897-01J	1200	157.417	22.615	0.1607	1.3E-16	0.023	6.4310	70.9	90.84	1434	16
5897-01K	1250	121.247	19.696	0.0273	5.2E-17	0.026	0.1103	94.6	98.63	1459	21
5897-01L	1300	141.438	19.012	0.1709	5.8E-18	0.027	0.1757	65.3	99.49	1252	170
5897-01M	1650	616.678	11.034	1.6074	3.4E-18	0.046	0.1270	23.1	100.00	1680	900
	total gas age		n=13		6.7E-16	0.066	0.0986			1106	59
ML 14-18-2 Hornblende, JM,		J=0.01073805			NM-42		1.14 mg				
5898-01A	700	789.680	2.426	2.5600	3.2E-17	0.210	0.1732	4.2	1.54	553	340
5898-01B	800	192.696	2.398	0.5035	4.6E-17	0.213	0.4156	22.9	3.74	700	62
5898-01C	900	-46.877	2.845	0.4139	3.1E-17	0.179	0.4169	360.5	5.23	0	678
5898-01D	950	153.136	6.687	0.3417	4.0E-17	0.076	0.5704	34.4	7.12	811	51
5898-01E	1000	117.731	11.438	0.1239	5.3E-17	0.045	0.3174	69.6	9.64	1146	23
5898-01F	1040	118.950	16.092	0.0867	5.5E-17	0.032	0.2588	79.5	12.24	1274	21
5898-01G	1080	114.290	19.008	0.0568	1.0E-16	0.027	0.1485	86.6	16.99	1318	12
5898-01H	1120	111.191	17.452	0.0153	4.1E-16	0.029	0.0459	97.1	36.20	1400.8	5.6
5898-01I	1160	111.081	16.602	0.0131	6.0E-16	0.031	0.0414	97.6	64.56	1404.6	4.1
5898-01J	1200	120.104	16.698	0.0516	2.0E-16	0.031	4.2790	88.4	74.06	1383.4	7.4
5898-01K	1250	114.625	17.485	0.0149	4.3E-16	0.029	0.2152	97.3	94.28	1432.8	4.4
5898-01L	1300	114.689	17.057	0.0176	8.8E-17	0.030	0.0417	96.6	98.46	1426	11
5898-01M	1650	132.655	16.298	0.0641	3.3E-17	0.031	0.0647	86.6	100.00	1462	27
	total gas age		n=13		2.1E-15	0.040	0.0738			1335	24
ML 14-18-2 Bulk Amphibole, JM,		J=0.01073225			NM-42		1.04 mg				
5899-01A	700	116.042	1.880	0.3409	1.6E-16	0.271	0.1007	13.3	5.39	277	28
5899-01B	800	49.496	2.191	0.0821	1.0E-16	0.233	0.1164	51.3	8.84	435	18
5899-01C	900	63.137	5.774	0.0938	5.5E-17	0.088	0.1670	56.8	10.71	589	26
5899-01D	950	62.269	12.311	0.0969	7.3E-17	0.041	0.2530	55.5	13.20	573	20
5899-01E	1000	55.609	10.940	0.0425	1.1E-16	0.047	0.1770	78.9	16.97	701	11
5899-01F	1040	70.979	17.278	0.0409	1.5E-16	0.030	0.1303	84.8	22.23	907.8	9.3
5899-01G	1080	96.805	18.579	0.0204	3.2E-16	0.027	0.0746	95.2	33.12	1252.6	5.4
5899-01H	1120	102.632	16.323	0.0081	5.3E-16	0.031	0.0414	98.9	51.19	1339.7	4.3
5899-01I	1160	91.321	15.008	0.0116	3.2E-16	0.034	0.1047	97.5	62.18	1219.2	5.0
5899-01J	1200	99.966	17.774	0.0171	3.6E-16	0.029	2.3456	96.3	74.52	1291.6	5.3
5899-01K	1250	109.701	22.142	0.0040	2.5E-16	0.023	0.0861	100.5	82.98	1423.6	5.6
5899-01L	1300	117.435	23.322	0.0043	3.4E-16	0.022	0.0467	100.4	94.50	1492.2	4.5
5899-01M	1650	109.286	21.683	0.0276	1.6E-16	0.024	0.0370	94.0	100.00	1355.7	8.7
	total gas age		n=13		2.9E-15	0.050	0.0834			1168.1	8.1
ML 10-8 Biotite, JM,		J=0.01072567			NM-42		0.68 mg				
5913-01A	600	46.903	0.345	0.1400	1.7E-16	1.477	0.1022	11.8	1.57	104	15
5913-01B	670	28.295	0.207	0.0241	2.0E-16	2.470	0.1124	74.8	3.43	369.1	6.5
5913-01C	730	31.931	0.105	0.0936	1.4E-17	4.864	0.0216	13.3	3.56	80	87
5913-01D	780	80.665	0.310	0.0142	4.2E-16	1.646	0.0417	94.8	7.54	1080.8	3.9
5913-01E	830	93.741	0.041	0.0072	5.8E-16	12.404	0.0216	97.7	12.99	1234.6	3.5
5913-01F	900	96.488	0.025	0.0020	1.0E-15	20.810	0.0134	99.3	22.75	1275.7	2.9
5913-01G	975	97.731	0.048	0.0030	8.4E-16	10.644	0.0216	99.1	30.63	1284.9	2.9
5913-01H	1050	96.378	0.101	0.0031	1.2E-15	5.046	0.0204	99.0	41.51	1271.8	3.0
5913-01I	1150	96.304	0.182	0.0012	3.7E-15	2.809	0.0089	99.6	76.30	1276.5	2.4
5913-01J	1250	98.008	0.141	0.0017	2.2E-15	3.624	0.4043	99.5	97.00	1291.4	2.6
5913-01K	1600	94.150	0.274	0.0105	3.2E-16	1.862	0.0634	96.7	100.00	1229.3	5.5
	total gas age		n=11		1.1E-14	6.020	6.0719			1231.3	3.2
ML 10-8 Actinolite, JM,		J=0.01071991			NM-42		0.16 mg				
5914-01A	700	906.107	2.511	1.6978	5.5E-17	0.203	0.4965	44.7	7.04	3024	53
5914-01B	800	108.302	3.749	0.1818	5.9E-17	0.136	0.2041	50.6	14.57	836	30
5914-01C	900	113.951	0.412	0.1440	7.1E-17	1.239	0.2525	62.7	23.72	1026	24
5914-01D	950	109.655	0.566	0.1253	6.2E-17	0.902	0.3395	66.2	31.71	1039	26
5914-01E	1000	105.462	0.786	0.1318	5.6E-17	0.650	0.3234	63.1	38.84	972	28
5914-01F	1040	107.064	1.377	0.0969	4.7E-17	0.370	0.3194	73.3	44.89	1102	28
5914-01G	1080	102.349	2.784	0.0548	6.0E-17	0.183	0.2587	84.4	52.56	1184	24
5914-01H	1120	100.212	3.805	0.0301	9.5E-17	0.134	0.1480	91.4	64.72	1236	13
5914-01I	1160	95.948	1.292	0.0131	1.6E-16	0.395	0.1505	96.0	85.45	1240.3	8.1
5914-01J	1200	102.406	6.693	0.0695	7.1E-17	0.076	12.8278	80.4	94.54	1146	17
5914-01K	1250	82.821	15.311	0.0092	3.3E-17	0.033	0.6776	98.1	98.71	1139	32
5914-01L	1300	514.857	26.369	-0.1500	2.4E-18	0.019	1.3726	109.0	99.02	3543	286
5914-01M	1650	790.157	16.000	0.2030	7.7E-18	0.032	0.6087	92.6	100.00	3950	120
	total gas age		n=13		7.8E-16	0.400	0.3778			1288	24

Run ID#	Temp	$^{40}Ar/^{39}Ar$	$^{37}Ar/^{39}Ar$	$^{36}Ar/^{39}Ar$	^{39}Ar moles	K/Ca	Cl/K	$\%^{40}Ar^*$	$\%^{39}Ar$	Age	± Err
ML 10-8 Hornblende, JM, J=0.01073843					NM-42		0.60 mg				
5916-01A	700	299.733	1.966	0.9540	1.3E-16	0.260	0.8792	6.0	4.62	319	64
5916-01B	800	129.470	0.663	0.2166	1.3E-16	0.770	0.3027	50.6	8.93	961	17
5916-01C	900	103.968	0.866	0.0964	1.3E-16	0.589	0.1754	72.7	13.46	1072	13
5916-01D	950	80.150	1.471	0.0525	1.2E-16	0.347	0.1843	80.8	17.53	953	14
5916-01E	1000	79.267	3.037	0.0240	9.2E-17	0.168	0.1973	91.3	20.70	1039	14
5916-01F	1040	91.236	6.654	0.0205	1.9E-16	0.077	0.1229	93.9	27.07	1180.7	7.1
5916-01G	1080	104.210	12.123	0.0113	4.4E-16	0.042	0.0529	97.7	42.10	1340.5	4.9
5916-01H	1120	101.921	8.478	0.0060	4.3E-16	0.060	0.0445	98.9	56.87	1328.7	4.3
5916-01I	1160	96.116	6.048	0.0094	2.5E-16	0.084	0.1197	97.6	65.58	1260.6	6.1
5916-01J	1200	108.762	12.483	0.0193	2.7E-16	0.041	3.5290	95.6	74.92	1361.1	6.0
5916-01K	1250	102.001	12.134	0.0051	4.1E-16	0.042	0.0510	99.4	88.90	1337.0	5.2
5916-01L	1300	83.257	9.690	0.0063	2.8E-16	0.053	0.0224	98.6	98.61	1146.5	5.5
5916-01M	1650	73.382	3.676	0.0357	4.0E-17	0.139	0.0663	86.0	100.00	935	28
	total gas age		n=13		2.9E-15	0.135	0.2329			1197.5	9.8
ML 10-8-2 Bulk Amphibole, JM, J=0.01077295					NM-42		0.42 mg				
5917-01A	700	761.223	3.034	2.5152	3.6E-17	0.168	0.4103	2.4	2.61	324	502
5917-01B	800	122.082	1.126	0.2275	5.3E-17	0.453	0.1004	45.0	6.43	839	45
5917-01C	900	145.314	1.847	0.2097	4.9E-17	0.276	0.1642	57.4	9.96	1158	36
5917-01D	950	167.947	3.098	0.2956	5.6E-17	0.165	0.3835	48.1	14.02	1132	40
5917-01E	1000	133.332	5.103	0.1688	6.8E-17	0.100	0.3516	62.9	18.92	1164	25
5917-01F	1040	123.110	9.924	0.1030	1.1E-16	0.051	0.1804	75.9	27.19	1262	14
5917-01G	1080	111.420	15.208	0.0316	3.1E-16	0.034	0.0634	92.6	49.63	1359.1	6.1
5917-01H	1120	102.533	7.705	0.0198	3.4E-16	0.066	0.0614	94.8	73.85	1297.9	5.2
5917-01I	1160	118.889	11.244	0.0704	1.6E-16	0.045	5.1226	83.2	85.62	1316	11
5917-01J	1200	110.547	17.433	0.0027	1.0E-16	0.029	0.0901	100.5	92.99	1432	13
5917-01K	1250	119.649	22.435	0.0035	2.9E-17	0.023	0.0870	100.6	95.05	1516	35
5917-01L	1300	110.106	21.754	0.0248	3.2E-17	0.023	0.0291	94.8	97.38	1375	33
5917-01M	1650	149.673	23.523	0.0663	3.6E-17	0.022	0.0650	88.1	100.00	1612	28
	total gas age		n=13		1.4E-15	0.080	0.1280			1274	27
CP-1-2b:a Muscovite, JM, J=0.01068425					NM-42		0.99 mg				
5919-01A	600	48.736	0.097	0.1145	9.0E-16	5.249	0.0132	30.6	1.76	266.4	6.5
5919-01B	650	78.456	0.071	0.0203	8.9E-16	7.219	0.0062	92.3	3.50	1034.0	3.1
5919-01C	700	101.548	0.035	0.0146	2.2E-16	14.587	0.0058	95.7	3.94	1284.9	6.2
5919-01D	750	107.213	0.022	0.0084	2.0E-15	23.539	0.0040	97.7	7.78	1354.6	2.9
5919-01E	800	106.445	0.010	0.0044	3.4E-15	52.224	0.0029	98.8	14.45	1358.3	2.8
5919-01F	825	104.617	0.007	0.0032	3.7E-15	73.796	0.0028	99.1	21.60	1344.8	2.6
5919-01G	850	103.968	0.006	0.0032	3.8E-15	82.545	0.0021	99.1	29.10	1338.9	2.6
5919-01H	875	103.827	0.005	0.0028	3.9E-15	101.149	0.0022	99.2	36.77	1338.8	2.6
5919-01I	900	104.239	0.004	0.0027	3.7E-15	115.313	0.0021	99.2	43.92	1342.8	2.7
5919-01J	925	104.742	0.004	0.0024	2.8E-15	117.528	0.0024	99.3	49.37	1348.3	2.7
5919-01K	950	105.554	0.006	0.0028	3.6E-15	92.270	0.0034	99.2	56.34	1354.5	2.7
5919-01L	975	105.303	0.005	0.0033	2.3E-15	107.783	0.0045	99.1	60.77	1350.9	2.8
5919-01M	1000	104.983	0.001	0.0042	1.7E-15	470.076	0.0056	98.8	64.11	1345.4	2.9
5919-01N	1040	105.411	0.004	0.0041	2.2E-15	113.839	0.0058	98.8	68.45	1349.6	2.8
5919-01O	1080	105.722	0.006	0.0027	2.9E-15	86.053	0.0050	99.2	74.14	1356.4	2.8
5919-01P	1120	106.017	0.008	0.0019	3.6E-15	64.141	0.0051	99.4	81.18	1361.1	2.5
5919-01Q	1180	106.872	0.020	0.0029	7.6E-15	25.846	0.1326	99.2	96.03	1366.1	2.7
5919-01R	1220	106.602	0.076	0.0007	1.5E-15	6.671	0.0118	99.8	99.01	1369.6	3.1
5919-01S	1400	113.210	0.833	0.0020	4.3E-16	0.612	0.0077	99.5	99.86	1426.1	5.1
5919-01T	1600	195.553	0.280	0.0140	7.0E-17	1.820	0.0157	97.9	100.00	2009	21
	total gas age		n=20		5.1E-14	83.821	101.9388			1329.0	2.8
CP-1-2b:b Muscovite, JM, J=0.01068425					NM-42		1.2 mg				
5920-01A	600	15.370	0.138	0.0388	1.7E-16	3.690	0.0142	25.3	0.36	74	10
5920-01B	650	33.933	0.083	0.0050	1.3E-15	6.132	0.0075	95.6	3.03	536.7	1.9
5920-01C	700	78.939	0.074	0.0039	2.7E-16	6.904	0.0055	98.5	3.59	1091.3	5.0
5920-01D	750	101.401	0.065	0.0011	2.0E-15	7.811	0.0038	99.7	7.77	1321.0	2.6
5920-01E	800	106.118	0.011	0.0008	2.6E-15	45.224	0.0013	99.8	13.29	1365.0	2.5
5920-01F	825	104.929	0.009	0.0005	2.8E-15	54.568	0.0008	99.8	19.22	1355.0	2.4
5920-01G	850	104.894	0.008	0.0006	3.6E-15	62.172	0.0009	99.8	26.72	1354.4	2.6
5920-01H	875	104.115	0.004	0.0002	3.7E-15	114.842	0.0006	99.9	34.46	1348.4	2.5
5920-01I	900	104.324	0.004	0.0004	3.1E-15	120.351	0.0013	99.9	40.85	1349.8	2.5
5920-01J	925	104.100	0.006	0.0001	2.8E-15	89.879	0.0015	100.0	46.61	1348.5	2.5
5920-01K	950	104.904	0.007	0.0003	3.5E-15	71.924	0.0016	99.9	53.96	1355.3	2.4
5920-01L	975	105.321	0.007	0.0001	2.3E-15	71.127	0.0024	100.0	58.71	1359.6	2.3
5920-01M	1000	105.319	0.007	0.0003	1.7E-15	78.183	0.0048	99.9	62.31	1359	15
5920-01N	1040	104.877	0.009	0.0004	2.1E-15	57.431	0.0045	99.9	66.77	1354.8	2.5
5920-01O	1080	105.351	0.009	0.0005	3.0E-15	56.329	0.0037	99.8	73.07	1358.7	2.8
5920-01P	1120	106.247	0.006	0.0001	5.1E-15	86.860	0.0030	99.9	83.68	1367.9	2.3
5920-01Q	1180	106.680	0.009	0.0004	5.9E-15	56.673	0.0863	99.9	95.92	1371.1	2.5
5920-01R	1220	106.702	0.042	0.0001	1.6E-15	12.232	0.0058	99.9	99.23	1372.1	2.8

Run ID#	Temp	$^{40}Ar/^{39}Ar$	$^{37}Ar/^{39}Ar$	$^{36}Ar/^{39}Ar$	^{39}Ar moles	K/Ca	Cl/K	$\%^{40}Ar^{*}$	$\%^{39}Ar$	Age	± Err
5920-01S	1400	109.725	0.896	0.0000	2.8E-16	0.570	0.0195	100.0	99.82	1400.7	5.8
5920-01T	1600	119.739	0.694	0.0054	8.8E-17	0.735	0.0405	98.7	100.00	1474	13
	total gas age		n=20		4.8E-14	66.851	38.4968			1329.9	3.0
JM-2 Muscovite, JM, J=0.01070879				NM-42		0.51 mg					
5921-01A	600	176.226	0.194	0.5468	1.0E-16	2.632	0.0618	8.3	0.56	263	49
5921-01B	650	40.790	0.099	0.0239	2.9E-16	5.131	0.0321	82.6	2.18	556.0	5.7
5921-01C	700	49.791	0.019	0.0006	7.4E-17	27.521	0.0291	99.6	2.59	768	18
5921-01D	750	69.052	0.052	0.0077	8.5E-16	9.862	0.0266	96.7	7.38	973.1	2.9
5921-01E	800	84.414	0.022	0.0051	1.1E-15	23.258	0.0102	98.2	13.40	1146.1	3.2
5921-01F	825	92.190	0.014	0.0034	1.3E-15	36.569	0.0053	98.9	20.83	1228.8	2.8
5921-01G	850	95.485	0.008	0.0024	1.3E-15	62.895	0.0049	99.2	28.08	1263.7	2.9
5921-01H	875	97.821	0.006	0.0012	1.3E-15	80.687	0.0046	99.6	35.14	1289.2	3.0
5921-01I	900	98.257	0.007	0.0025	1.2E-15	70.894	0.0055	99.2	41.64	1289.6	3.2
5921-01J	925	98.910	0.008	0.0025	8.7E-16	60.833	0.0065	99.2	46.55	1295.8	3.2
5921-01K	950	99.260	0.026	0.0035	1.5E-15	19.440	0.0076	98.9	54.73	1296.5	3.0
5921-01L	975	100.156	0.032	0.0035	1.1E-15	16.094	0.0092	99.0	61.15	1305.0	3.6
5921-01M	1000	100.402	0.019	0.0045	1.1E-15	26.847	0.0087	98.7	67.42	1304.4	3.3
5921-01N	1040	101.732	0.015	0.0053	1.4E-15	33.331	0.0103	98.4	75.13	1314.7	2.8
5921-01O	1080	103.527	0.011	0.0079	1.1E-15	44.849	0.0151	97.7	81.39	1324.1	3.4
5921-01P	1120	104.018	0.012	0.0070	1.1E-15	41.863	0.0186	98.0	87.34	1331.3	3.2
5921-01Q	1180	106.886	0.037	0.0205	8.1E-16	13.901	1.1678	94.3	91.89	1320.9	3.4
5921-01R	1220	110.413	0.030	0.0338	3.7E-16	17.007	0.0219	90.9	93.98	1317.0	5.6
5921-01S	1400	100.176	0.067	0.0045	9.3E-16	7.598	0.0058	98.6	99.22	1302.3	3.1
5921-01T	1600	106.968	0.032	0.0238	1.4E-16	15.875	0.0153	93.4	100.00	1312.4	9.6
	total gas age		n=20		1.8E-14	36.338	22.8771			1251.8	3.6
JM-4:a Muscovite, JM, J=0.010612				NM-42		1.52 mg					
5923-01A	600	66.706	0.022	0.1121	1.5E-15	23.068	0.0082	50.3	2.94	549.7	5.0
5923-01B	650	72.047	0.016	0.0114	1.7E-15	31.202	0.0028	95.3	6.11	987.5	2.5
5923-01C	700	83.790	0.010	0.0068	1.7E-15	50.697	0.0022	97.6	9.42	1126.9	2.7
5923-01D	750	89.981	0.007	0.0039	3.9E-15	71.054	0.0015	98.7	16.92	1197.8	2.4
5923-01E	800	95.485	0.007	0.0032	5.7E-15	76.642	0.0010	99.0	27.79	1253.2	2.5
5923-01F	825	96.754	0.005	0.0032	4.9E-15	94.071	0.0013	99.0	37.28	1265.4	2.5
5923-01G	850	97.899	0.005	0.0054	5.3E-15	111.978	0.0016	98.4	47.44	1270.0	2.5
5923-01H	875	98.541	0.004	0.0071	4.3E-15	123.744	0.0019	97.8	55.79	1271.3	2.5
5923-01I	900	99.957	0.006	0.0085	3.6E-15	85.678	0.0026	97.5	62.66	1280.7	2.5
5923-01J	925	100.623	0.006	0.0095	2.7E-15	88.523	0.0039	97.2	67.92	1284.3	3.0
5923-01K	950	102.922	0.006	0.0127	2.3E-15	82.451	0.0055	96.3	72.32	1296.9	3.0
5923-01L	975	102.358	0.006	0.0119	2.4E-15	91.232	0.0061	96.5	76.94	1293.7	2.9
5923-01M	1000	102.464	0.007	0.0096	2.2E-15	70.432	0.0065	97.2	81.19	1301.2	2.7
5923-01N	1040	102.796	0.008	0.0083	2.4E-15	61.943	0.0071	97.6	85.82	1307.9	2.8
5923-01O	1080	103.784	0.006	0.0108	2.4E-15	82.585	0.0072	96.9	90.43	1310.0	2.9
5923-01P	1120	103.626	0.007	0.0057	2.9E-15	76.759	0.0095	98.3	95.98	1322.6	2.6
5923-01Q	1180	108.777	0.011	0.0181	1.8E-15	45.566	0.5933	95.1	99.44	1336.2	2.8
5923-01R	1220	105.635	0.021	0.0060	1.3E-16	24.039	0.0645	98.3	99.69	1340	10
5923-01S	1400	117.401	0.022	0.0295	6.4E-17	22.945	0.0382	92.5	99.82	1383	20
5923-01T	1600	118.972	0.049	0.0054	9.6E-17	10.332	0.0275	98.6	100.00	1459	15
	total gas age		n=20		5.2E-14	81.639	31.6409			1242.1	2.8
JM-4:b Muscovite, JM, J=0.010612				NM-42		0.8 mg					
5924-01A	600	44.445	0.091	0.0468	3.8E-16	5.591	0.0302	68.8	2.37	507.2	4.8
5924-01B	650	88.394	0.000	0.0000	6.8E-17	0.000	0.0045	100.0	2.79	1193	17
5924-01C	700	90.311	0.023	0.0047	2.6E-16	22.482	0.0133	98.4	4.43	1198.8	5.1
5924-01D	750	94.229	0.016	0.0021	1.1E-15	32.293	0.0062	99.3	11.53	1244.4	2.6
5924-01E	800	96.280	0.010	0.0015	1.3E-15	51.854	0.0039	99.5	19.71	1265.5	2.8
5924-01F	825	95.237	0.008	0.0008	1.4E-15	61.098	0.0031	99.7	28.53	1257.6	2.5
5924-01G	850	94.790	0.006	0.0010	1.5E-15	87.279	0.0027	99.7	38.19	1252.8	2.5
5924-01H	875	95.200	0.013	0.0009	1.1E-15	39.549	0.0039	99.7	45.20	1256.9	2.7
5924-01I	900	95.418	0.008	0.0009	1.0E-15	66.897	0.0041	99.7	51.46	1259.1	2.7
5924-01J	925	95.780	0.010	0.0014	1.0E-15	49.757	0.0059	99.5	57.93	1261.1	2.9
5924-01K	950	95.881	0.006	0.0009	5.8E-16	92.648	0.0077	99.7	61.58	1263.5	3.8
5924-01L	975	96.782	0.006	0.0011	7.3E-16	78.922	0.0099	99.6	66.19	1271.5	3.1
5924-01M	1000	95.875	0.005	0.0016	7.4E-16	108.532	0.0093	99.5	70.81	1261.5	3.1
5924-01N	1040	96.557	0.008	0.0007	6.2E-16	61.936	0.0097	99.8	74.70	1270.4	3.2
5924-01O	1080	97.914	0.004	0.0009	1.1E-15	133.662	0.0115	99.7	81.28	1282.6	3.0
5924-01P	1120	99.725	0.013	0.0016	1.4E-15	39.790	0.0102	99.5	90.37	1297.7	2.7
5924-01Q	1180	102.626	0.017	0.0028	1.4E-15	30.834	0.4736	99.2	99.11	1321.3	2.7
5924-01R	1220	112.124	0.064	0.0022	1.3E-16	8.016	0.4381	99.4	99.90	1408.1	9.8
5924-01S	1400	274.399	2.048	-0.0582	6.9E-18	0.249	0.9443	106.3	99.95	2546	147
5924-01T	1600	329.102	1.234	0.3204	8.3E-18	0.414	0.1073	71.2	100.00	2255	176
	total gas age		n=20		1.6E-14	60.655	38.2551			1252.8	3.2
JM-5 Muscovite, JM, J=0.01070913				NM-42		0.71 mg					
5925-01A	600	45.754	0.021	0.0387	1.0E-15	24.429	0.0085	75.0	3.89	564.5	3.3

Run ID#	Temp	^{40}Ar/^{39}Ar	^{37}Ar/^{39}Ar	^{36}Ar/^{39}Ar	^{39}Ar moles	K/Ca	Cl/K	%^{40}Ar*	%^{39}Ar	Age	± Err
5925-01B	650	72.000	0.019	0.0034	1.5E-15	27.234	0.0047	98.6	9.45	1019.9	2.5
5925-01C	700	76.873	0.009	0.0016	1.4E-15	59.695	0.0034	99.4	14.92	1078.4	2.6
5925-01D	750	84.597	0.008	0.0013	4.2E-15	64.855	0.0017	99.5	30.92	1159.4	2.5
5925-01E	800	96.642	0.006	0.0010	4.6E-15	86.986	0.0009	99.7	48.50	1278.6	2.3
5925-01F	825	102.239	0.004	0.0013	3.6E-15	125.289	0.0006	99.6	62.29	1330.4	2.6
5925-01G	850	103.739	0.003	0.0015	2.6E-15	180.371	0.0013	99.6	72.31	1343.7	2.6
5925-01H	875	104.657	0.005	0.0025	2.0E-15	110.709	0.0015	99.3	79.75	1349.4	2.7
5925-01I	900	106.477	0.004	0.0038	1.6E-15	122.873	0.0024	98.9	85.71	1362.5	2.8
5925-01J	925	107.872	0.007	0.0046	1.1E-15	78.124	0.0048	98.7	89.90	1373.0	3.0
5925-01K	950	110.089	0.007	0.0036	5.4E-16	78.054	0.0073	99.0	91.93	1395.4	4.4
5925-01L	975	110.441	0.005	0.0069	6.4E-16	98.018	0.0096	98.1	94.37	1389.8	3.6
5925-01M	1000	111.080	0.000	0.0035	4.6E-16	6363.114	0.0145	99.0	96.11	1404.4	4.3
5925-01N	1040	111.660	0.000	0.0060	3.4E-16	0.000	0.0200	98.4	97.41	1403.0	5.3
5925-01O	1080	112.603	0.002	0.0154	2.1E-16	293.158	0.0438	95.9	98.22	1386.6	7.3
5925-01P	1120	111.547	0.015	0.0128	1.7E-16	34.530	0.0694	96.6	98.86	1384.1	9.2
5925-01Q	1180	112.836	0.009	0.0150	2.3E-16	56.111	2.3650	96.1	99.72	1390.0	6.9
5925-01R	1220	143.642	0.045	0.1106	4.6E-17	11.384	0.0465	77.2	99.90	1413	32
5925-01S	1400	102.917	0.006	-0.0222	2.2E-17	90.503	0.0523	106.3	99.98	1399	51
5925-01T	1600	403.413	0.111	0.5248	4.8E-18	4.593	0.1412	61.6	100.00	2340	362
total gas age			n=20		2.6E-14	203.905	1406.2543			1246.2	3.0
JM-7:a Muscovite, JM, J=0.01071319				NM-42			1.05 mg				
5927-01A	600	42.468	0.026	0.0736	3.4E-15	19.386	0.0055	48.7	8.49	361.0	3.5
5927-01B	650	85.891	0.017	0.0132	2.2E-15	30.776	0.0018	95.4	13.97	1137.2	2.7
5927-01C	700	99.931	0.008	0.0084	2.3E-15	66.508	0.0017	97.5	19.80	1289.5	2.7
5927-01D	750	103.409	0.007	0.0060	4.2E-15	72.995	0.0015	98.3	30.25	1328.7	2.7
5927-01E	800	104.241	0.005	0.0047	4.9E-15	93.363	0.0013	98.6	42.34	1340.0	2.5
5927-01F	825	104.132	0.005	0.0046	3.9E-15	99.991	0.0013	98.7	51.90	1339.1	2.6
5927-01G	850	105.054	0.005	0.0093	3.5E-15	100.572	0.0017	97.4	60.63	1334.8	2.6
5927-01H	875	108.355	0.004	0.0192	3.2E-15	120.774	0.0027	94.7	68.54	1338.2	2.8
5927-01I	900	109.366	0.007	0.0229	2.4E-15	68.578	0.0042	93.8	74.59	1337.6	2.8
5927-01J	925	109.792	0.004	0.0239	1.9E-15	126.536	0.0052	93.6	79.28	1338.8	3.0
5927-01K	950	111.539	0.007	0.0277	1.4E-15	73.442	0.0073	92.6	82.69	1344.4	3.1
5927-01L	975	111.454	0.005	0.0250	1.6E-15	96.735	0.0083	93.4	86.65	1351.1	3.3
5927-01M	1000	110.138	0.005	0.0219	1.4E-15	106.421	0.0094	94.1	90.12	1347.3	3.4
5927-01N	1040	109.641	0.006	0.0185	1.4E-15	78.959	0.0095	95.0	93.64	1352.0	3.2
5927-01O	1080	108.804	0.009	0.0172	1.3E-15	55.435	0.0124	95.3	96.79	1348.0	3.2
5927-01P	1120	110.380	0.013	0.0212	8.8E-16	40.646	0.0231	94.3	98.96	1351.5	3.3
5927-01Q	1180	129.805	0.032	0.0890	3.7E-16	15.711	2.3961	79.7	99.88	1345.9	7.4
5927-01R	1220	109.176	0.000	0.0029	2.4E-17	0.000	0.2244	99.2	99.94	1390	39
5927-01S	1400	175.026	0.000	0.0179	1.9E-17	0.000	0.1692	97.0	99.99	1869	53
5927-01T	1600	1110.155	0.077	0.4816	4.2E-18	6.662	0.2093	87.2	100.00	4386	305
total gas age			n=20		4.0E-14	79.685	40.6808			1243.2	3.0
JM-7:b Muscovite, JM, J=0.01071319				NM-42			1.1 mg				
5928-01A	600	28.745	0.142	0.0546	1.5E-16	3.590	0.0556	43.8	3.99	228	12
5928-01B	650	68.359	0.056	0.0183	1.4E-16	9.103	0.0899	92.1	7.69	929.8	8.3
5928-01C	700	87.149	0.103	0.0092	8.6E-17	4.960	0.0574	96.9	10.01	1162	12
5928-01D	750	97.683	0.021	0.0085	3.3E-16	24.026	0.0220	97.4	18.86	1267.8	5.0
5928-01E	800	99.750	0.017	0.0040	4.3E-16	30.017	0.0135	98.8	30.44	1300.1	3.7
5928-01F	825	99.782	0.000	0.0013	4.3E-16	0.000	0.0143	99.6	42.17	1308.0	3.6
5928-01G	850	101.062	0.010	0.0018	3.8E-16	52.939	0.0156	99.4	52.39	1318.4	4.3
5928-01H	875	100.304	0.004	-0.0002	3.2E-16	144.909	0.0171	100.0	60.91	1316.7	4.4
5928-01I	900	101.700	0.024	0.0012	2.6E-16	21.192	0.0253	99.6	67.82	1326.0	4.7
5928-01J	925	100.838	0.007	0.0062	2.3E-16	69.297	0.0356	98.1	74.01	1304.1	5.2
5928-01K	950	102.952	0.008	0.0008	1.4E-16	61.990	0.0402	99.8	77.92	1338.7	7.9
5928-01L	975	102.902	0.000	-0.0025	1.7E-16	0.000	0.0475	100.7	82.46	1347.2	7.5
5928-01M	1000	102.245	0.024	-0.0032	1.5E-16	20.966	0.0479	100.9	86.46	1342.9	7.5
5928-01N	1040	102.658	0.000	0.0034	1.7E-16	0.000	0.0520	99.0	91.08	1328.8	7.9
5928-01O	1080	104.225	0.023	0.0007	1.5E-16	22.074	0.0646	99.8	95.24	1350.6	8.1
5928-01P	1120	102.763	0.024	0.0051	1.1E-16	21.047	0.1150	98.5	98.28	1325	11
5928-01Q	1180	113.820	0.292	0.0525	3.5E-17	1.749	20.2878	86.4	99.23	1298	29
5928-01R	1220	92.697	0.000	-0.2023	2.7E-18	0.000	2.9757	164.5	99.30	1747	240
5928-01S	1400	221.693	0.000	0.0015	2.8E-18	0.000	0.6027	99.8	99.38	2192	235
5928-01T	1650	152.914	1.144	0.0750	2.3E-17	0.446	0.0142	85.5	100.00	1581	43
total gas age			n=20		3.7E-15	34.553	35.5000			1256.1	6.7
JM-8:a Muscovite, JM, J=0.01062287				NM-42			0.75 mg				
5929-01A	600	47.326	0.050	0.1302	1.1E-15	10.295	0.0088	18.6	5.94	161.6	6.9
5929-01B	650	73.402	0.068	0.0431	5.6E-16	7.475	0.0035	82.6	8.92	897.0	4.4
5929-01C	700	94.157	0.129	0.0250	1.8E-16	3.945	0.0016	92.1	9.90	1178.3	6.9
5929-01D	750	102.235	0.017	0.0154	1.4E-15	30.684	0.0015	95.5	17.49	1283.9	2.9
5929-01E	800	105.488	0.007	0.0063	2.3E-15	70.798	0.0006	98.2	29.54	1339.0	2.9
5929-01F	825	104.737	0.005	0.0052	2.3E-15	104.897	0.0005	98.5	41.46	1335.2	2.7
5929-01G	850	104.309	0.005	0.0048	2.2E-15	110.130	0.0009	98.6	52.90	1332.2	3.0

Run ID#	Temp	$^{40}Ar/^{39}Ar$	$^{37}Ar/^{39}Ar$	$^{36}Ar/^{39}Ar$	^{39}Ar moles	K/Ca	Cl/K	%$^{40}Ar^*$	%^{39}Ar	Age	± Err
5929-01H	875	104.988	0.006	0.0085	2.1E-15	91.436	0.0010	97.6	64.09	1328.6	2.8
5929-01I	900	107.439	0.003	0.0153	1.8E-15	153.657	0.0027	95.8	73.75	1332.6	2.9
5929-01J	925	110.733	0.008	0.0265	1.4E-15	60.586	0.0067	92.9	81.13	1332.2	3.5
5929-01K	950	115.010	0.000	0.0355	5.5E-16	0.000	0.0108	90.8	84.06	1347.0	4.3
5929-01L	975	117.445	0.003	0.0447	8.2E-16	157.134	0.0155	88.7	88.41	1344.5	4.0
5929-01M	1000	119.505	0.002	0.0469	5.6E-16	204.316	0.0190	88.4	91.38	1357.3	4.7
5929-01N	1040	122.335	0.004	0.0517	5.4E-16	115.427	0.0234	87.5	94.26	1370.0	4.8
5929-01O	1080	122.878	0.000	0.0523	5.1E-16	0.000	0.0278	87.4	96.97	1373.3	5.4
5929-01P	1120	127.831	0.014	0.0630	3.8E-16	35.364	0.0409	85.4	98.98	1389.3	5.5
5929-01Q	1180	200.437	0.036	0.2534	1.7E-16	14.279	3.8080	62.6	99.86	1529	15
5929-01R	1220	188.255	0.000	0.0412	7.7E-18	0.000	0.5304	93.5	99.90	1902	122
5929-01S	1400	332.604	0.295	0.1183	1.1E-17	1.731	0.2240	89.5	99.96	2573	87
5929-01T	1600	631.277	0.000	0.2919	7.8E-18	0.000	0.1432	86.3	100.00	3455	156
	total gas age		n=20		1.9E-14	83.448	63.8356			1254.0	3.8

JM-8:b Muscovite, JM, J=0.01062287 NM-42 1.05 mg

Run ID#	Temp	$^{40}Ar/^{39}Ar$	$^{37}Ar/^{39}Ar$	$^{36}Ar/^{39}Ar$	^{39}Ar moles	K/Ca	Cl/K	%$^{40}Ar^*$	%^{39}Ar	Age	± Err
5930-01A	600	18.225	0.112	0.0150	6.8E-16	4.549	0.0248	75.6	7.91	246.5	2.3
5930-01B	650	66.305	0.091	0.0082	3.3E-16	5.623	0.0378	96.3	11.73	934.3	4.5
5930-01C	700	84.243	0.004	0.0070	3.0E-16	125.116	0.0244	97.5	15.21	1131.8	4.3
5930-01D	750	93.114	0.015	0.0037	6.9E-16	34.520	0.0143	98.8	23.29	1230.0	3.1
5930-01E	800	100.132	0.008	0.0024	1.0E-15	66.513	0.0090	99.3	35.03	1300.3	2.8
5930-01F	825	101.207	0.007	0.0014	9.5E-16	76.977	0.0062	99.6	46.09	1312.8	3.0
5930-01G	850	100.869	0.000	0.0020	8.3E-16	0.000	0.0071	99.4	55.77	1308.0	3.0
5930-01H	875	100.735	0.010	0.0010	7.2E-16	49.270	0.0078	99.7	64.15	1309.7	3.2
5930-01I	900	100.893	0.004	0.0025	5.7E-16	139.496	0.0111	99.2	70.75	1307.0	3.2
5930-01J	925	100.532	0.006	0.0023	4.8E-16	86.139	0.0163	99.3	76.38	1304.3	3.7
5930-01K	950	98.861	0.009	0.0017	3.5E-16	59.013	0.0251	99.5	80.42	1290.3	4.7
5930-01L	975	99.866	0.009	0.0000	3.4E-16	56.835	0.0243	100.0	84.40	1304.4	4.3
5930-01M	1000	99.952	0.000	-0.0023	3.0E-16	0.000	0.0266	100.7	87.89	1311.5	4.8
5930-01N	1040	101.756	0.000	-0.0025	3.5E-16	0.000	0.0283	100.7	91.91	1328.7	4.2
5930-01O	1080	103.979	0.016	0.0022	3.2E-16	31.880	0.0431	99.4	95.61	1336.3	4.3
5930-01P	1120	103.074	0.037	-0.0002	2.4E-16	13.675	0.1913	100.0	98.40	1334.4	5.0
5930-01Q	1180	105.387	0.231	0.0107	7.6E-17	2.210	10.2346	97.0	99.29	1326	12
5930-01R	1220	86.224	0.000	-0.0851	1.1E-17	0.000	1.5150	129.1	99.41	1408	60
5930-01S	1400	94.456	0.307	-0.0119	2.1E-17	1.660	1.4899	103.7	99.65	1287	35
5930-01T	1650	127.759	0.936	0.0074	3.0E-17	0.545	0.2507	98.3	100.00	1530	29
	total gas age		n=20		8.6E-15	48.465	4.4E+01			1199.7	3.8

D=	1.00510	0.00200
Ca 39/37=	0.00070	0.00005
Ca 36/37=	0.00026	0.00002
K 38/39=	0.01190	
K 40/39=	0.02700	0.00200

This thesis is accepted on behalf of the faculty
of the Institute by the following committee:

Advisor

Date

I release this document to the New Mexico Institute of Mining and Technology.

Student's Signature 1/27/92 Date